Cooperative Techniques for Next Generation HF Communication Systems

by

Mohammad Reza Heidarpour

A thesis
presented to the University of Waterloo
in fulfillment of the
thesis requirement for the degree of
Doctor of Philosophy
in
Electrical and Computer Engineering

Waterloo, Ontario, Canada, 2013

AUTHOR'S DECLARATION

I hereby declare that I am the sole author of this thesis. This is a true copy of the thesis, including any required final revisions, as accepted by my examiners.

I understand that my thesis may be made electronically available to the public.

Abstract

The high frequency (HF) band lies within 2-30 MHz of the electromagnetic spectrum. For decades, the HF band has been recognized as the primary means of long-range wireless communications. When satellite communication first emerged in 1960s, HF technology was considered to be obsolete. However, with its enduring qualities, HF communication survived through this competition and positioned itself as a powerful complementary and/or alternative technology to satellite communications.

HF systems have been traditionally associated with low-rate data transmission. With the shift from analog to digital in voice communication, and increasing demands for high-rate data transmission (e.g., e-mail, Internet, FTP), HF communication has been going through a renaissance. Innovative techniques are required to push the capacity limits of the HF band.

In this dissertation, we consider cooperative communication as an enabling technology to meet the challenging expectations of future generation HF communication systems. Cooperative communication exploits the broadcast nature of wireless transmission and relies on the cooperation of users relaying the information to one another. We address the design, analysis, and optimization of cooperative HF communication systems considering both multi-carrier and single-carrier architectures. As the multi-carrier HF system, we consider the combination of the orthogonal frequency division multiplexing (OFDM) with the bit interleaved coded modulation (BICM) as the underlying physical layer platform. It is assumed that cooperating nodes may use different HF propagation mechanisms, such as near-vertical-incidence sky wave (NVIS) and surface wave, to relay their received signals to the destination in different environmental scenarios. Diversity gain analysis, optimum relay selection strategy and power allocation between the source and relays are investigated for the proposed cooperative HF system.

For single-carrier HF systems, we first derive a matched-filer-bound (MFB) on the error rate performance of the non-regenerative cooperative systems. The results from the MFB analysis are also used for relay selection and power allocation in the multi-relay cooperative systems. To overcome the intersymbol interference impairment induced by frequency-selectivity of the HF channel, equalization is inevitable at the destination in a single-carrier system. In this work, we investigate the minimum-mean-square-error (MMSE) based linear/decision-feedback frequency domain equalizers (FDEs). Both symbol-spaced and fractionally-spaced implementations of the proposed FDEs are considered and their performance is compared under different channel conditions and sampling phase errors at the relay and destination nodes.

Acknowledgements

"In the Name of Allah, the Most Beneficent, the Most Merciful,
All praise is due to Allah, the Lord of the Worlds,
The Most Beneficent, the Most Merciful,
The Master of the Day of Judgment,
You (Alone) we worship, and you (Alone) we ask for help."

[The Holy Quran, Chapter 1, verses 1-5]

Table of Contents

List of Figures

List of Tables

List of Abbreviations

AaF	Amplify-and-forward
ALE	Automatic link establishment
APS	Average power scaling
ARQ	Automatic-repeat-request
AS	All subcarrier selection
AWGN	Additive white Gaussian noise
BER	Bit error rate
BICM	Bit interleaved coded modulation
BLOS	Beyond line of sight
BPSK	Binary phase shift keying
BW	Burst waveform
CFO	Carrier frequency offsets
CIR	Channel impulse response
CP	Cyclic prefix
CPSC	Cyclic prefix single-carrier
CSI	Channel state information
DaF	Decode-and-forward
DFE	Decision feedback equalization
DFT	Discrete Fourier transform
DRM	Digital Radio Mondiale
EPA	Equal power allocation
FaF	Filter-and-forward
FDE	Frequency domain equalization
FEC	Forward-error-correction

FIR	Finite impulse response
FSE	Fractionally spaced equalization
FS-FDE	Fractionally-spaced frequency-domain equalization
GP	Geometric programming
GPS	Global positioning system
HARQ	Hybrid automatic-repeat-request
HDL	High-rate data link
IDFT	Inverse discrete Fourier transform
i.i.d.	Independent and identically distributed
IPS	Instantaneous power scaling
IR-HARQ	Incremental-redundancy hybrid automatic-repeat-request
ISB	Independent sideband
ISI	Inter-symbol interference
LDL	Low-rate data link
LOS	Line of sight
LUF	Lowest usable frequency
MC	Multi-carrier
MFB	Matched filter bound
MIL-STD	Military standard
MIMO	Multiple-input-multiple-output
ML	Maximum likelihood
MLSD	Maximum likelihood sequence detection
MUF	Maximum usable frequency
NVIS	Near vertical incidence sky wave
OFDM	Orthogonal frequency division multiplexing
OPA	Optimum power allocation

OTH	Over the horizon
PEP	Pairwise error probability
PHY	Physical layer
PS	Per subcarrier selection
PSD	Power spectral density
PSK	Phase shift keying
QAM	Quadrature amplitude modulation
SC	Single-carrier
SER	Symbol error rate
SINR	Signal-to-interference-plus-noise ratio
SNR	Signal-to-noise ratio
SSE	Symbol-spaced equalization
SS-FDE	Symbol-spaced frequency-domain equalization
STANAG	Standardization agreement
TDE	Time domain equalization
TDL	Tapped-delay-line
TR-STBC	Time-reversal space time block coding
WBHF	Wideband high-frequency

Notation

Bold upper-case letter	Matrix
Bold lower-case letter	Column vector
$\overline{(\cdot)}$	Conjugate operator
$(\cdot)^{\mathrm{T}}$	Transpose operator
$(\cdot)^{*}$	Conjugate transpose operator
$*$	linear convolution operator
$\otimes$	Kronecker product
$<\cdot>_N$	Modulo N operation
$[k]_N$	is equal to k if $k \leq N$, and equal to $k - 2N$ if $k > N$
$\mathrm{E}[\cdot]$	Expectation of a random variable
$\mathbf{v}(k)$	The kth entry of vector $\mathbf{v}$
$\mathbf{X}(k,l)$	The (k,l)th entry of matrix $\mathbf{X}$
$\|.\|$	Euclidean norm of a vector
$\mathbf{I}_K$	Identity $K \times K$ matrix
$\mathbf{0}_{M \times N}$	An $M \times N$ all-zero matrix
$\mathbf{1}_{M \times N}$	An $M \times N$ all-one matrix
$\mathbf{Q}_N = [q_{n,k}]$	The N-point discrete Fourier transform (DFT) matrix $(n,k = 0,1,\cdots,N-1)$ with $q_{n,k} = W_N^{kn}/\sqrt{N}$ and $W_N \triangleq \exp(-j2\pi/N)$
$\|\Omega\|$	Cardinality of the set Ω
$\exp(\mathbf{v})$	A vector in which the ith entry is $\exp(\mathbf{v}(i))$
$\|x(.)\|$	Square root of the energy of the signal $x(.)$
$X \sim \mathcal{G}(\alpha,\beta)$	X is a Gamma random variable with parameters α and β
$\delta(n)$	Kronecker delta function
$E_1(\cdot)$	Exponential integral function

$W_{\mu,\nu}(\cdot)$	Whittaker W function with parameters μ and ν
$\Gamma(\cdot)$	Gamma function
$\mathrm{diag}\{\mathbf{v}\}$	A diagonal matrix with the elements of vector $\mathbf{v}$ on its diagonal
$\mathrm{Diag}\{\mathbf{A},\mathbf{B},\cdots\}$	A block matrix which can be partitioned into submatrices $\mathbf{A},\mathbf{B},\cdots$ (possibly of different dimensions) on the diagonal and zero submatrices elsewhere

Chapter 1

Introduction

1.1 HF Communication

For decades, the high frequency (HF) band has been recognized as the primary means of long-range wireless communications. The HF band lies within 2-30 MHz of the electromagnetic spectrum. In this part of the spectrum, propagation via direct wave, surface wave, near-vertical-incidence sky wave (NVIS), and sky wave provides a means of communication from line-of-sight (LOS) to beyond-line-of-sight (BLOS), and over-the-horizon (OTH) ranges [1], [2].

As a worldwide communication medium, spectrum utilization and allocation of the HF band is regulated by the International Telecommunication Union (ITU). Allocations are made on the basis of service type, which includes a wide range of applications, some of which are explained in the following:

- **Fixed radio communication:** HF communication between specified land stations provides service to isolated or remote areas where alternative services (e.g., satellite) are unavailable or too expensive to use.

- **Mobile radio communication:** HF communication between portable stations or between such stations and fixed land stations is particularly useful in establishing redundant links for disaster recovery, rescue operations, emergency responses, and battlefield scenarios.

- **Broadcasting:** With its long range, the HF band makes international broadcasting possible. Numerous broadcasting stations (e.g., the BBC World Service, the Voice of America) exist in the HF band and are known as world band radios. Analog modulation techniques have been traditionally employed for broadcasting in the HF band. The digital

HF broadcasting standard, known as Digital Radio Mondiale (DRM), was introduced in 2003 [3].

- **Amateur (ham) radio:** A portion of the HF band is allocated for the use of people interested in radio technology as a hobby. An estimated six million people worldwide are regularly involved with amateur radio.

Since Marconi demonstrated the first transatlantic radio transmission in 1901, HF communication has been widely used for long-range transmission and worldwide coverage during most of the 20th century. When satellite communication first emerged in the 1960s, HF technology was considered obsolete. However, later in the satellite area, it became clear that satellites were not the panacea they first appeared. The main disadvantages of satellite communication include the vulnerability of ground stations in disaster situations, problems with indoor reception, requirement for an unobstructed view of the satellite, high investment and maintenance costs among others. Also, in northern latitudes, the access to geosynchronous satellites and the majority of commercial services is limited by the low horizon angles. With its enduring qualities, HF communication has survived through this competition and positioned itself as a powerful complementary and/or alternative technology to satellite communications.

1.1.1 Early Period

The first HF modems typically used continuous wave (CW), frequency shift keying (FSK), and single side band (SSB) modulation to convey Morse, teletype, and voice signals, respectively [1]. The earliest multi-carrier HF modem was the Kineplex system introduced by the Collins Radio company in 1957 and was based on orthogonal frequency division multiplexing (OFDM). This system used 16 parallel tones with differential quadrature phase-shift keying (DQPSK) modulation at a symbol rate of 75 bauds to achieve a data rate of 2400 bps. In the 1960-1970s, other OFDM-based HF modems were introduced such as Kathryn (by General Atronics in 1961),

Andeft (by General Dynamics in 1967), and Codem (by General Atronics in 1971) [4]. Since the severe frequency-selectivity nature of HF channels requires a relatively high complexity for single-carrier receivers, a multi-carrier architecture with differential modulation was preferred in these modems. Following the advances in DSP and VLSI technologies, practical implementation barriers to advanced communication signal processing (such as adaptive channel estimation and equalization) were removed, resulting in the dominancy of single-tone modems. Progress in the areas of channel coding, modulation (e.g., coherent M-ary PSK/QAM), and adaptive channel estimation/equalization have further contributed to the evolution of HF radio [5].

1.1.2 Second Generation

A major problem in the early HF radios was the need for manual operation to identify suitable transmission frequencies and maintain transmission in the presence of ionospheric changes. The introduction of automatic link establishment (ALE) in the 1980s was a major milestone for HF systems. The ALE system is used to continually monitor the available channels, rank them according to their quality and ensure the high quality of the transmissions. Such automated frequency management systems removed the need for the highly trained and experienced crews used in the past. In this context, manually-controlled HF modems (before the introduction of the ALE technology) are typically referred to as the first generation (1G). The HF standards based on asynchronous ALE and synchronous ALE are, respectively, known as the second generation (2G) and the third generation (3G) [5].

In 1988, MIL-STD 188-141A was introduced as a standard for asynchronous ALE systems that can scan the spectrum at a rate of 2 or 5 channels per second. These ALE systems are used in conjunction with a physical layer (PHY) standard, e.g., MIL-STD 188-110A/B/C, STANAG 4285/4539, and a data link standard, e.g., STANAG 5066. The PHY standard MIL-STD 188-110A (released in 1991) uses a half-rate convolutional code, QPSK modulation, and a 50%

frame-pattern efficiency (i.e., the fraction of data symbols) to achieve a data rate of 1200 bps. Different coding rates, interleavers, constellation sizes (e.g., BPSK, QPSK, 8PSK, 16/32/64 QAM), and frame-pattern efficiencies determine the overall data rate as well as the robustness of different waveforms. MIL-STD 188-110A supports data rates of 75, 150, 300, 600, 1200, and 2400 bps in different configurations.

In MIL-STD 188-110B (released in 2000), data rates as high as 9600 bps are supported. Furthermore, this standard describes an optional mode of HF data modem operation over multiple discrete channels (including independent sidebands of a single carrier), and specifies a waveform that supports data rates of 9600 to 19200 bps over two independent sideband (2-ISB) radios. In addition to the mandatory serial-tone waveforms, MIL-STD 188-110B considers an optional operation based on the 16- or 39-tone waveforms for data rates from 75 to 2400 bps.

In 2011, MIL-STD 188-110C was released which involves a family of wideband high-frequency (WBHF) radio modem waveforms and coding specifications. The WBHF family of waveforms uses single contiguous bandwidths greater than 3 kHz, up to 24 kHz, supporting data rates in the range of 75 bps and 120,000 bps. Although it suppresses the 16-tone mode, this standard still retains the optional 39-tone parallel waveform.

1.1.3 Third Generation

While 2G HF standards are based on asynchronous ALE, 3G HF standards (such as MIL-STD 188-141B and STANAG 4538) employ synchronous ALE as a result of the employed global positioning system (GPS) time reference, and therefore, provide shorter call times than the earlier asynchronous ALEs. It should be noted that 2G technology has not been made obsolete by 3G systems, but rather coexists with them as a result of backward compatibility.

In 1999, MIL-STD 188-141B was released by the US department of defence (DoD). This standard supports backward compatibility for the 2G systems. Furthermore, unlike 2G standards,

it is a stand-alone standard and includes the specifications for PHY and data link layers. Specifically, MIL-STD 188-141B includes two data link protocols: the high-rate data link protocol (HDL), for large messages and/or good channel conditions, and the low-rate data link protocol (LDL), for short messages and/or poor channel conditions. At the PHY layer, different burst waveforms (BWs) are defined for the various kinds of signalling required in the system, such as 3G-ALE (BW0), traffic management and HDL acknowledgement (BW1), HDL traffic data (BW2), LDL traffic data (BW3), and LDL acknowledgement (BW4). All BWs use the basic 8-PSK modulation at 2400 bauds (also used in the MIL-STD 188-110A serial tone modem waveform). On the other hand, different code rates, interleaving lengths, and payload volumes are deployed in different BWs. For instance, BW2 uses a 1/4-rate convolutional code, a 66% frame-pattern efficiency, and contains $1881 \times n$ bits ($n = 3, 6, 12, 24$).

In 2011, the US DoD released another revision of the 3G standard, referred to as MIL-STD 188-141C, which also contains WBHF specifications to support high speed HF data communication.

1.1.4 Current Status

In this high-tech information age, HF communication continues to be used for a wide range of civilian, government, and military applications as a powerful alternative to a myriad of more sophisticated communication systems. Current HF communication systems are not used only for traditional voice transmission, but also for data communication (including file transfer, facsimile, e-mail, internet access), still-image transmission, and even real-time video conferencing [6], [7]. Unfortunately, the data rates offered in conventional 3 kHz HF channel allocations rarely exceed 9.6 kbps, and 128 kbps in the 24 kHz aggregated channels which are far away from today's user demands. Traditional analog voice transmission has been also replaced by digital techniques, as seen in the recent introduction of DRM broadcasting [3]. With the shift from analog to digital in

voice communication, and increasing demands for high-rate data transmission, HF communication has been going through a renaissance. Innovative techniques are required to push the capacity limits of the HF band. One of the promising techniques for deployment in the HF band is cooperative communication which is discussed in the next section.

1.2 Cooperative Communication

Within the last fifteen years, we have witnessed exciting developments in the area of wireless communication theory, most notably, multiple-input multiple-output (MIMO) and cooperative communication techniques. MIMO systems involve the deployment of multiple antennas at the transmitter and/or the receiver side(s), and achieve significant improvements in transmission reliability and throughput [8]–[10]. Multiple-antenna systems have been studied extensively in the context of transmission in the UHF (300 MHz - 3 GHz) and SHF (3 GHz - 30 GHz) bands assigned for cellular phones, cordless phones, Wi-Fi, and WiMax systems.

Cooperative diversity exploits the broadcast nature of wireless transmission and relies on the cooperation of users relaying each other's data. When a source node transmits its signal, this signal is received by the destination node and also overheard by other nodes in the vicinity. If these nodes are willing to share their resources, they can forward the overheard information to the destination as a second replica of the original signal, and act as relays for the source node (see Fig. 1.1).

The basic ideas behind user cooperation can be traced back to 1971 when Van Der Meulen investigated the average mutual information rate for the "three-terminal communication channels" [11]. The rigorous information theoretical analysis of the relay assisted transmission over the AWGN channels was first established by Cover and Gamal in 1979 [12]. However, the recent surge of interest in cooperative communication was subsequent to the works of Sendonaris et al. [13], [14], in which user cooperation is adopted to overcome the fading

6
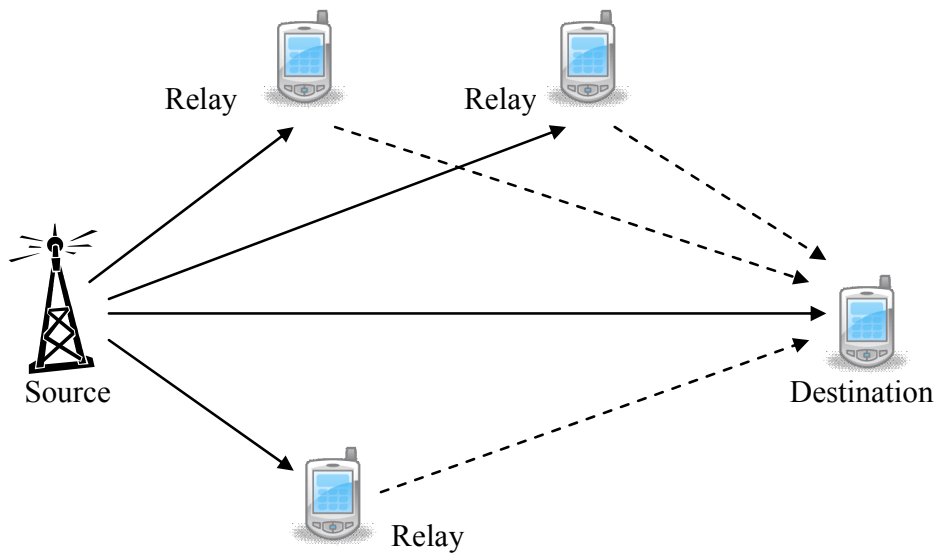
Figure 1.1 Cooperative communication.

impairment induced by multipath propagation in wireless networks. The user cooperation scheme in [13], [14] effectively realizes beamforming in a distributed manner based on the assumption that the channels' phases are available at the transmitters. In an independent work, Laneman et al. [15]–[17] proposed user cooperation over fading channels assuming no channel-state-information (CSI) at the transmitters. Specifically, it is demonstrated that a spatial diversity on the order of relay numbers can be achieved by using a two-phase cooperation protocol. In the first phase, i.e., the broadcasting phase, the source transmits its signal which is received by both the destination and the relays. In the second phase, i.e., the relaying phase, the relays transmit their signals to the destination through either orthogonal channels, in the so-called repetition based cooperative diversity approach [15], [16], or the same channel, in the so-called distributed space-time coded cooperative diversity approach [17]. Although distributed space time coding offers high spectral efficiency with respect to the repetition based method, it adds significant complexity to the system due to the required synchronization among the distributed nodes and a

7

priori knowledge about the number of relays which are successful in decoding of their received signals. In order to alleviate the complexity of relaying phase without sacrificing the spectral efficiency, Bletsas et al. [18] proposed the opportunistic relaying as an alternative technique. In the opportunistic relaying, the best relay from the set of available relays is selected and is used for cooperation between the source and the destination.

In general, relay nodes operate in either regenerative or non-regenerative mode. A regenerative, also called as decode-and-forward (DaF), relay decodes the received signal, and re-encodes the retrieved information before forwarding to the destination [15]. On the other hand, a non-regenerative relay, without any attempt to decode, just scales and forwards a processed version of its received signal. Based on the type of processing, non-regenerative relaying takes different forms such as amplify-and-forward (AaF) [15] and filter-and-forward (FaF) [19].

1.3 Thesis Motivation and Contributions

With a few recent exceptions (e.g., [20]–[22]), neither MIMO nor cooperative communication techniques have been extensively investigated for the HF band. Being cautious on the concept of MIMO HF is understandable because the required separation between antennas to extract diversity is of the order of several hundred meters considering that the wavelengths in HF band are in the range of 10-150 meters. This fact limits the potential use of MIMO HF to certain fixed applications for which the deployment area of HF station permits such wide uses of space.

On the other hand, cooperative communication is an effective means to exploit the spatial dimension of the wireless channel in the HF band. An initial performance study of a cooperative HF system has already demonstrated the potential of this emerging concept [21], [22]. In [21], Sharp et al. have proposed several single-carrier and multi-carrier cooperative systems with DaF relaying based on distributed randomized space time block coding. Based on simulation results, they have concluded that time-reversal space time block coding (TR-STBC) outperforms the

alternative methods. In [22], Banwell et al. have discussed the carrier synchronization and carrier frequency offset estimation for a DaF cooperative HF system.

This dissertation aims to address the design, analysis, and optimization of cooperative HF communication systems. Although there already exists a rich literature on cooperative communication, the current results are mainly limited to channel models developed for UHF and lower portion of SHF bands and are not directly applicable to HF communications. This motivates us to investigate the promising combination of HF communication and cooperative diversity techniques taking into account the intrinsic characteristics of HF band.

The outline of the thesis and the original contributions in each chapter are as follows. Chapter 2 presents an overview of HF communication basics. First, characteristics and mechanisms of different HF propagation approaches are reviewed. Then, the HF channel model that is used in the later chapters is introduced.

In Chapter 3, we address the analysis and design of a multi-carrier HF cooperative system with AaF relaying. The source and the destination terminals are separated far away from each other and achieve OTH communications via sky wave propagation. A number of relay terminals are located around the destination terminal and provide communication to the destination through either surface wave or NVIS. We consider the use of the OFDM with the bit-interleaved-coded-modulation (BICM) [23] as the outer coder at the transmitter. BICM is currently used in many point-to-point communication standards (e.g., IEEE 802.11 and 802.16 families) [24] and known to be robust to possible variations in the underlying channel's specification such as the number of paths and their relative delays [25]. BICM-OFDM was recently applied to AaF cooperative systems in [26] assuming a generic fading model. However, an in-depth study of BICM-OFDM cooperative systems taking into account the inherent characteristics of HF channels and propagation mechanisms does not yet exist and will be pursued in this chapter. We derive a pairwise error probability (PEP) expression for cooperative BICM-OFDM systems over HF

channels and determine the achievable diversity orders. Moreover, we derive a power allocation rule for performance improvement in cooperative HF system, and discuss relay selection criteria to enable an efficient opportunistic relaying strategy for multi-relay scenarios.

In Chapter 4, we focus our attention on single-carrier (SC) HF cooperative systems. The analysis and design of cooperative SC transmission has been studied in [19], [27]–[30] either through Monte Carlo simulations or the derivation of performance metrics such as instantaneous signal-to-interference-plus-noise ratio (SINR) and PEP. The existence of intersymbol interference (ISI) due to the frequency-selectivity and noise propagation due to the non-regenerative operation in the relays make the derivation of closed-form expressions for bit error rate and symbol error rate mathematically difficult, if not intractable. In Chapter 4, we address this issue by deriving a matched filter bound (MFB) on the error rate performance of cooperative SC systems with non-regenerative (in the form of either AaF or FaF) relaying. MFB analysis is a mature concept in point-to-point communication [31]–[34]. However, it has not yet been studied in detail in the context of cooperative communications except for some numerical results [28], [29].

In the MFB analysis, the performance is evaluated for the special case of transmitting only one isolated symbol, and therefore, MFB provides an upper bound on the performance of any kind of equalizer. It was shown in the literature [34] that the gap between the performance of maximum likelihood sequence detection (MLSD) and MFB bound is zero in many cases meaning that, within a multiplicative constant, the error probability of the MLSD is the same as MFB. We derive a closed form MFB expression on the error rate performance of non-regenerative SC cooperative systems. Through MFB analysis, we derive the achievable diversity order and obtain relay selection criterion in multi-relay systems. Moreover, we optimize power allocation to tighten the derived MFB expression which also provides an optimum (from an MFB perspective) method to allocate power between the source and relays in practical systems.

10

In Chapter 5, we discuss fractionally spaced equalization (FSE) and its application in single-carrier HF cooperative systems. In the conventional symbol-spaced equalizers (SSEs), the received signal is sampled at the symbol (or baud) rate before applying to the equalization filter. As a result, in practical systems using pulse-shaping filters with non-zero roll-off factor, the equalization filter operates on an aliased spectrum of the received signal rendering performance acutely sensitive to the receiver sampling phase [35], [36]. The sampling phase sensitivity of SSEs can be avoided by the implementation of FSEs in which the received signal is sampled at least as fast as the Nyquist rate [35], [37]. In [35], it is shown that unconstraint-length FSE achieves the optimum, in the minimum-mean-square-error (MMSE) sense, performance of the linear receivers. On the other hand, in the high data-rate communication, specifically in highly dispersive channels, the complexity demand of the time domain equalization (TDE) becomes prohibitively high, whereas, the frequency domain equalization (FDE) exhibits a low complexity growth by increasing the data rate and/or the length of the underlying channel impulse response [38].

Although the theory of equalization is enriched for the point-to-point communications including MIMO systems [38], [39], it is an under-explored concept for the case of cooperative systems and limited to a few publications (see [30], [19], [28], [29] and references therein). One of the earliest works on this topic is [30], where Mheidat et. al. proposed some symbol spaced FDE (SS-FDE) techniques for several cooperative systems. Based on maximizing signal-to-noise ratio (SNR), the design of symbol spaced TDE (SS-TDE) for cooperative beamforming transmission is investigated in [19], [28]. Considering the use of SS-FDE filters instead of SS-TDE ones, the design of cooperative beamforming systems is also revisited in [29].

To the best of our knowledge, FSE has not yet been studied in the context of cooperative systems. In Chapter 5, we investigate fractionally spaced FDE (FS-FDE) technique for a cooperative multi-relay system. Our motivation stems from the elegant properties reported for

the FSEs in the point-to-point communication systems (i.e., its robustness to sampling phase errors and potential in achieving the optimum performance) and the scalability of the FDEs. In particular, we propose a $T_S/2$-spaced equalizer [40] that transforms the temporal sample sequence to the frequency domain, applies MMSE linear/decision-feedback equalization, and returns the resulting signal back to the time domain for detection. The vital importance of using FSE method in cooperative systems is disclosed in practical scenarios where the transmitted signals have non-zero roll-off components and sampling phase error may occur in relay(s) and destination terminals. Analytical and numerical results are reported to compare the performance of FS-FDE and SS-FDE based cooperative systems. Specifically, it is observed that, under specific channel realizations and sampling errors, the cooperative systems with SS-FDE fail to harvest the available cooperative diversity and the performance approaches to that of no relay scenario. On the other hand, the performance of cooperative system with FS-FDE method becomes independent of sampling phase errors, and full benefit of cooperation is retained.

In Chapter 6, we summarize the contributions of the work presented in this dissertation and discuss potential extensions to our work.

It should be also noted that while this thesis considers the HF channel, the results are general, and the system designs and analyses are applicable to any cooperative system with underlying frequency selective channels.

Chapter 2

Overview of HF Propagation Methods and Channel Models

In HF band, propagation takes place via space wave, surface wave, near-vertical-incidence sky wave (NVIS), and sky wave [1], [2]. Space wave propagation (see Fig.2.1.a) supports LOS communication, whereas the surface wave mechanism (see Fig.2.1.b) provides BLOS communication, typically in the range of 100-150 kilometers or more based on the terrain conditions.

(a)   (b)

(c)   (d)
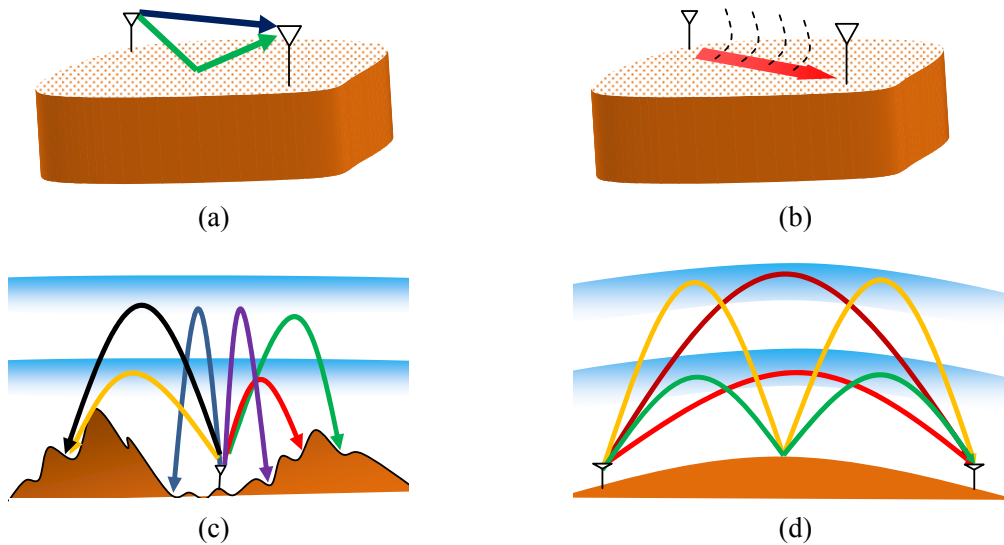
Figure 2.1 Different propagation mechanisms in the HF band: (a) space wave; (b) surface wave; (c) NVIS; (d) sky wave

On the other hand, the ionosphere, which is composed of a number of ionized regions above the Earth's surface, provides a natural mirror for HF electromagnetic waves. In NVIS (see Fig.2.1.c), HF signals are transmitted in a near vertical direction towards the ionosphere, which upon the refraction, gives an omnidirectional umbrella-like coverage as far as 300 kilometers. This method of communication becomes particularly useful in mountain and forest areas. Furthermore, in sky wave propagation (see Fig.2.1.d), the oblique transmission towards the ionosphere lets HF radio achieve OTH communications with nearly worldwide coverage.

In this chapter, we first provide an overview of HF propagation methods. Then, we present HF channel models including path loss, fading, noise and interference which will be used in the rest of the thesis.

2.1 HF Propagation Methods

2.1.1. Ground Wave Propagation

Ground wave propagation can be divided into two modes known as space and surface waves [1]. The dominancy of each mode differs based on the height of the transmitter and receiver antennas with respect to the carrier wave length. For low antenna heights, two components of the space-waves, i.e. the direct waves and indirect (ground reflected) waves cancel each other (see Fig. 2.1.a) and ground wave propagation mainly takes place along the surface of the earth (see Fig. 2.1.b). On the other hand, for high antenna heights, space waves become dominant [1]. Considering the wavelengths used in the HF band, it is the surface wave that predominates in the ground wave propagation, because the antennas are unlikely to be elevated by more than a few wavelengths (except in the case of aircraft to aircraft links).

Surface waves propagate along the (conductive) surface of the Earth. Therefore, vertical polarizations are required for their effective propagations [1]. The surface wave follows the curvature of the Earth and its range does not depend upon the height of the antenna. However,

the range depends upon the transmitter power and the operating frequency. Low frequencies travel further than high frequencies. Surface wave communications also vary by diurnal and seasonal changes in terrain electrical parameters. However these changes are much less than sky wave's variations and often negligible [1].

2.1.2. Sky Wave Propagation

The ionosphere is a region of the earth's atmosphere lying in the altitude range of 50-1000 km. In this region, the molecules of the atmosphere can be ionized by radiation from the Sun. Ionization is an energy consuming process in which neutral molecules are decomposed into negative-charge electrons and positive-charge ions. There is also an inverse de-ionization operation in which electric charged particles absorb each other and form neutral molecules. Although the name of ionosphere layer directly points out to the existence of ions in this layer, these are the much lighter and more freely moving electrons which are responsible for the refraction and reflection of the electromagnetic waves [41].

In different altitudes of the ionosphere, different chemical compositions and pressures exist. The amount of solar radiation energy, which provides the fuel for the ionization process, also decreases in its path from higher to lower altitudes. Therefore, different ionization/deionization equilibriums occur in different altitudes of the ionosphere. During the day, there are four principal layers with different electron densities in the ionosphere, called D layer (50-90 km), E layer (90-140 km), F1 layer (140-210 km), and F2 layer (over 210 km). F1 layer sometimes merges into F2 layer and only three distinct ionospheric layers are observed [41]. Electromagnetic waves are mainly reflected from either E or F (F2 and F1 if present) layers. The D layer, with lower electron density, is principally responsible for the attenuation of the cross-passing waves. In addition to these principal layers, there exist spatially and temporally variable patches of ionization, called sporadic-E (Es) at altitudes of 90 to 140 km (the E region). Because

15

of its high electron density, Es region can sometimes reflect HF signals which are normally intended to be reflected by F layer [41].

Electron life-time in F2 layer is much higher than F1 and E layers. Typical electron life-time in F2 layer is 20 minutes while this is 1 minute and 20 seconds for F1 and E layers respectively [41]. Furthermore, upper atmosphere wind currents from day-lit to night-side hemispheres can interchange the free electron content of F2 layer in different parts of ionospheres with each other. These are the main reasons that why during the night when there is no solar radiation any more, it is only the F2 layer which keeps ionized and all the other layers will be depleted from electrons.

Influence of the ionosphere on the incident electromagnetic waves comes from the fact that the speed of the wave (and therefore the refractive index) in the ionosphere is different from that in free space. The ionospheric refractive index is a function of electron density (inversely) and the frequency of incident wave (directly) [42]. According to Snell's law, the electromagnetic wave starts deviating from the straight line that it travels when it arrives, with the incident angle θ, from the lower parts of the atmosphere (with refractive index close to one) to the ionosphere. This deviation remains continuous until the point where the refractive index becomes equal to $\sin(\theta)$. From this point forth, upwards movement is converted to the downwards one and the electromagnetic wave comes back to the earth.

The choice of carrier frequency is critical in sky wave propagation. By definition, the maximum frequency which is reflected back to the earth by the ionosphere under the vertical transmission (incidence) is called "critical frequency" [1]. The "maximum usable frequency (MUF)" for any given transmission distance is calculated from the product of critical frequency and the MUF factor which is a function of the transmission distance. This distance is associated with a certain angle of elevation of the transmitted wave. On the other hand, the absorption of an HF radio wave in the D region, which is proportional to the inverse square of the frequency,

defines a lower band for the operating frequency [1]. This bound is called the "lowest usable frequency (LUF)".

The distance between the transmitter and the receiver determines which layer (E or F) of the ionosphere can act as the principal mirror for the transmitted signal. Consequently, the elevation angle of the transmitter antenna and the carrier frequency can be adjusted properly. The carrier frequency is selected to be greater than the LUF and less than the MUF of the corresponding layer.

NVIS and sky wave communications are subject to frequency selective fading because of the multipath propagation (see Fig. 2.1). In addition to the multipath-induced fading experienced in the NVIS/sky wave propagation, another source of fading in the HF channel comes from the effect of the Earth's magnetic field on moving electrons, i.e., the Faraday effect [2]. More specifically, each electromagnetic wave, in its path through the ionosphere, applies an electric force on free electrons. The direction of this force is the same as the direction of the wave's electric field. On the other hand, moving electrons re-radiate an electromagnetic wave whose polarization, in the absence of the Earth's magnetic field, would be the same as the incident wave's. However, in reality, moving electrons become subject to the force applied by the geomagnetic field. As a result, electrons will move in complicated twisted orbits and the received wave will have a different polarization than that of the transmitted wave. In other words, the reflected wave is the superposition of two components. One of them is the ordinary (O) component which is produced by moving electrons in the absence of the Earth's magnetic field. The other one is called extraordinary (X) component which comes from the effect of the geomagnetic field on moving electrons. Although most of the time they have approximately the same delay and so are not distinguishable, the interference between O and X components results in an outcome wave with a time-variant polarization. Rotation of the axes of the received polarization ellipse forms a kind of fading called the polarization fading.

17

Ionospheric variations also highly affect the sky wave propagation, and therefore, the fading strength. The ionization process is mostly dependent on the energy receiving from solar radiations, and thus, on the solar activity and the solar zenith angle (which is different in various seasons and latitudes). The solar activity is determined by the number of sunspots appearing on the surface of the sun (the higher the solar activity is, the higher the number of sunspots), and undergoes an 11-year cycle. As a result, the ionosphere has annual, seasonal and diurnal variations. High electron density occurs within the duration of the maximum received solar radiation, i.e. at noon in a day, during the summer in a year, and in the period of the maximum number of sunspots (called the solar maximum) in an 11-year solar cycle. This is exactly the case for the D layer. For the E layer, the ionization does not show significant seasonal variations and does not change much as a function of sunspot numbers. However, this layer obeys diurnal changes as expected. The ionization in the F2 layer is highly and directly related to the sunspot number and it also shows anomalous behaviors with respect to the solar zenith angle. In particular, during the winter, higher ionization is observed in this layer than during the summer which is called the "winter anomaly" [42].

In addition to temporal variations, ionosphere is also subject to latitudinal variations. During the day, with increasing latitude, the solar radiation strikes the atmosphere more obliquely, so less ionization is expected with increasing the latitude. The F2 layer shows an anomaly in this context. Daytime electron density of the F2 layer reaches its maximum not in the equatorial region, but 15-20° north and south of it, which is called "equatorial anomaly" [41]. As mentioned earlier, the F2 layer also remains ionized in the night hemisphere and the minimum electron density occurs in mid latitude regions which is called the "mid latitude trough" [41]. Another solar-terrestrial interaction becomes important in high latitude regions (i.e., the polar zones). Energetic particles of sun winds after reshaping the earth's magnetic field come to the atmosphere from polar zones and participate in the ionization process which is sometimes

18

observable via their aurora effect [2]. Thus, in high latitudes, ionosphere is particularly complicated and will often be significantly different to that observed at mid and lower latitudes.

2.2 HF Channel Model

In this section, we present the path loss, fading, noise and intereference models commonly used for different HF propagation mechanisms.

2.2.1 Path Loss

Path Loss for Ground Wave: Assuming that the surface wave is the dominant component in the ground wave propagation, the typical path loss behavior is given by [1]

$$PL_{surf} \propto \begin{cases} d^2, & \text{at small distances from the transmitter} \\ d^4, & d < 10\lambda^{1/3} \\ \exp(\alpha d), & d > 10\lambda^{1/3} \text{ and for some } \alpha \geq 0 \end{cases} \tag{2.1}$$

where d is the distance from the transmitter in km and λ is the carrier wavelength in meters. The calculation of exact path loss is complicated, because it is affected by various parameters such as the troposphere refractive index, the curvature of the Earth, and the terrain type (e.g., sea/fresh water, wet/dry ground). The GRWAVE software [43], freely available at the ITU website, includes such factors, and provides a convenient tool to predict the path loss of the surface wave propagation.

Path Loss for NVIS and Sky Wave: Ionosphere has temporal and latitudinal variations and is even dependent on the weather conditions and particular time of transmission. Several software packages such as IONCAP family (REC533, VOACAP, ICEPAC) are available for ionospheric propagation predictions [44]. In NVIS or sky wave transmission, HF electromagnetic wave goes up to the ionosphere, gets reflected and returns back to the Earth. This is the first "hop". The second hop takes place as a result of the reflection from the Earth's surface towards the ionosphere and so on. Moreover, although reflection from only one of the ionospheric layers (E

or F layer) is intended, non-zero antenna beam can lead to the contribution of other layers. As a result, there may exist many paths by which an NVIS or a sky wave travels from the transmitter to the receiver (c.f., Figs. 2.1.c and 2.1.d). Fig. 2.2 depicts the sky wave propagation with a single hop.
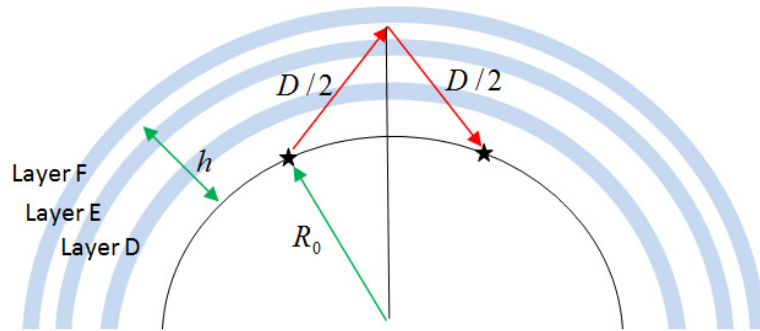
Figure 2.2 A simplified geometry of sky wave propagation with a single hop.

A simplified formula for path loss associated to each path of an NVIS or sky wave link (with up to 7000 km length) is given by [45]

$$PL_{sky} = 32.45 + 20\log f_c + 20\log p' + 2(n-1) + PL_w \quad \text{[dB]} \tag{2.2}$$

where f_c is the carrier frequency in MHz, p' is the virtual slant range in km (which is a function of total path length D and elevation angle), n is the number of hops, and L_w is the loss term that includes ionospheric absorption loss, above the MUF loss (which is zero for the carrier frequencies less than or equal to the MUF, and non-zero otherwise), and auroral signal losses (which is zero for geomagnetic latitude less than 45°, and non-zero otherwise). One simplification is to use D instead of p'. D can be readily approximated from the geometrical relation between the earth radius (R_0) and the equivalent plane-mirror reflection height (h).

2.2.2 Fading

In sky wave propagation, path loss determines the average received signal-to-noise ratio (SNR), while small-scale fading causes fluctuations around the average value. Dynamic variations in the heights of ionospheric layers induce Doppler spread into the refracted signals. Further Doppler shifts are also possible due to the speed of the mobile units in mobile HF applications. Besides the frequency dispersion that occurs independently for each path, another source of fading is the interference between two or more propagation paths. Different paths can have different numbers of hops and can be refracted from different ionospheric layers (the E and F layers). Therefore, large delay spreads on the order of several milliseconds are typically observed. All these effects result in a doubly-selective (i.e., time-selective and frequency-selective) fading channel.

The widely adopted fading channel model for narrowband HF transmission (up to 12 kHz bandwidth) is Watterson model [46]. Let L denote the number of resolvable propagation paths. In the Watterson model, HF NVIS/sky wave channel is represented by a tapped-delay-line (TDL) model where the ith path with delay τ_i has a Rayleigh fading gain $G_i(t)$, $i = 1, \cdots, L$. Each $G_i(t)$ has a bi-Gaussian Doppler power spectral density (PSD), $S_{G_i}(\nu)$, which consists of two Gaussian components with a frequency shift in relative to each other. Mathematically, it is given by

$$S_{G_i}(\nu) = \sum_{m=1}^{2} \frac{1}{A_{i,m}} \sqrt{\frac{2}{\pi f_{d_{i,m}}^2}} \exp\left(\frac{-2\left(\nu - \nu_{i,m}\right)^2}{f_{d_{i,m}}^2} \right) \tag{2.3}$$

where $A_{i,m}$, $\nu_{i,m}$, and $f_{d_{i,m}}$ are, respectively, the attenuations, Doppler shifts, and Doppler spreads for the mth component, m=1,2. Each Gaussian component in $S_{G_i}(\nu)$ corresponds to either O or X component of the ith path. When the O/X components are indistinguishable, $S_{G_i}(\nu)$ becomes a uni-Gaussian function. Based on the ITU recommendation [47], a Watterson model with zero Doppler shift (i.e., $\nu_{i,m} = 0$, $m = 1, 2$) uni-Gaussian PSD is commonly used. Moreover,

ITU also recommends considering equal mean attenuation (i.e., $A = A_{i,m}$, $i, m = 1, 2$) and equal Doppler spreads (i.e., $f_d = f_{d_{i,m}}$, $i, m = 1, 2$) for both paths.

2.2.3 Noise and Interference

Noise in the HF band includes thermal, atmospheric (due to lightening), galactic (due to disturbances originating outside the Earth's atmosphere) and man-made noises. Although the typical HF noise is non-Gaussian, the actual distribution of the noise makes very little difference on the performance of the narrow band HF modems [48], and based on ITU recommendations, noise is commonly modeled as additive white Gaussian noise (AWGN) [47], [49].

Another impairment in the HF band is the ambient interference. Since the energy generated in one location within the HF band can propagate through the ionosphere and might affect receiver antennas far away, the presence of other HF users operating all over the world in the same frequency band can be considered as the potential source of the interference in HF communication. As a result, the amount of HF interference depends on ionosphere conditions, and therefore, on solar activities.

Let Q_k denote the probability that the interference power (in dBm) in a channel located in the kth ITU allocation with the center frequency f_k (in MHz) exceeds a predefined power threshold x. According to the Laycock-Gott empirical model [50], Q_k is given by

$$Q_k = \frac{1}{1 + \exp\left(-\left(\beta x + \alpha_k + (b_0 + b_1 f_k)\log_{10}(B) + b_2 [\log_{10}(B)]^2\right)\right)} \tag{2.4}$$

where B (in kHz) is the bandwidth of the channel, β, b_0, b_1, and b_2 are some fitting parameters, and α_k is a function of f_k, the time of the measurement, the sunspot number, and a bias for the kth ITU band. The time between two interference power transitions can be modeled by an exponential distribution whose mean is in the order of a few minutes. In frequency, a separation of 1 kHz and more results in almost independent interference powers. On the other

22

hand, in the spatial dimension, interference powers are highly correlated. Experimental results demonstrate that there is no significant difference between interference powers measured simultaneously at two sites separated by about 100 km [50].

Chapter 3

Multi-Carrier Cooperative HF Systems

3.1 Introduction

In this chapter, we address the analysis and design of a multicarrier HF cooperative system with amplify-and-forward (AaF) relaying. The underlying waveform is based on the combination of orthogonal frequency division multiplexing (OFDM) and bit-interleaved coded modulation (BICM). We investigate the performance of OFDM-BICM scheme over HF channels through the derivation of pairwise error probability and quantify the maximum achievable diversity. Furthermore, we study optimum power allocation for performance improvements and discuss relay selection criterion for multi-relay scenarios. Exhaustive Monte Carlo simulation results are also conducted to confirm the analytical derivations and present performance comparisons.

The rest of the chapter is organized as follows. In Sections 3.2 and 3.3, we introduce the channel and system models under consideration, respectively. In Section 3.4, we present a diversity order analysis through the derivation of pairwise error probability (PEP) for an orthogonal (i.e., TDMA-based) scheme in which relays scale and transmit their received OFDM signals in different time slots. In Sections 3.5 and 3.6, we discuss power allocation and relay selection rules, respectively. In Section 3.7, we present the simulation results.

3.2 Channel Model

In the light of discussions in Chapter 2, we assume an aggregate HF channel model which consists of both long-term path loss and (if present) short-term fading effects. By normalizing the

path loss in the $A \rightarrow B^{1}$ link with respect to the path loss between the source and destination, the relative geometrical gain [51] in the $A \rightarrow B$ link is defined by $G_{AB} = PL(A,B)/PL(S,D)$ where $PL(A,B)$ denotes the path loss between the nodes A and B, and $PL(S,D)$ is the path loss between the source and destination.

The short-term variations of the underlying sky wave/NVIS channel in the $A \rightarrow B$ link are modeled by a tapped-delay-line (TDL) with L_{AB} resolvable propagation paths based on the Watterson model (see Section 2.2 of Chapter 2). For mathematical tractability in our analytical derivations, we assume that sky wave/NVIS channels remain constant within the duration of one block transmission (i.e., $f_{d}T \ll 1$ where T is the block duration). This assumption is reasonable since typical Doppler spreads in the HF band are less than 2 Hz [1], and therefore, HF channel can be classified as a slowly time-varying channel for most practical purposes. Later, in our simulations, we will further study the impact of frequency dispersion on the performance by considering time-variation of the NVIS/sky wave links based on the Doppler PSD given in (2.3).

The channel impulse response (CIR) of the $A \rightarrow B$ link is modeled by $G_{AB}h_{AB}(t)$ where $h_{AB}(t) = \sum_{n=0}^{L_{AB}-1} \mathbf{h}_{AB}(n)\delta(t - \boldsymbol{\tau}_{AB}(n))$, $\boldsymbol{\tau}_{AB}$ is a vector including the delays associated with different paths, and the entries of random vector $\mathbf{h}_{AB}$ are independent identically distributed (i.i.d.) zero-mean complex Gaussian random variables with variances $1/L_{AB}$. In the frequency domain, the corresponding frequency response of the $A \rightarrow B$ link in the kth frequency bin $(k = 0, \cdots, K-1)$, is given by $G_{AB}\tilde{\mathbf{h}}_{AB}(k)$ where $\tilde{\mathbf{h}}_{AB}(k) = \mathbf{v}_{AB,k}^{*}\mathbf{h}_{AB}$, $\mathbf{v}_{AB,k} = \exp(j2\pi k\boldsymbol{\tau}_{AB}/KT_{S})$, K is the number of OFDM subcarriers, and T_{S} is the sampling time of the system. If surface wave is used in the $A \rightarrow B$ link, this can be considered as a special case of frequency-selective channel model considered here. In this case, CIR contains only one *deterministic* tap with the gain of G_{AB} (i.e., $\mathbf{h}_{AB} = 1$).

---

[1] A→B signifies the link between nodes A and B.

3.3 System Model

We consider a cooperative HF system where the source node S transmits information to the destination node D with the assistance of M relay nodes, $R_1, \cdots, R_M$. We assume the orthogonal cooperation protocol of [15]: During the first phase (i.e., the broadcasting phase), the source broadcasts an OFDM symbol to the relay terminals. In the second phase (i.e., the relaying phase), the source stops transmission, and the relay nodes take turns to forward a scaled version of the signals received from the source. We assume that relays are connected to the destination through either NVIS or surface wave links (See Figs. 3.1 and 3.2).

We assume OFDM transmission with K subcarriers and a linear modulation scheme such as PSK or QAM. The constellation set χ is assumed to have unit average energy. Let $\mathbf{c}$ denote a codeword with a length of $K \log_2 |\chi|$ bits produced from a convolutional code C with free distance d_f. The codeword $\mathbf{c}$ is then passed through the interleaver Π and linearly modulated

—————— Sky wave (Source-to-Relays/Destination)

············ Surface wave (Relays-to-Destination)
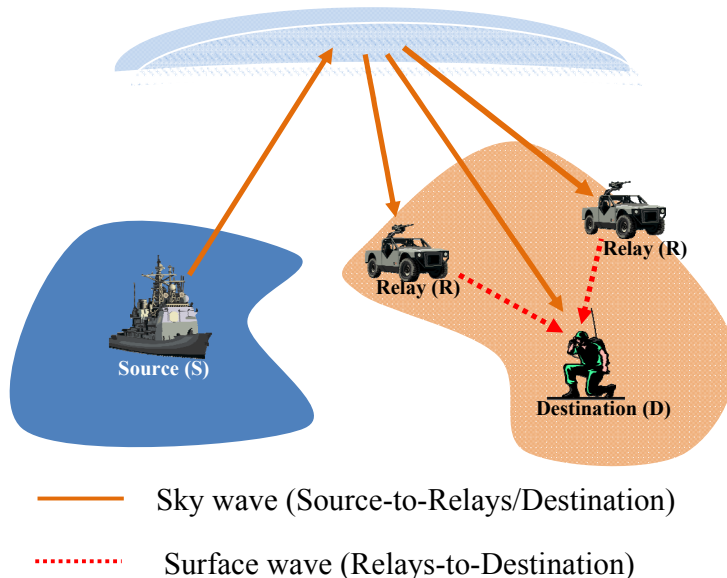
Figure 3.1 Illustration of cooperative HF communications using surface wave in relay-to-destination links.
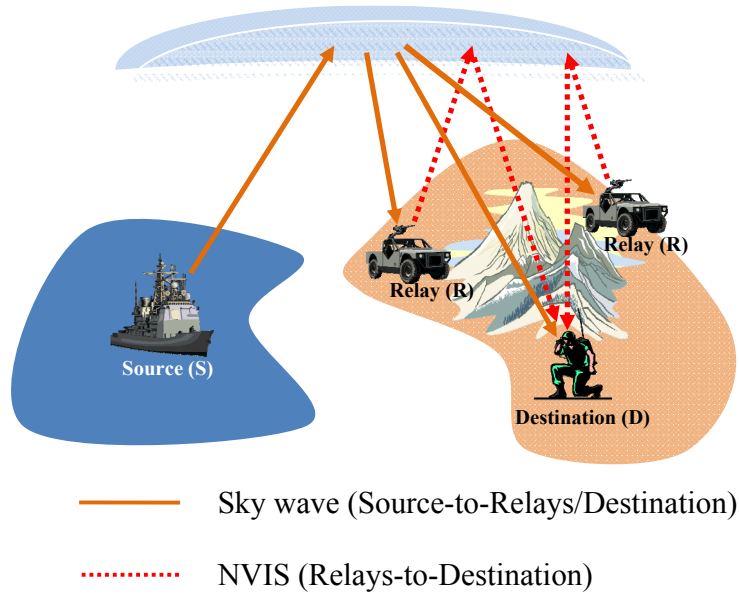
Figure 3.2 Illustration of cooperative HF communications using NVIS in relay-to-destination links.

with Gray mapping. The resulting vector of constellation points with size $K \times 1$ is denoted by $\tilde{\mathbf{x}}$.

For a convolutional code, the minimum-length interval, including all distinct bits between any two minimum distance codewords, spans a specific number of bits which is denoted by $d_0 (\geq d_f)$. As discussed in [24], the key point to exploit the full multipath diversity under BICM-OFDM transmission is to design the interleaver such that each d_0 consecutive bits of $\mathbf{c}$ is carried by different subcarriers. In particular, define the interleaver permutation rule as $\Pi : k_i' \rightarrow (k_i, m)$ meaning that the k_i'th bit of $\mathbf{c}$, i.e., $\mathbf{c}(k_i')$, is mapped to the mth bit of the Gray label of a constellation point to be carried by the k_ith subcarrier, i.e., $\tilde{\mathbf{x}}(k_i)$. Accordingly, we can say that if $0 < | k_i' - k_j' | \leq d_0$, then $k_i \neq k_j$.

The signal $\tilde{\mathbf{x}}$ is applied to the inverse DFT (IDFT). The output vector is $\mathbf{x} = \mathbf{Q}^* \tilde{\mathbf{x}}$ where $\mathbf{Q}$ is the DFT matrix. Finally, a cyclic prefix (CP) longer than the length of CIRs is appended to $\mathbf{x}$ and the resulting OFDM signal is transmitted through the sky wave link which is received by M relay terminals and the destination.

After removing the CP, the received data blocks at the destination and the nth relay node are, respectively, given by

$$\mathbf{r}_{\mathrm{SD}} = \sqrt{P_0}\,\mathbf{H}_{\mathrm{SD}}\mathbf{x} + \mathbf{z}_{\mathrm{SD}} \tag{3.1}$$

$$\mathbf{r}_{\mathrm{SR}_n} = \sqrt{P_0 G_{\mathrm{SR}_n}}\,\mathbf{H}_{\mathrm{SR}_n}\mathbf{x} + \mathbf{z}_{\mathrm{SR}_n} \tag{3.2}$$

where $\mathbf{H}_{\mathrm{SD}}$ and $\mathbf{H}_{\mathrm{SR}_n}$ are circulant channel matrices with entries of $\mathbf{H}_{\mathrm{SD}}(i,j) = \mathbf{h}_{\mathrm{SD}}(<i-j>_K)$, and $\mathbf{H}_{\mathrm{SR}_n}(i,j) = \mathbf{h}_{\mathrm{SR}_n}(<i-j>_K)$. In (3.1) and (3.2), $\mathbf{z}_{\mathrm{SD}}$ and $\mathbf{z}_{\mathrm{SR}_n}$ are the Gaussian noise vectors with zero mean and covariance matrix of $N_0\mathbf{I}_K$, $P_0 = K_0 P_T$ $(0 < K_0 \leq 1)$ is the transmit power per symbol (or subcarrier) at the source, and P_T is the overall average power budget per subcarrier.

To ensure that the power budget is not violated, relay nodes scale their received signals. In the average-power-scaling (APS) method [52], the power scaling factor for the nth relay is given by $\alpha_{\mathrm{R}_n} = 1/(P_0 G_{\mathrm{SR}_n} + N_0)$. After scaling operation, relays insert new CPs and forward their resulting signals to the destination one-by-one in different time slots. After CP removal, the received signals at the destination are given by

$$\mathbf{r}_{\mathrm{R}_n\mathrm{D}} = \sqrt{\alpha_{\mathrm{R}_n} P_n G_{\mathrm{R}_n\mathrm{D}} P_0 G_{\mathrm{SR}_n}}\,\mathbf{H}_{\mathrm{R}_n\mathrm{D}}\mathbf{H}_{\mathrm{SR}_n}\mathbf{x} + \sqrt{\alpha_{\mathrm{R}_n} P_n G_{\mathrm{R}_n\mathrm{D}}}\,\mathbf{H}_{\mathrm{R}_n\mathrm{D}}\mathbf{z}_{\mathrm{SR}_n} + \mathbf{z}_{\mathrm{R}_n\mathrm{D}},\ n=1,\cdots,M \tag{3.3}$$

where $P_n = K_n P_T$ $(0 \leq K_n \leq 1)$ is the transmit power per subcarrier in the nth relay, $\mathbf{H}_{\mathrm{R}_n\mathrm{D}}$ is the circulant channel matrix with entries of $\mathbf{H}_{\mathrm{R}_n\mathrm{D}}(i,j) = \mathbf{h}_{\mathrm{R}_n\mathrm{D}}(<i-j>_K)$, and $\mathbf{z}_{\mathrm{R}_n\mathrm{D}}$ is the Gaussian noise vector with zero mean and covariance matrix of $N_0\mathbf{I}_K$.

Taking DFT of the signals received over the broadcasting phase and the relaying phase yields

$$\mathbf{y}_{\mathrm{SD}} = \mathbf{Q}\mathbf{r}_{\mathrm{SD}} = \sqrt{P_0}\,\mathbf{D}_{\mathrm{SD}}\tilde{\mathbf{x}} + \mathbf{v}_{\mathrm{SD}} \tag{3.4}$$

$$\mathbf{y}_{\mathrm{R}_n\mathrm{D}} = \mathbf{Q}\mathbf{r}_{\mathrm{R}_n\mathrm{D}} = \sqrt{\beta_n}\,\mathbf{D}_{\mathrm{R}_n\mathrm{D}}\mathbf{D}_{\mathrm{SR}_n}\tilde{\mathbf{x}} + \mathbf{v}_{\mathrm{R}_n\mathrm{D}},\ n=1,\cdots,M \tag{3.5}$$

where $\mathbf{D}_{\mathrm{SD}} = \mathrm{diag}\{\tilde{\mathbf{h}}_{\mathrm{SD}}\}$, $\mathbf{D}_{\mathrm{SR}_n} = \mathrm{diag}\{\tilde{\mathbf{h}}_{\mathrm{SR}_n}\}$, $\mathbf{D}_{\mathrm{R}_n\mathrm{D}} = \mathrm{diag}\{\tilde{\mathbf{h}}_{\mathrm{R}_n\mathrm{D}}\}$, $\beta_n = \alpha_{\mathrm{R}_n} P_n G_{\mathrm{R}_n\mathrm{D}} P_0 G_{\mathrm{SR}_n}$, $\mathbf{v}_{\mathrm{SD}}$ is the Gaussian noise vector with zero mean and the covariance matrix of $N_0\mathbf{I}_K$, and $\mathbf{v}_{\mathrm{R}_n\mathrm{D}}$ is

conditionally Gaussian (conditioned on $\mathbf{h}_{\mathrm{R}_n\mathrm{D}}$) with zero mean and the covariance matrix of

$N_0(\alpha_{\mathrm{R}_n}P_nG_{\mathrm{R}_n\mathrm{D}}\mathbf{D}_{\mathrm{R}_n\mathrm{D}}\mathbf{D}_{\mathrm{R}_n\mathrm{D}}^* + \mathbf{I}_K)$.

The maximum likelihood (ML) metric for each bit is calculated by taking into account all OFDM symbols. Under the assumption of known CIRs, the ML bit-metric for $\mathbf{c}(k')$, denoted by $\mu_{\mathbf{c}(k')}$, is given by

$$\mu_{\mathbf{c}(k')} = \min_{x' \in \chi^m_{\mathbf{c}(k')}} \left\{ \Lambda(x',k) \right\} \tag{3.6}$$

where $\Lambda(x',k)$ is expressed as

$$\Lambda(x',k) = \left\| \mathbf{y}_{\mathrm{SD}}(k) - \sqrt{P_0}\tilde{\mathbf{h}}_{\mathrm{SD}}(k)x' \right\|^2 + \sum_{n=1}^{M} \frac{\left\| \mathbf{y}_{\mathrm{R}_n\mathrm{D}}(k) - \sqrt{\beta_n}\tilde{\mathbf{h}}_{\mathrm{R}_n\mathrm{D}}(k)\tilde{\mathbf{h}}_{\mathrm{SR}_n}(k)x' \right\|^2}{\sigma^2_{n,k}} \tag{3.7}$$

with $\sigma^2_{n,k} = \alpha_{\mathrm{R}_n}P_nG_{\mathrm{R}_n\mathrm{D}}\left\| \tilde{\mathbf{h}}_{\mathrm{R}_n\mathrm{D}}(k) \right\|^2 + 1$. In (3.6), the minimization is carried over $\chi^m_{\mathbf{c}(k')}$ which is a set of constellation points that the mth bit of their corresponding (Gray) bit-label is equal to $\mathbf{c}(k')$. Finally, the ML decoder makes decisions based on

$$\hat{\mathbf{c}} = \arg\min_{\mathbf{c} \in \mathrm{C}} \sum_{k'} \mu_{\mathbf{c}(k')} . \tag{3.8}$$

3.4 Diversity Gain Analysis

In this section, we derive a PEP expression for the system under consideration and present the achievable diversity order. Assume that the codeword $\mathbf{c}$ is transmitted and codeword $\hat{\mathbf{c}}$ is erroneously detected. Defining $\mathbf{h}_{\mathrm{SR}} = [\mathbf{h}_{\mathrm{SR}_1}^{\mathrm{T}}, \cdots, \mathbf{h}_{\mathrm{SR}_M}^{\mathrm{T}}]^{\mathrm{T}}$ and $\mathbf{h}_{\mathrm{RD}} = [\mathbf{h}_{\mathrm{R}_1\mathrm{D}}^{\mathrm{T}}, \cdots, \mathbf{h}_{\mathrm{R}_M\mathrm{D}}^{\mathrm{T}}]^{\mathrm{T}}$, the conditional PEP of this codeword pair is given by

$$P\left(\mathbf{c} \to \hat{\mathbf{c}} \,|\, \mathbf{h}_{\mathrm{SD}}, \mathbf{h}_{\mathrm{SR}}, \mathbf{h}_{\mathrm{RD}}\right) = P\left(\sum_{k' \in \Omega'} \mu_{\mathbf{c}(k')} \geq \sum_{k' \in \Omega'} \mu_{\hat{\mathbf{c}}(k')} \,|\, \mathbf{h}_{\mathrm{SD}}, \mathbf{h}_{\mathrm{SR}}, \mathbf{h}_{\mathrm{RD}} \right) \tag{3.9}$$

where $\mathbf{c}$ and $\hat{\mathbf{c}}$ differ only in d_f bits and in the locations specified by the index set Ω' (i.e. $\mathbf{c}(i) \neq \hat{\mathbf{c}}(i)$ iff $i \in \Omega'$, $|\Omega'| = d_f$). Moreover, let Ω denote the index set of subcarriers which are

selected by the interleaver to carry these distinct bits. Since the interleaver is supposed to assign each $d_0 (\geq d_f)$ consecutive coded bits to different subcarriers, the cardinality of Ω is also equal to d_f. Based on (3.6), we can rewrite (3.9) as

$$P\left(\mathbf{c} \rightarrow \hat{\mathbf{c}} \mid \mathbf{h}_{\mathrm{SD}}, \mathbf{h}_{\mathrm{SR}}, \mathbf{h}_{\mathrm{RD}}\right) = P\left(\sum_{k \in \Omega} \Lambda(x_k, k) \geq \sum_{k \in \Omega} \Lambda(\hat{x}_k, k)\right) \tag{3.10}$$

where x_k and $\hat{x}_k$ are the constellation points, respectively, given by

$$x_k = \arg \min_{x' \in \mathcal{X}_{\mathbf{c}(k')}^m} \left\{\Lambda(x', k)\right\},$$

$$\hat{x}_k = \arg \min_{x' \in \mathcal{X}_{\hat{\mathbf{c}}(k')}^m} \left\{\Lambda(x', k)\right\}.$$

Since the transmitted signal $\tilde{\mathbf{x}}(k) \in \mathcal{X}_{\mathbf{c}(k')}^m$, we have $\sum_{k \in \Omega} \Lambda\left(\tilde{\mathbf{x}}(k), k\right) \geq \sum_{k \in \Omega} \Lambda\left(x_k, k\right)$, and therefore, we can write

$$P\left(\mathbf{c} \rightarrow \hat{\mathbf{c}} \mid \mathbf{h}_{\mathrm{SD}}, \mathbf{h}_{\mathrm{SR}}, \mathbf{h}_{\mathrm{RD}}\right) \leq P\left(\sum_{k \in \Omega} \Lambda\left(\tilde{\mathbf{x}}(k), k\right) \geq \sum_{k \in \Omega} \Lambda(\hat{x}_k, k)\right)$$

$$= Q\left(\sqrt{\sum_{k \in \Omega}\left(\frac{\left\|\sqrt{P_0}\tilde{\mathbf{h}}_{\mathrm{SD}}(k)\left(\tilde{\mathbf{x}}(k) - \hat{x}_k\right)\right\|^2}{2} + \sum_{n=1}^{M} \frac{\left\|\sqrt{\beta_n}\tilde{\mathbf{h}}_{\mathrm{R}_n\mathrm{D}}(k)\tilde{\mathbf{h}}_{\mathrm{SR}_n}(k)\left(\tilde{\mathbf{x}}(k) - \hat{x}_k\right)\right\|^2}{2\sigma_{n,k}^2}\right)}\right) \tag{3.11}$$

Using the Chernoff bound, an upper bound for the average PEP is given by

$$P\left(\mathbf{c} \rightarrow \hat{\mathbf{c}}\right) \leq \frac{1}{2} \underbrace{\mathrm{E}_{\mathbf{h}_{\mathrm{SD}}}\left\{\exp\left(-\frac{d_{\min}^2 P_0}{4} \sum_{k \in \Omega}\left\|\tilde{\mathbf{h}}_{\mathrm{SD}}(k)\right\|^2\right)\right\}}_{PEP_{\mathrm{SD}}}$$

$$\times \underbrace{\mathrm{E}_{\mathbf{h}_{\mathrm{SR}}, \mathbf{h}_{\mathrm{RD}}}\left\{\prod_{n=1}^{M} \exp\left(-\beta_n d_{\min}^2 \sum_{k \in \Omega} \frac{\left\|\tilde{\mathbf{h}}_{\mathrm{R}_n\mathrm{D}}(k)\tilde{\mathbf{h}}_{\mathrm{SR}_n}(k)\right\|^2}{4\sigma_{n,k}^2}\right)\right\}}_{PEP_{\mathrm{SRD}}} \tag{3.12}$$

30

where $d_{\min}$ represents the minimum distance of the constellation set $\mathcal{X}$. Let PEP_{SD} and PEP_{SRD} denote the first and the second expectation terms, respectively. Noting that $\tilde{\mathbf{h}}_{SD}(k) = \mathbf{v}_{SD,k}^{*}\mathbf{h}_{SD}$ and by performing expectation with respect to the complex Gaussian random vector $\mathbf{h}_{SD}$, we obtain

$$PEP_{SD} = \prod_{i=1}^{r_0}\left(1 + \frac{d_{\min}^2 P_0}{4}\lambda_i\right)^{-1} \tag{3.13}$$

where r_0 and λ_i, $i = 1, \cdots, r_0$ are, respectively, the rank and eigenvalues of the matrix $\mathbf{C}_{SD}\sum_{k\in\Omega}\mathbf{v}_{SD,k}\mathbf{v}_{SD,k}^{*}$ with $\mathbf{C}_{SD} = (1/L_{SD})\mathbf{I}_{L_{SD}}$.

Now we focus on the second expectation term of (3.12). Noting that $\tilde{\mathbf{h}}_{SR_n}(k) = \mathbf{v}_{SR_n,k}^{*}\mathbf{h}_{SR_n}$, by taking expectation with respect to the complex Gaussian random vector $\mathbf{h}_{SR}$, we have

$$PEP_{SRD} = E_{\mathbf{h}_{RD}}\left\{\prod_{n=1}^{M}\det^{-1}\left(\mathbf{I}_{L_{SR_n}} + \beta_n d_{\min}^2 \mathbf{C}_{SR_n}\sum_{k\in\Omega}\frac{\left\|\tilde{\mathbf{h}}_{R_nD}(k)\right\|^2 \mathbf{v}_{SR_n,k}\mathbf{v}_{SR_n,k}^{*}}{4\sigma_{n,k}^2}\right)\right\} \tag{3.14}$$

where $\mathbf{C}_{SR_n} = (1/L_{SR_n})\mathbf{I}_{L_{SR_n}}$. Following the steps in Appendix A, we obtain

$$PEP_{SRD} \leq \prod_{n=1}^{M}\sum_{m=0}^{r_n}\xi_{n,m}\frac{L_{R_nD}^{L_{R_nD}}}{(L_{R_nD}-1)!}\underbrace{\int_0^{\infty}\frac{x_n^{L_{R_nD}-1+m}\exp(-L_{R_nD}x_n)\ dx_n}{(\beta_n' x_n + 4)^{r_n}}}_{\Upsilon_{n,m}} \tag{3.15}$$

where $r_n = \min(L_{SR_n}, d_f)$, $\xi_{n,m}$ is the coefficient of the term x_n^m in the binomial expansion of $(4 + 4\alpha_{R_n}P_n G_{R_nD}L_{R_nD}x_n)^{r_n}$. In (3.15), $\beta_n' = \beta_n d_{\min}^2 \mu_n / L_{SR_n}$, and μ_n is the minimum of the non-zero eigenvalues of the sub-matrices located in the last L_{SR_n} rows and the last L_{SR_n} columns of all possible matrices in the form of $\mathbf{U}_n^{*}\mathbf{J}_n\mathbf{U}_n$, where $\mathbf{J}_n = \sum_{k\in\Omega}\tilde{\mathbf{V}}_{n,k}\mathbf{v}_{SR_n,k}(\tilde{\mathbf{V}}_{n,k}\mathbf{v}_{SR_n,k})^{*}$, $\tilde{\mathbf{V}}_{n,k} = \mathbf{I}_{L_{SR_n}}\otimes\mathbf{v}_{R_nD,k}$, and $\mathbf{U}_n$ can be any orthonormal matrix of size $L_{SR_n}L_{R_nD}\times L_{SR_n}L_{R_nD}$. Using (3.13) and (3.15), we obtain the unconditional PEP as

$$P(\mathbf{c}\to\hat{\mathbf{c}}) \leq \frac{1}{2}\left(\prod_{i=1}^{r_0}\left(1 + \frac{d_{\min}^2 P_0}{4}\lambda_i\right)^{-1}\right)\left(\prod_{n=1}^{M}\sum_{m=0}^{r_n}\xi_{n,m}\frac{L_{R_nD}^{L_{R_nD}}}{(L_{R_nD}-1)!}\int_0^{\infty}\frac{x_n^{L_{R_nD}-1+m}\exp(-L_{R_nD}x_n)\ dx_n}{(\beta_n' x_n + 4)^{r_n}}\right) \tag{3.16}$$

31

Using similar arguments as in [24], it can be shown that the rank of the matrix $\mathbf{C}_{\mathrm{SD}} \sum_{k\in\Omega} \mathbf{v}_{\mathrm{SD},k} \mathbf{v}_{\mathrm{SD},k}^*$ in (3.13) is equal to $\min(d_f, L_{\mathrm{SD}})$. Therefore, a diversity order of $\min(d_f, L_{\mathrm{SD}})$ is provided by the direct link.

For the diversity orders contributed by the cascaded relay links, i.e. PEP_{SRD} given in (3.15), we need to consider distinct values of r_n and $L_{\mathrm{R}_n\mathrm{D}} + m$. Specifically, we can identify the following three cases for $\Upsilon_{n,m}$:

Case1: For $r_n < L_{\mathrm{R}_n\mathrm{D}} + m$,

$$\Upsilon_{n,m} \le \left(\beta_n'\right)^{-r_n} \int_0^\infty x_n^{L_{\mathrm{R}_n\mathrm{D}}-1+m-r_n} \exp(-L_{\mathrm{R}_n\mathrm{D}} x_n) \ dx_n \ . \tag{3.17}$$

Case 2: For $r_n > L_{\mathrm{R}_n\mathrm{D}} - 1 + m$,

$$\Upsilon_{n,m} \le \left(\beta_n'\right)^{-L_{\mathrm{R}_n\mathrm{D}}-m} \int_0^\infty \frac{x_n^{L_{\mathrm{R}_n\mathrm{D}}-1+m}}{\left(x_n+4\right)^{r_n}} dx_n \ . \tag{3.18}$$

Case 3: For $r_n = L_{\mathrm{R}_n\mathrm{D}} + m$,

$$\Upsilon_{n,m} \le \left(\beta_n'\right)^{-r_n} \int_0^\infty x_n^{-1} \exp(-L_{\mathrm{R}_n\mathrm{D}} x_n) dx_n \approx \left(\beta_n'\right)^{-r_n} \int_{\frac{1}{\beta_n'}}^\infty x_n^{-1} \exp(-L_{\mathrm{R}_n\mathrm{D}} x_n) dx_n = \left(\beta_n'\right)^{-r_n} E_1\left(\frac{L_{\mathrm{R}_n\mathrm{D}}}{\beta_n'}\right) \tag{3.19}$$

where $E_1(\cdot)$ is the exponential integral function defined in [53]. Since $E_1(z) \to \log(1/z)$, as $z \to 0$, for large enough β_n', we have $E_1(L_{\mathrm{R}_n\mathrm{D}}/\beta_n') \to \log(\beta_n'/L_{\mathrm{R}_n\mathrm{D}})$. Therefore, from (3.19), we can write

$$\Upsilon_{n,m} \le \left(\beta_n'\right)^{-r_n+\frac{\log\log\beta_n'}{\log\beta_n'}} \left(1-\log_{\beta_n'} L_{\mathrm{R}_n\mathrm{D}}\right) \tag{3.20}$$

On the other hand, as $P_T \to \infty$, $\beta_n' \to (K_n G_{\mathrm{R}_n\mathrm{D}} d_{\min}^2 \mu_n / L_{\mathrm{SR}_n}) P_T$, and therefore, based on (3.17)-(3.20), we have $\Upsilon_{n,m} \le \alpha_{n,m} (P_T)^{-\min(d_f, L_{\mathrm{SR}_n}, L_{\mathrm{R}_n\mathrm{D}}+m)}$ where $\alpha_{n,m}$ is a constant with respect to P_T. This indicates a diversity order of $\sum_{n=1}^M \min(d_f, L_{\mathrm{SR}_n}, L_{\mathrm{R}_n\mathrm{D}})$ for the relaying link. Considering further the diversity order contributed by the direct link, a total diversity of

$$\min(d_f, L_{\mathrm{SD}}) + \sum_{n=1}^M \min(d_f, L_{\mathrm{SR}_n}, L_{\mathrm{R}_n\mathrm{D}}) \tag{3.21}$$

is available.

Under the assumption of surface wave relaying links (See Fig 3.1), we have $L_{R_nD} = 1$, $\mathbf{h}_{R_nD} = 1$, $n = 1, \cdots, M$, and hence, based on (3.13) and (3.14), the total diversity order becomes $\min(d_f, L_{SD}) + \sum_{n=1}^{M} \min(d_f, L_{SR_n})$.

3.5 PEP-based Power Allocation

As illustrated in Figs. 3.1 and 3.2, relays are connected to the destination through either NVIS or surface wave links. Their path losses are much smaller than those of the sky wave link which connects the source and the destination. Therefore, under a fixed overall system power budget, equal power allocation (EPA) among the source and relays does not realize the full potential of HF cooperative communication. In this section, we investigate the optimum choice of power coefficients, i.e. $K_0, K_1, \cdots, K_M$, as to minimize PEP. The minimization of the derived PEP for coded HF system is intractable, if not impossible (see Appendix A for details). Therefore, we re-formulate this problem for an uncoded OFDM system. In an uncoded OFDM cooperative AaF system, the resulting SNR at the kth subcarrier is given by

$$\gamma_D(k) = \gamma_{SD}(k) + \sum_{n=1}^{M} \underbrace{\frac{\gamma_{SR_n}(k)\gamma_{R_nD}(k)}{\gamma_{R_nD}(k) + \overline{\gamma}_{SR_n} + 1}}_{\gamma_{SR_nD}(k)} \tag{3.22}$$

where $\gamma_{SD}(k) = \overline{\gamma}_{SD} \left\| \tilde{\mathbf{h}}_{SD}(k) \right\|^2$, $\gamma_{SR_n}(k) = \overline{\gamma}_{SR_n} \left\| \tilde{\mathbf{h}}_{SR_n}(k) \right\|^2$, and $\gamma_{R_nD}(k) = \overline{\gamma}_{R_nD} \left\| \tilde{\mathbf{h}}_{R_nD}(k) \right\|^2$ are instantaneous SNRs respectively in the $S \to D$, $S \to R_n$, and $R_n \to D$ links. Here, the corresponding average SNRs are given by $\overline{\gamma}_{SD} = K_0 P_T / N_0$, $\overline{\gamma}_{SR_n} = G_{SR_n} K_0 P_T / N_0$, and $\overline{\gamma}_{R_nD} = G_{R_nD} K_n P_T / N_0$. In the sequel, we drop the index k for the convenience of the presentation. Note that $\tilde{\mathbf{h}}_{AB}$ is a normalized complex Gaussian random variable, and therefore, the moment generating function (MGF) of γ_D can be easily found as

$$\Phi_{\gamma_D}^{NVIS}(s) = \Phi_{\gamma_{SD}}(s) \prod_{n=1}^{M} \Phi_{\gamma_{SR_nD}}^{NVIS}(s)$$

33

$$= \frac{1}{\overline{\gamma}_{\mathrm{SD}}s+1} \prod_{n=1}^{M} \left(\frac{1}{\overline{\gamma}_{\mathrm{SR}_n}s+1} + \frac{\left(\overline{\gamma}_{\mathrm{SR}_n}+1\right)\overline{\gamma}_{\mathrm{SR}_n}se^{\frac{\overline{\gamma}_{\mathrm{SR}_n}+1}{\overline{\gamma}_{\mathrm{R}_n\mathrm{D}}\left(\overline{\gamma}_{\mathrm{SR}_n}s+1\right)}}}{\overline{\gamma}_{\mathrm{R}_n\mathrm{D}}\left(\overline{\gamma}_{\mathrm{SR}_n}s+1\right)^2} E_1 \left(\frac{\overline{\gamma}_{\mathrm{SR}_n}+1}{\overline{\gamma}_{\mathrm{R}_n\mathrm{D}}\left(\overline{\gamma}_{\mathrm{SR}_n}s+1\right)} \right) \right). \tag{3.23}$$

The Chernoff bound on the PEP between x_0 and $\hat{x}_0$ is given by

$$\Pr(x_0 \rightarrow \hat{x}_0) \le \mathrm{E}\left[\exp\left(-\frac{\gamma_{\mathrm{D}}d_{\min}^2}{4} \right) \right] = \Phi_{\gamma_{\mathrm{D}}}^{NVIS}\left(\frac{d_{\min}^2}{4} \right) \tag{3.24}$$

where $\left\| x_0 - \hat{x}_0 \right\|^2 = d_{\min}^2$. At high SNR region, $\Phi_{\gamma_{\mathrm{D}}}^{NVIS}(d_{\min}^2/4)$ can be approximated by the following *posynomial[1]* function with respect to $K_0, K_1, \cdots, K_M$ (see Appendix C)

$$\Phi_{\gamma_{\mathrm{D}}}^{NVIS}\left(\frac{d_{\min}^2}{4} \right) \simeq \frac{4}{K_0 \overline{\gamma} d_{\min}^2} \prod_{n=1}^{M} \left(\frac{4}{G_{\mathrm{SR}_n} K_0 \overline{\gamma} d_{\min}^2} + \frac{4\ln\left(\overline{\gamma}\right)}{G_{\mathrm{R}_n\mathrm{D}} K_n \overline{\gamma} d_{\min}^2} \right) \tag{3.25}$$

where $\overline{\gamma} = P_T/N_0$. It is worth noting that the approximation in (3.25) gets closer to the actual value as $G_{\mathrm{R}_n\mathrm{D}}$ increases. In the HF cooperative system under our consideration, since the direct link is a long distance sky wave and the relay-to-destination links are NVIS, we have $G_{\mathrm{R}_n\mathrm{D}} \gg 1$ leading to a very accurate approximation.

Our optimum power allocation (OPA) problem can be now stated as

$$\min \Phi_{\gamma_{\mathrm{D}}}^{NVIS}\left(\frac{d_{\min}^2}{4} \right)$$

$$\text{s.t. } K_0 + \sum_{n=1}^{M} K_n = 1,\ K_0, K_1, \cdots, K_M \ge 0 \tag{3.26}$$

As SNR increases, the OPA problem in (3.26) approaches to a geometric programming (GP) [54]. GP problems define an important class of non-convex optimization problems that can be easily transformed into convex programming of the so-called log-sum-exponential form, and

---

[1] A function in the form of $f(x_1, \cdots, x_n) = \sum_{k=1}^{K} c_k x_1^{a_{1,k}}, \cdots, x_n^{a_{n,k}}$ is called posynomial where $c_k > 0$ and the exponents, $a_{1,k}, \cdots, a_{n,k}$, can be any real numbers.

thus, their global minima can be efficiently found by using numerical methods such as the interior point. In particular, we use "fmincon" command available in MATLAB optimization toolbox which is designed to find the minimum of a given constrained nonlinear multivariable function. It should be also emphasized that these OPA problems do not need to be solved in real time for practical systems, because optimization does not depend on the instantaneous channel information or the input data. This means that the OPA values can be calculated a priori for given values of operating SNR and propagation parameters, and then, stored to be used as a lookup table in practical implementation.

For the case of surface wave relaying links ($L_{R_nD} = 1$, $\mathbf{h}_{R_nD} = 1$, $n = 1, \cdots, M$), (3.22) reduces to

$$\gamma_D = \gamma_{SD} + \sum_{n=1}^{M} \frac{\overline{\gamma}_{R_nD}}{\overline{\gamma}_{R_nD} + \overline{\gamma}_{SR_n} + 1} \gamma_{SR_n} .$$ (3.27)

The corresponding MGF is given by

$$\Phi_{\gamma_D}^{Surf}(s) = \frac{1}{\overline{\gamma}_{SD} s + 1} \prod_{n=1}^{M} \frac{1}{\dfrac{\overline{\gamma}_{R_nD} \overline{\gamma}_{SR_n}}{\overline{\gamma}_{R_nD} + \overline{\gamma}_{SR_n} + 1} s + 1} .$$ (3.28)

The power allocation for this case has the similar form as in (3.26) and, for high SNR values, can be solved by efficient convex optimization engines.

3.6 Opportunistic Relaying

Although orthogonal cooperation provides full spatial diversity, it suffers from low spectral efficiency. Relay selection, also known as opportunistic relaying, provides an alternative to orthogonal relaying [18]. In relay selection over frequency-flat fading channels, only the relay with the strongest end-to-end path is allowed to transmit. Therefore, instead of *M* time slots, relaying phase takes place in only one time slot.

35

Conventional relay selection can be extended to OFDM signaling via two principal approaches [55]. In the first approach, the best relay is selected for each subcarrier. Then, each of the selected relays amplifies and forwards its assigned subcarriers and sets the other subcarriers to zero. Therefore, in this *per-subcarrier (PS) relay selection* scheme, different subcarriers of the OFDM symbol, transmitted towards the destination in the relaying phase, can come from different relays. On the other hand, in *all-subcarrier (AS) relay selection* scheme, a single relay is selected for all subcarriers and that is the only relay that participates in the relaying phase. PS and AS schemes have the same bandwidth efficiency, since relaying phase for both of them lasts only one time slot. Based on the PEP expression in (3.12), relay selection rules for PS and AS relay selection schemes can be respectively given as

$$n_k^{\mathrm{PS}} = \arg \max_{n=1,\cdots,M} \left\{ \frac{\beta_n \left\| \tilde{\mathbf{h}}_{\mathrm{R}_n\mathrm{D}}(k)\tilde{\mathbf{h}}_{\mathrm{SR}_n}(k) \right\|^2}{\sigma_{n,k}^2} \right\} , \quad k = 1,\cdots,K \tag{3.29}$$

$$n^{\mathrm{AS}} = \arg \max_{n=1,\cdots,M} \left\{ \sum_{k=1}^{K} \frac{\beta_n \left\| \tilde{\mathbf{h}}_{\mathrm{R}_n\mathrm{D}}(k)\tilde{\mathbf{h}}_{\mathrm{SR}_n}(k) \right\|^2}{\sigma_{n,k}^2} \right\} . \tag{3.30}$$

3.7 Simulation Results

In this section, we present the error rate performance of HF cooperative system under consideration through Monte Carlo simulations. We consider an HF communication link between a task force (including a destination terminal and a number of relay terminals) and their headquarters separated apart by 700 km (See Figs. 3.1 and 3.2). We assume QPSK modulation, a bandwidth of 9 kHz, and 192 subcarriers with frequency spacing $\Delta f = 46.875$ Hz [3]. A convolutional code with rate $R_{\mathrm{C}} = 1/2$ and free distance $d_f = 7$ is employed. In sky wave/NVIS channels, we assume $L_{\mathrm{SD}} = L_{\mathrm{SR}_n} = L_{\mathrm{R}_n\mathrm{D}} = 2$ and equal tap attenuations. Unless otherwise stated,

we assume that sky wave/NVIS channels remain constant within the duration of one block transmission.

Based on (2.2), the path loss for the sky wave and NVIS links are, respectively, calculated as 114 dB and 103 dB assuming $f_c = 5\,\text{MHz}$, $n = 1$, and $L_w = 10$ dB. Path loss for surface wave link is calculated through GRWAVE software assuming electrical parameters for the medium dry ground (i.e., relative permittivity $\varepsilon = 15$ and conductivity $\sigma = 0.001$ Siemens per meter [1]). For a range of 3.5 km (which denotes the distance between the destination and each relay), the path loss for surface wave is found to be 84 dB. Therefore, the path gains for sky wave $S \to D$ and $S \to R_n$, $n = 1, \cdots, M$, links, which have approximately the same length, are 0 dB (i.e. $G_{SD} = G_{SR_n} = 0\,\text{dB}$) while the gain for the $R_n \to D$, $n = 1, \cdots, M$, links depend on the propagation method. Specifically, we have $G_{R_nD} = 11\,\text{dB}$ and $30\,\text{dB}$, respectively, for the NVIS and surface wave methods.

In Fig. 3.3, we illustrate the bit error rate (BER) of the cooperative HF system with $M = 1$ and $M = 2$ relays under the assumption that relay terminals communicate through NVIS (See Fig. 3.2). We consider both orthogonal and opportunistic relaying methods. As a benchmark, we include the performance of direct transmission ($M = 0$). Moreover, the BER of the uncoded no-relay system over AWGN channel with $G_{SD} = 0$ is also depicted. Note that orthogonal and opportunistic relaying coincide for $M = 1$. To make a fair comparison between different schemes, the adopted modulation schemes for the direct transmission, opportunistic relaying, and orthogonal relaying with $M = 2$ are BPSK, QPSK, and 8PSK, respectively. Different constellation sizes balance the overall rate of different methods. Optimum power allocation parameters are found from (3.26) and listed in Table 3.1. In Fig. 3.3, we observe that the amount of SNR required by the direct transmission to achieve BER=10^{-3} is 14.7 dB. The cooperative scheme with $M = 1$ outperforms the direct transmission by 6 dB. This climbs up to 8.5 dB for opportunistic PS relaying with $M = 2$.
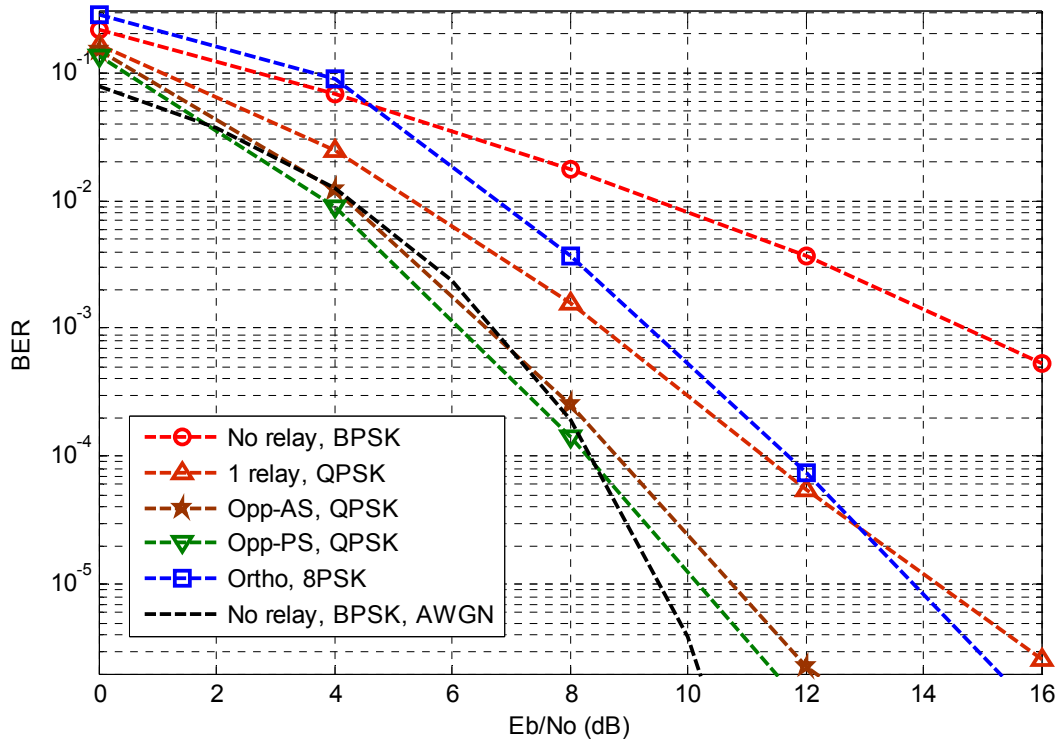
Figure 3.3 BER performance for the cooperative systems with NVIS relay-to-destination link(s)

Table 3.1 System parameters for different cooperative systems under consideration

	M	Modulation	NVIS	Surface wave
Direct Transmission	0	BPSK	$K_0 = 1$	$K_0 = 1$
Orthogonal/opportunistic	1	QPSK	$K_0 = 0.77, K_1 = 0.23$	$K_0 = 0.98, K_1 = 0.02$
Opportunistic Relaying (PS)	2	QPSK	$K_0 = 0.67, K_1 = 0.33$	$K_0 = 0.96, K_1 = 0.04$
Opportunistic Relaying (AS)	2	QPSK	$K_0 = 0.67, K_1 = 0.33$	$K_0 = 0.96, K_1 = 0.04$
Orthogonal	2	8PSK	$K_0 = 0.70, K_1 = K_2 = 0.15$	-

From Fig. 3.3, it is also observed that a diversity order of 2 is achieved for the direct transmission. On the other hand, based on (3.21), the maximum diversity order for cooperative systems with $M = 1$ and $M = 2$ is 4 and 6, respectively. However, the cascaded nature of Rayleigh channels in relaying links allows only partial diversity to be observed in the practical SNR range under consideration [56]. Accordingly, in the SNR region of Fig. 3.3, we see a diversity order of 3.3 for cooperative system with $M = 1$, 5.1 for both PS and AS opportunistic systems with $M = 2$, and 4.7 for the orthogonal relaying with $M = 2$. Higher spectral efficiency of the opportunistic relaying results in outperforming the orthogonal relaying approach. In particular, at the target BER of 10^{-3}, the performance gap between PS-opportunistic and orthogonal relaying is more than 3 dB. Moreover, the performance gap between PS- and AS-opportunistic relaying is less than 0.5 dB. This result reveals that for the HF network under our consideration, using the much simpler, yet suboptimal AS relay selection method does not considerably sacrifice the performance.

Fig. 3.4 illustrates the BER performance of cooperative systems under the assumption that relay terminals communicate through surface wave. Optimum power allocation parameters for this case are listed in Table 3.1. The performance gains (with respect to the direct communication) for cooperative system with $M = 1$, and PS-opportunistic relaying with $M = 2$ are given by 8.5 dB and 11 dB at the target BER of 10^{-3}, respectively. The increase in performance gains in comparison to those achieved through NVIS are due to the fading-free nature of surface wave links and their relatively less path losses.

Our results indicate that path loss becomes the dominating factor in the performance discrepancy of two propagation mechanisms. To further highlight this performance difference resulting from path loss, Fig. 3.5 illustrates the corresponding BER performance versus relay-to-destination distance for a fixed SNR=10 dB. It is observed that by increasing the distance, the path loss of the surface wave increases, and therefore, the associated performance gets worse.

39
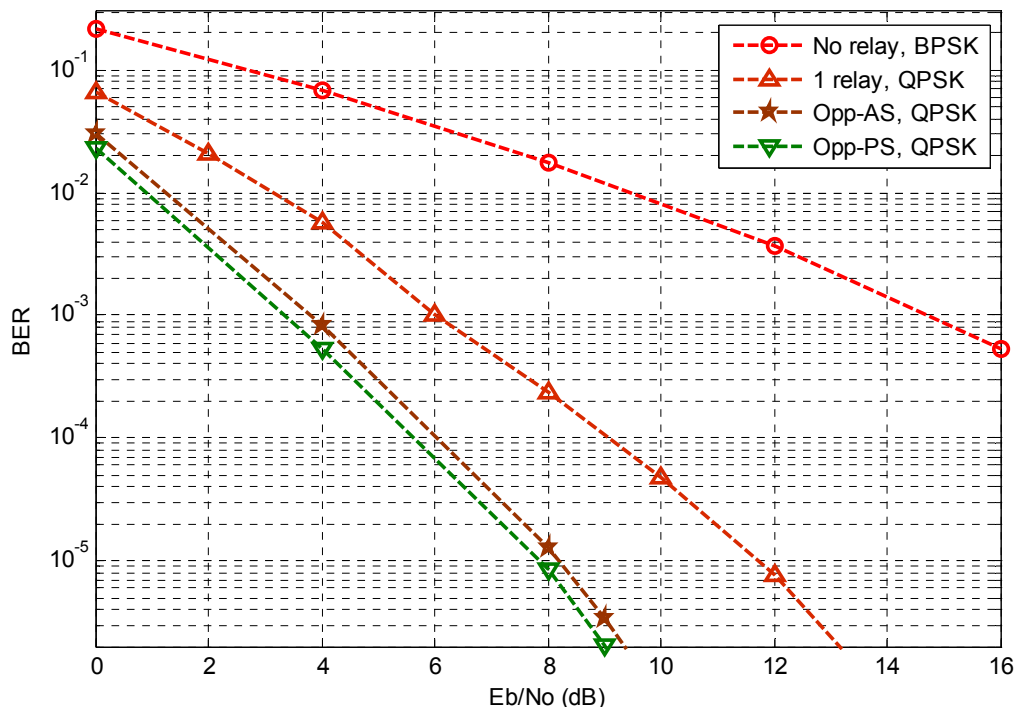
Figure 3.4 BER performance for the cooperative systems with surface wave relay-to-destination link(s)

On the other hand, if NVIS is used, the path loss is almost fixed, so the corresponding performance remains unchanged. As a result, for small distances between the relay and the destination, using a surface wave link is better than NVIS. For larger distances, the situation is however reversed.

In Fig. 3.6, we investigate the effect of time-variation on the performance of the cooperative systems. Based on ITU recommendations [47], we consider uni-Gaussian PSD and 2 milliseconds delay between the two paths. We assume different Doppler spreads, namely $f_d = 2$, 5, and 10 Hz. Comparison with Fig. 3.3 for the same number of relays indicates that time
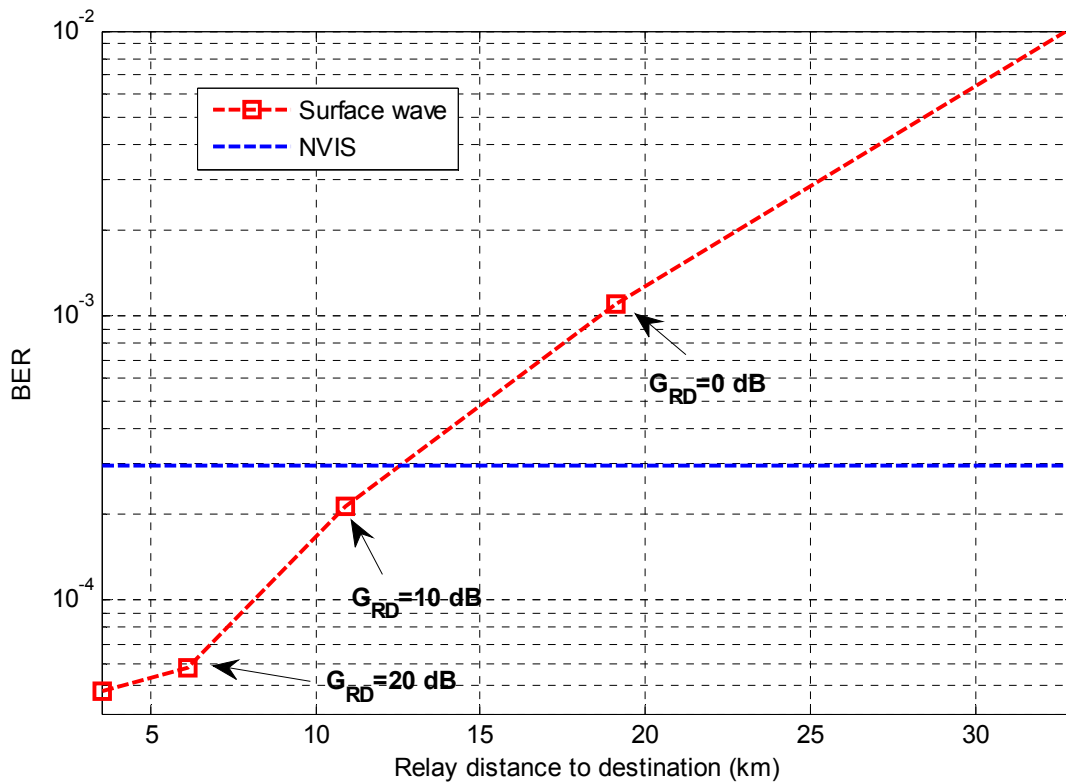
Figure 3.5 BER performance as a function of relay-to-destination distance

selectivity induced by ionosphere brings negligible degradation for typical HF channels with 2 Hz Doppler spread. However, as Doppler spread increases, the amount of inter-carrier-interference (ICI) impairment in the OFDM signals (resulting from the time selectivity of the channel) increases [57], and therefore, the performance of the system is gradually degraded. The effect of the induced ICI can be reduced by properly designed equalizers [58].
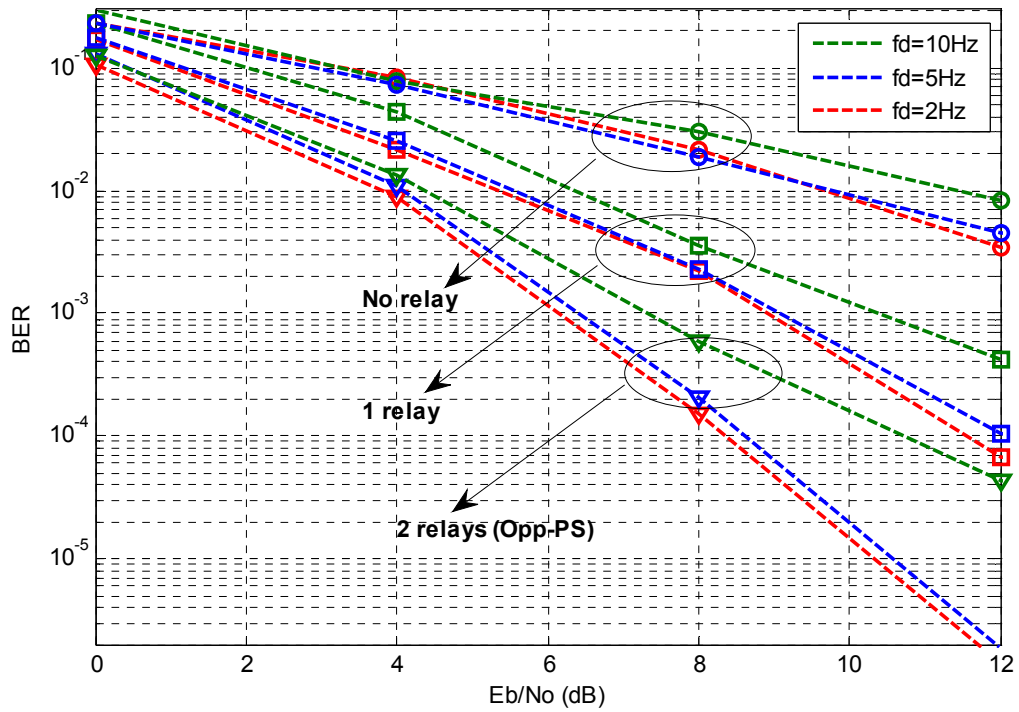
Figure 3.6 BER performance of the cooperative systems with NVIS relay-to-destination link(s) under the time varying channel assumption.

Chapter 4

Matched Filter Bound for Single-Carrier Cooperative HF Systems

4.1 Introduction

Single-carrier (SC) modulation, as discussed in Chapter 1, is the primary mode of operation in many tactical HF standards. Therefore, the objective of this chapter and the next is to investigate the cooperative communication for an HF system in which different nodes are equipped with SC modems.

In this chapter, we form our analytical framework for the design of SC cooperative systems by using the notion of matched filter bound (MFB). In particular, a closed form MFB on the error rate performance is derived for SC cooperative systems with non-regenerative relaying, i.e., in the form of either amplify-and-forward (AaF) or filter-and-forward (FaF) relaying. It is demonstrated that the MFB analysis of AaF/FaF cooperative systems over frequency-selective Rayleigh fading channels (due to ISI and noise propagation impairments) can be reduced to the analysis of the AaF/FaF cooperative systems over non-frequency selective (i.e., frequency-flat) Nakagami-m fading channels. Based on the derived MFB, we further investigate the optimum power allocation and relay selection rules.

This chapter is organized as follows. In Section 4.2, we introduce the system model. In Section 4.3, we present the MFB derivation and discuss its relationship to the existing results. In Section 4.4, we discuss diversity gain analysis and introduce optimum relay selection strategies. In Section 4.5, we propose an optimal power allocation scheme to minimize the derived MFB on the symbol error rate (SER). Finally, we present numerical results in Section 4.6.

43

4.2 System Model

We consider a multi-relay cooperative system where the source node S transmits information to the destination node D through the assistance of M relay nodes $R_1, \cdots, R_M$ (Fig. 4.1). The relay nodes operate in half-duplex mode and perform non-regenerative relaying.
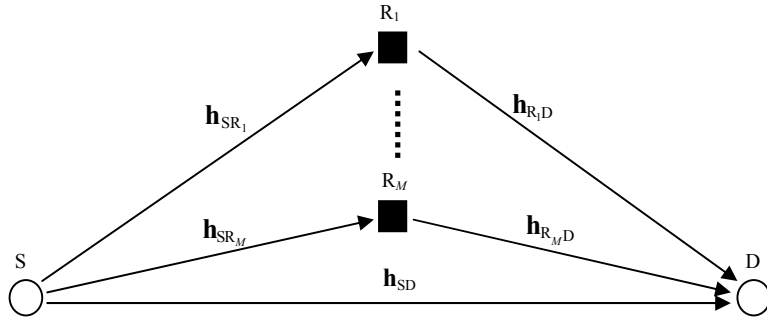
Figure 4.1 The cooperative system under consideration

We adopt the HF channel models presented in Section 3.2 of Chapter 3 for the underlying links. Let the baseband source signal be a single pulse $x_0 C_S(t)$ where x_0 is a complex-valued modulation symbol belonging to a normalized linear constellation (e.g., PSK, QAM) with unit average energy, and $C_S(t)$ is the impulse response of the pulse shaping filter in the source. During the broadcasting phase, the received signals at the destination and the relay node R_n ($n = 1, \cdots, M$) are, respectively, given by

$$r_{SD}(t) = \sqrt{P_0} x_0 \sum_{l=0}^{L_{SD}-1} \mathbf{h}_{SD}(l) C_S(t - \boldsymbol{\tau}_{SD}(l)) + n_{SD}(t) \tag{4.1}$$

$$r_{SR_n}(t) = \sqrt{G_{SR_n} P_0} x_0 \sum_{l=0}^{L_{SR_n}-1} \mathbf{h}_{SR_n}(l) C_S(t - \boldsymbol{\tau}_{SR_n}(l)) + n_{SR_n}(t) \tag{4.2}$$

where $n_{SD}(t)$ and $n_{SR_n}(t)$ are the complex additive white Gaussian noise (AWGN) terms with zero mean and double sided power spectral density N_0. In (4.1) and (4.2), P_0 is the average

source power per symbol and can be written as $P_0 = K_0 P_T$ ($K_0 \geq 0$) where P_T denotes the average total power budget (i.e., total power of the source and relay nodes) for transmitting one symbol.

At the destination, the received signal $r_{\mathrm{SD}}(t)$ is passed through the normalized matched-filter (MF), i.e., $g_{\mathrm{SD}}^*(T_{\mathrm{SD}} - t)/\|g_{\mathrm{SD}}(t)\|$ where $g_{\mathrm{SD}}(t) = \sum_{l=0}^{L_{\mathrm{SD}}-1} \mathbf{h}_{\mathrm{SD}}(l) C_{\mathrm{S}}(t - \boldsymbol{\tau}_{\mathrm{SD}}(l))$, and T_{SD} is the temporal support of $g_{\mathrm{SD}}(t)$. Sampling the output of the normalized MF at time instant T_{SD} yields the sufficient statistic given by

$$y_{\mathrm{SD}} = \sqrt{P_0} \, \|g_{\mathrm{SD}}(t)\| x_0 + z_{\mathrm{SD}} \tag{4.3}$$

where z_{SD} is the zero-mean complex Gaussian noise term with the variance of N_0. Similarly, at the nth relay, $n = 1, \cdots, M$, after applying the corresponding normalized MF to the received signal and sampling at time instant T_{SR_n}, we have

$$y_{\mathrm{SR}_n} = \sqrt{G_{\mathrm{SR}_n} P_0} \, \|g_{\mathrm{SR}_n}(t)\| x_0 + z_{\mathrm{SR}_n} \tag{4.4}$$

where $g_{\mathrm{SR}_n}(t) = \sum_{l=0}^{L_{\mathrm{SR}_n}-1} \mathbf{h}_{\mathrm{SR}_n}(l) C_{\mathrm{S}}(t - \boldsymbol{\tau}_{\mathrm{SR}_n}(l))$, T_{SR_n} is the support of $g_{\mathrm{SR}_n}(t)$, and z_{SR_n} is the zero-mean complex Gaussian noise term with the variance of N_0.

During the relaying phase, relays transmit their signals towards the destination in consecutive time intervals. The received signal at the destination, coming from the nth relay within the nth time slot, is given by

$$r_{\mathrm{R}_n\mathrm{D}}(t) = \sqrt{\alpha_n P_n G_{\mathrm{R}_n\mathrm{D}}} \, y_{\mathrm{SR}_n} \sum_{l=0}^{L_{\mathrm{R}_n\mathrm{D}}-1} \mathbf{h}_{\mathrm{R}_n\mathrm{D}}(l) C_{\mathrm{R}_n}(t - \boldsymbol{\tau}_{\mathrm{R}_n\mathrm{D}}(l)) + n_{\mathrm{R}_n\mathrm{D}}(t) \tag{4.5}$$

where $P_n = K_n P_T$ ($K_n \geq 0$) is the average power of the nth relay for each symbol, $C_{\mathrm{R}_n}(t)$ is the impulse response of the pulse shaping filter in the nth relay, and $n_{\mathrm{R}_n\mathrm{D}}(t)$ is the complex AWGN term with zero mean and double-sided power spectral density N_0. In (4.5), α_n represents the scaling factor and can take different values based on the availability of channel state information

at the relay. Specifically, under the so-called average power scaling (APS) and instantaneous power scaling (IPS) [52], we have

$$\alpha_n = \begin{cases} \dfrac{1}{N_0 + G_{SR_n}P_0} & \text{for APS} \\ \\ \dfrac{1}{N_0 + G_{SR_n}P_0 \left\| g_{SR_n}(t) \right\|^2} & \text{for IPS} \end{cases} \tag{4.6}$$

The received signal given in (4.5) is then applied to its corresponding MF, i.e., $g^*_{R_nD}(T_{R_nD} - t)$ where $g_{R_nD}(t) = \sum_{l=0}^{L_{R_nD}-1} \mathbf{h}_{R_nD}(l)C_{R_n}(t - \tau_{R_nD}(l))$, and T_{R_nD} is the support of $g_{R_nD}(t)$. Accordingly, the sampled output of the MF at time instant T_{R_nD} is given by

$$y_{R_nD} = \sqrt{\alpha_n P_n G_{R_nD}} \left\| g_{R_nD}(t) \right\|^2 y_{SR_n} + z_{R_nD} \tag{4.7}$$

where z_{R_nD} is the complex Gaussian noise component with zero mean and the variance of $N_0 \left\| g_{R_nD}(t) \right\|^2$. At the destination, maximum ratio combining (MRC) is applied on the received signals from the $S \rightarrow D$ and $S \rightarrow R_n \rightarrow D$ ($n = 1, \cdots, M$) links.

4.3 Matched Filter Bound (MFB) on Error Rate

In this section, we derive MFBs on SER and BER of SC cooperative systems with non-regenerative relaying. Let $\overline{\gamma}_{AB}$ denote the average SNR in the $A \rightarrow B$ link. Therefore, we can write $\overline{\gamma}_{SD} = P_0/N_0$, $\overline{\gamma}_{SR_n} = G_{SR_n}P_0/N_0$, and $\overline{\gamma}_{R_nD} = G_{R_nD}P_n/N_0$. Accordingly, the instantaneous SNR of the $A \rightarrow B$ link is given by $\gamma_{AB} = \overline{\gamma}_{AB} \left\| g_{AB}(t) \right\|^2$ which can be expressed as

$$\gamma_{AB} = \overline{\gamma}_{AB} \sum_{m=0}^{L_{AB}-1} \sum_{l=0}^{L_{AB}-1} \mathbf{h}_{AB}(m)\mathbf{h}^*_{AB}(l)R_A\left(\tau_{AB}(m) - \tau_{AB}(l)\right) \tag{4.8}$$

where $R_A(.)$ is the autocorrelation function of the impulse response of the pulse shaping filter at node A, i.e., $C_A(t)$. Under the assumption that received signals from different paths are orthogonal, we can write $R_A(\tau_{AB}(m) - \tau_{AB}(l)) = 0$, for any $m \neq l$, and therefore, (4.8) yields

46

$$\gamma_{\mathrm{AB}} = \overline{\gamma}_{\mathrm{AB}} \left\| \mathbf{h}_{\mathrm{AB}} \right\|^2 \tag{4.9}$$

which indicates that the MF detector is equivalent to optimal multipath diversity combining [31], and therefore, yields the highest amount of SNR[1].

For the cooperative system under consideration, the instantaneous SNR at the destination is given by

$$\gamma_{\mathrm{D}} = \gamma_{\mathrm{SD}} + \sum_{n=1}^{M} \gamma_{\mathrm{SR}_n \mathrm{D}} \tag{4.10}$$

where $\gamma_{\mathrm{SR}_n \mathrm{D}}$ is

$$\gamma_{\mathrm{SR}_n \mathrm{D}} = \frac{\gamma_{\mathrm{SR}_n} \gamma_{\mathrm{R}_n \mathrm{D}}}{\gamma_{\mathrm{R}_n \mathrm{D}} + a \gamma_{\mathrm{SR}_n} + b_n} \tag{4.11}$$

with $a=1$ and $b_n=1$ for IPS, and $a=0$ and $b_n = 1 + \overline{\gamma}_{\mathrm{SR}_n}$ for APS. Using MGF, the SER/BER can be evaluated for a wide variety of modulation schemes [59]. For instance, the average SER for the M-PSK modulation is given by [59, pp. 230]

$$P_s(e) = \frac{1}{\pi} \int_0^{\frac{(M-1)\pi}{M}} \Phi_{\gamma_{\mathrm{D}}} \left(\frac{g_{\mathrm{PSK}}(1)}{\sin^2 \theta} \right) d\theta \tag{4.12}$$

where $g_{\mathrm{PSK}}(k) = \sin^2(k\pi/\mathrm{M})$ and $\Phi_{\gamma_{\mathrm{D}}}(s)$ denotes the MGF of γ_{D}. Furthermore, defining P_k as the probability that, for a given transmitted phase, the received signal vector falls in the kth decision region away from the one corresponding to the transmitted phase, we have [59, pp. 233]

---

[1] The assumed orthogonality of the received multipath signals is satisfied in various cases. For instance, assume that the pulse shaping filter $C_{\mathrm{A}}(t)$ is designed for a baud rate of $1/T_s$ based on the Nyquist criterion (i.e., $R_{\mathrm{A}}(kT_s) = 0, k \neq 0$). Then, the orthogonality of the received multipath signals is satisfied for all channels that can be modeled by the so-called tapped-delay-line with subsequent T_s second delays (i.e., the most common model for the multipath channels). Another example is the transmission over channels in which the relative delay between different propagation paths is much more than T_s seconds (typical HF NVIS/skywave channels have this property).

$$P_k = \frac{1}{2\pi}\int_0^{\pi\left(1-\frac{2k-1}{M}\right)}\Phi_{\gamma_D}\left(\frac{g_{PSK}(2k-1)}{\sin^2\theta}\right)d\theta - \frac{1}{2\pi}\int_0^{\pi\left(1-\frac{2k+1}{M}\right)}\Phi_{\gamma_D}\left(\frac{g_{PSK}(2k+1)}{\sin^2\theta}\right)d\theta. \tag{4.13}$$

Accordingly, the exact BER of the M-PSK, using Gray bit-to-symbol mapping, is determined in terms of P_k, $k=1,\cdots,M-1$. For example, for $M=4,\ 8,$ and 16, we have [59, pp. 233]

$$P_b(e) = \frac{1}{2}\left(P_1 + 2P_2 + P_3\right),\ M = 4$$

$$P_b(e) = \frac{1}{3}\left(P_1 + 2P_2 + P_3 + 2P_4 + 3P_5 + 2P_6 + P_7\right),\ M = 8$$

$$P_b(e) = \frac{1}{2}\left(\sum_{k=1}^{8}P_k + \sum_{k=2}^{5}P_k + P_5 + 2P_6 + P_7\right),\ M = 16 \tag{4.14}$$

Calculation of SER and BER expressions in (4.12) and (4.14) requires the derivation of $\Phi_{\gamma_D}(s)$ which is given by

$$\Phi_{\gamma_D}(s) = \Phi_{\gamma_{SD}}(s)\prod_{n=1}^{M}\Phi_{\gamma_{SR_nD}}(s) \tag{4.15}$$

where $\Phi_{\gamma_{SD}}(s)$ and $\Phi_{\gamma_{SR_nD}}(s)$ are the MGFs of γ_{SD} and γ_{SR_nD}. In order to calculate $\Phi_{\gamma_D}(s)$, first, note that $\mathbf{h}_{AB}$ is a vector of i.i.d. complex zero-mean Gaussian random variables. Therefore, $\gamma_{AB} \sim \mathcal{G}(L_{AB}, \overline{\gamma}_{AB}/L_{AB})$ with probability density function (pdf) [59, pp. 126]

$$f_{\gamma_{AB}}(x) = \frac{L_{AB}^{L_{AB}}x^{L_{AB}-1}e^{-\frac{L_{AB}x}{\overline{\gamma}_{AB}}}}{\overline{\gamma}_{AB}^{L_{AB}}\Gamma(L_{AB})}. \tag{4.16}$$

where $\Gamma(.)$ is the gamma function [60]. Therefore, we have $\gamma_{SD} \sim \mathcal{G}(L_{SD}, \overline{\gamma}_{SD}/L_{SD})$, $\gamma_{SR_n} \sim \mathcal{G}(L_{SR_n}, \overline{\gamma}_{SR_n}/L_{SR_n})$, and $\gamma_{R_nD} \sim \mathcal{G}(L_{R_nD}, \overline{\gamma}_{R_nD}/L_{R_nD})$. As a result, the MGF of the direct $S \rightarrow D$ link is given by [59, pp. 126]

$$\Phi_{\gamma_{SD}}(s) = E\left[e^{-s\gamma_{SD}}\right] = \left(1 + \frac{\overline{\gamma}_{SD}}{L_{SD}}s\right)^{-L_{SD}}. \tag{4.17}$$

On the other hand, the following proposition is used to derive the MGF of the SNR contribution of the cascaded relay links, i.e., $\Phi_{\gamma_{\mathrm{SR}_n\mathrm{D}}}(s), n = 1, \cdots, M$.

Proposition: Consider a cascaded $\mathrm{A} \to \mathrm{B} \to \mathrm{C}$ non-regenerative relaying link where $\mathrm{A} \to \mathrm{B}$ and $\mathrm{B} \to \mathrm{C}$ links experience *frequency-selective Rayleigh fading channels* with uniform power delay profiles in which the number of resolvable paths are, respectively, L_{AB} and L_{BC}. Now consider another $\mathrm{A} \to \mathrm{B} \to \mathrm{C}$ non-regenerative relay channel in which $\mathrm{A} \to \mathrm{B}$ and $\mathrm{B} \to \mathrm{C}$ links experience *frequency-flat Nakagami-m fading channels* whose fading parameters are, respectively, $m_1 = L_{\mathrm{AB}}$ and $m_2 = L_{\mathrm{BC}}$. From MFB perspective, these two channels yield the same end-to-end SNR.

Proof: Based on the preceding MFB analysis, the received SNR at the output of the cascaded frequency selective $\mathrm{A} \to \mathrm{B} \to \mathrm{C}$ channel follows the same formula given in (4.11) which can be readily checked by replacing $\gamma_{\mathrm{SR}_n\mathrm{D}}$, γ_{SR_n}, and $\gamma_{\mathrm{R}_n\mathrm{D}}$ by γ_{ABC}, γ_{AB}, and γ_{BC}, respectively. Moreover, we have $\gamma_{\mathrm{AB}} \sim \mathcal{G}(\mathrm{L}_{\mathrm{AB}}, \overline{\gamma}_{\mathrm{AB}}/\mathrm{L}_{\mathrm{AB}})$ and $\gamma_{\mathrm{BC}} \sim \mathcal{G}(\mathrm{L}_{\mathrm{BC}}, \overline{\gamma}_{\mathrm{BC}}/\mathrm{L}_{\mathrm{BC}})$. On the other hand, it is well known [61] that the generic formula in (4.11) also holds between γ_{AB}, γ_{BC}, and γ_{ABC} when both $\mathrm{A} \to \mathrm{B}$ and $\mathrm{B} \to \mathrm{C}$ links are frequency-flat fading channels. Under the Nakagami-m fading assumption with fading parameter m_1 in the $\mathrm{A} \to \mathrm{B}$ link and m_2 in the $\mathrm{B} \to \mathrm{C}$ link, we have $\gamma_{\mathrm{AB}} \sim \mathcal{G}(m_1, \overline{\gamma}_{\mathrm{AB}}/m_1)$ and $\gamma_{\mathrm{BC}} \sim \mathcal{G}(m_2, \overline{\gamma}_{\mathrm{BC}}/m_2)$. As a result, the proof is complete by setting $m_1 = L_{\mathrm{AB}}$ and $m_2 = L_{\mathrm{BC}}$.

Based on the Proposition, we use the MGF derived for Nakagami-m relay channels to obtain the MGF of $\gamma_{\mathrm{SR}_n\mathrm{D}}$ as [61]

$$\Phi_{\gamma_{\mathrm{SR}_n\mathrm{D}}}(s) = \mathrm{E}\left[e^{-s\gamma_{\mathrm{SR}_n\mathrm{D}}}\right]$$

$$= \begin{cases} 1 - 2s \displaystyle\sum_{l=0}^{L_{\mathrm{SR}_n}-1} \sum_{k=0}^{L_{\mathrm{R}_n\mathrm{D}}-1} \sum_{m=0}^{k} C_1(l,k,m) \sum_{q=0}^{l+m+2} \binom{l+m+2}{q} J_1(l,k,m,q) & \text{for IPS} \\ 1 - 2s \displaystyle\sum_{l=0}^{L_{\mathrm{SR}_n}-1} \sum_{k=0}^{L_{\mathrm{R}_n\mathrm{D}}-1} C_2(l,k) J_2(l,k) & \text{for APS} \end{cases}$$

(4.18)

where $C_1(l,k,m)$, $C_2(l,k)$, $J_1(l,k,m,q)$ and $J_2(l,k)$ are given by

$$C_1(l,k,m) = \frac{\left(\dfrac{\overline{\gamma}_{SR_n}}{L_{SR_n}}\right)^{\frac{l-m+1-2L_{SR_n}}{2}} \left(\dfrac{\overline{\gamma}_{R_nD}}{L_{R_nD}}\right)^{\frac{m-l-1-2k}{2}}}{m!(k-m)!l!\left(L_{SR_n}-l-1\right)!}$$

$$C_2(l,k) = \frac{\left(\dfrac{\overline{\gamma}_{SR_n}}{L_{SR_n}}\right)^{\frac{l-k+1-2L_{SR_n}}{2}} \left(\dfrac{\left(1+\overline{\gamma}_{SR_n}\right)L_{R_nD}}{\overline{\gamma}_{R_nD}}\right)^{\frac{l+k+1}{2}}}{k!l!\left(L_{SR_n}-l-1\right)!}$$

$$J_1(l,k,m,q) = \sqrt{\frac{\overline{\gamma}_{SR_n}\overline{\gamma}_{R_nD}}{L_{SR_n}L_{R_nD}}} \frac{\Gamma(l+2)\Gamma(m+1)}{2(-1)^{L_{SR_n}+k-q+1}} \frac{d^{L_{SR_n}+k-q+1}}{dt^{L_{SR_n}+k-q+1}}$$

$$\times \left\{ e^{\frac{t}{2}} W_{-\frac{l+m+2}{2},\frac{l-m+1}{2}}\left(\frac{t}{2}-\sqrt{\frac{t^2}{4}-\frac{\overline{\gamma}_{SR_n}\overline{\gamma}_{R_nD}}{L_{SR_n}L_{R_nD}}}\right) W_{-\frac{l+m+2}{2},\frac{l-m+1}{2}}\left(\frac{t}{2}+\sqrt{\frac{t^2}{4}-\frac{\overline{\gamma}_{SR_n}\overline{\gamma}_{R_nD}}{L_{SR_n}L_{R_nD}}}\right) \right\} \Bigg|_{t=s+\frac{\overline{\gamma}_{SR_n}}{L_{SR_n}}+\frac{\overline{\gamma}_{R_nD}}{L_{R_nD}}}$$

$$J_2(l,k) = \frac{\Gamma\left(L_{SR_n}+1\right)\Gamma\left(L_{SR_n}+k-l\right)}{2\sqrt{\dfrac{\overline{\gamma}_{SR_n}\overline{\gamma}_{R_nD}}{L_{SR_n}L_{R_nD}}}\left(1+\overline{\gamma}_{SR_n}\right)}\left(s+\frac{\overline{\gamma}_{SR_n}}{L_{SR_n}}\right)^{\frac{l-k-2L_{SR_n}}{2}}$$

$$\times e^{\frac{L_{SR_n}L_{R_nD}\left(1+\overline{\gamma}_{SR_n}\right)}{2\overline{\gamma}_{R_nD}\left(L_{SR_n}+\overline{\gamma}_{SR_n}s\right)}} W_{\frac{l-2L_{SR_n}-k}{2},\frac{l-k+1}{2}}\left(\frac{L_{SR_n}L_{R_nD}\left(1+\overline{\gamma}_{SR_n}\right)}{\overline{\gamma}_{R_nD}\left(L_{SR_n}+\overline{\gamma}_{SR_n}s\right)}\right).$$

in which $W_{\mu,\nu}(.)$ is the Whittaker W function [62, pp. 340].

Replacing (4.17) and (4.18) in (4.15), we have the MGF of the received signal at the destination, $\Phi_{\gamma_D}(s)$. Using the resulting expression in (4.12) and (4.14) yields the MFB on the SER and BER, respectively.

4.4 Diversity Gain Analysis and Optimum Relay Selection

For sufficiently large SNR values, (4.18) can be simplified as (see Appendix D for the proof)

$$\Phi_{\gamma_{\mathrm{D}}}(s) \simeq \eta_0(\overline{\gamma}s)^{-L_{\mathrm{SD}}} \prod_{n=1}^{M}\left(\eta_{0,n}(\overline{\gamma}s)^{-L_{\mathrm{SR}_n}} + \eta_{1,n}(\overline{\gamma}s)^{-L_{\mathrm{R}_n\mathrm{D}}}\right) \tag{4.19}$$

where $\overline{\gamma} = P_T/N_0$ is the overall SNR per transmitted symbol in the system, $\eta_0 = (K_0/L_{\mathrm{SD}})^{-L_{\mathrm{SD}}}$, and $\eta_{0,n}$ and $\eta_{1,n}$ are some constants with respect to s, defined in the Appendix D, for different scaling methods and channel conditions. The asymptotical MGF in (4.19) can be used to determine the available diversity order of the uncoded SC cooperative system. The diversity order is, conventionally, defined as the (negative) slope of the SER versus SNR curve in a log-log scale at high SNR regime, i.e.,

$$O_d = -\lim_{\overline{\gamma} \to \infty} \frac{\log P_s(e)}{\log \overline{\gamma}}. \tag{4.20}$$

On the other hand, it can be shown that diversity order also governs the decaying behavior of the MGF [63]. In particular, as $s \to \infty$, $\left|\Phi_{\gamma_{\mathrm{D}}}(s)\right| \to c|s|^{-O_d}$. As a result, based on (4.19), the achievable diversity order of uncoded SC cooperative systems is given by

$$O_d = L_{\mathrm{SD}} + \sum_{n=1}^{M} \min\left(L_{\mathrm{SR}_n}, L_{\mathrm{R}_n\mathrm{D}}\right). \tag{4.21}$$

MFB analysis also can be used to derive an optimum (from MFB perspective) relay selection rule for opportunistic multi-relay cooperative systems. In particular, from (4.10) and (4.11), the relay with the highest contribution in the ultimate SNR at the destination terminal is determined by

$$n^{Opt} = \arg\max_{n}\left\{\frac{\gamma_{\mathrm{SR}_n}\gamma_{\mathrm{R}_n\mathrm{D}}}{\gamma_{\mathrm{R}_n\mathrm{D}} + a\gamma_{\mathrm{SR}_n} + b_n}\right\}. \tag{4.22}$$

4.5 MFB Optimization through Optimum Power Allocation

In this section, we aim to optimize the derived MFBs by finding the optimum power allocation values (i.e., K_0 and K_n, $n = 1, \cdots, M$). Since, under the Gray code mapping, SER and BER

expressions differ by only one multiplicative constant at high SNR region [59], the optimization of the MFB-BER and MFB-SER become equivalent. As a result, here we just investigate the power allocation problem to minimize the MFB on SER.

Recall that we have $P_0 = K_0 P_T$ and $P_n = K_n P_T$ $(n = 1, \cdots, M)$ where P_T denotes the average system power budget for transmitting one symbol. Therefore, the minimization problem can be expressed as

$$\min P_s(e)$$
$$\text{s.t.} \sum_{n=0}^{M} K_n = 1, \tag{4.23}$$
$$K_0, K_1, \cdots, K_M \geq 0$$

Since no closed-form solution is available for (4.23), we resort to numerical methods to solve this optimization problem. From the Appendix D, it is easy to verify that $\eta_{0,n}$ and $\eta_{1,n}$ are posynomial functions in terms of $K_0, \cdots, K_M$. As a result, based on (4.14) and (4.19), $P_S(e)$ becomes a posynomial function with respect to $K_0, \cdots, K_M$, and therefore, at high SNR region, the problem in (4.23) approaches to a GP problem. As an example, Table 4.1 and Table 4.2 show the OPA parameter, K_0, based on the solution of (4.23) for different G_{SR_n}, G_{R_nD}, at $\bar{\gamma} = 20$ dB assuming $L_{SD} = L_{SR_n} = L_{R_nD} = 2$.

Table 4.1 The optimum power allocation parameter, K_0, for the one relay scenario with $L_{SD} = L_{SR_1} = L_{R_1D} = 2$ (the fraction of the power allocated to the relay can be also obtained by $K_1 = 1 - K_0$).

	$[G_{SR_1}$ (dB), G_{R_1D} (dB)]								
	[0,0]	[0,5]	[0,10]	[5,0]	[5,5]	[5,10]	[10,0]	[10,5]	[10,10]
IPS	0.6682	0.7046	0.7725	0.6171	0.6227	0.6723	0.5948	0.5764	0.5925
APS	0.6549	0.7482	0.8458	0.5609	0.6335	0.7505	0.5149	0.5357	0.6265

Table 4.2 The optimum power allocation parameter, K_0, for the two relay scenario with $L_{SD} = L_{SR_n} = L_{R_nD} = 2, \quad n = 1, 2$ (the fraction of the power allocated to each relay can be also obtained by $K_2 = K_1 = (1 - K_0)/2$).

	[G_{SR_n} (dB), G_{R_nD} (dB)]								
	[0,0]	[0,5]	[0,10]	[5,0]	[5,5]	[5,10]	[10,0]	[10,5]	[10,10]
IPS	0.5889	0.6488	0.7480	0.4765	0.5190	0.6290	0.3962	0.3990	0.4851
APS	0.6060	0.6326	0.7045	0.5756	0.5190	0.5756	0.4837	0.4395	0.4623

4.6 Numerical Results and Discussions

In this section, we present numerical results to verify the derived MFB bound on SER/BER, compare it with the simulation results of some practical equalization schemes, and discuss the effect of some system parameters. We assume that all underlying channels are either sky wave or NVIS links. Unless otherwise specified, based on ITU recommendations [47], we consider two propagation paths in each of the underlying channels (i.e., $L_{SD} = L_{SR_n} = L_{R_nD} = 2$) with equal attenuations and a 2 millisecond delay spread.

Fig. 4.2 depicts the MFB-BER performance of cooperative systems. Cooperative systems with one and two relays are considered. We assume the HF communication scenario depicted in Fig. 3.2 of Chapter 3 (i.e., the sky wave source-to-relay(s)/destination and NVIS relay(s)-to-destination links) with $G_{SD} = G_{SR_n} = 0$ dB and $G_{R_nD} = 10$ dB. The OPA values can be found in Table 4.1 and Table 4.2. As a benchmark, the performance of non-cooperative point-to-point scenario with $K_0 = 1$ is also included. To make a fair comparison, we consider BPSK modulation for the point-to-point system, QPSK for the one-relay system, and 8-PSK for the two-relay system. From Fig. 4.2, it is observed that diversity orders of 4 and 6 are achieved by the single- and two-relay systems, respectively. This result is in agreement with the derived diversity order given by (4.21). Furthermore, it is observed that the IPS-based system outperforms its APS-based
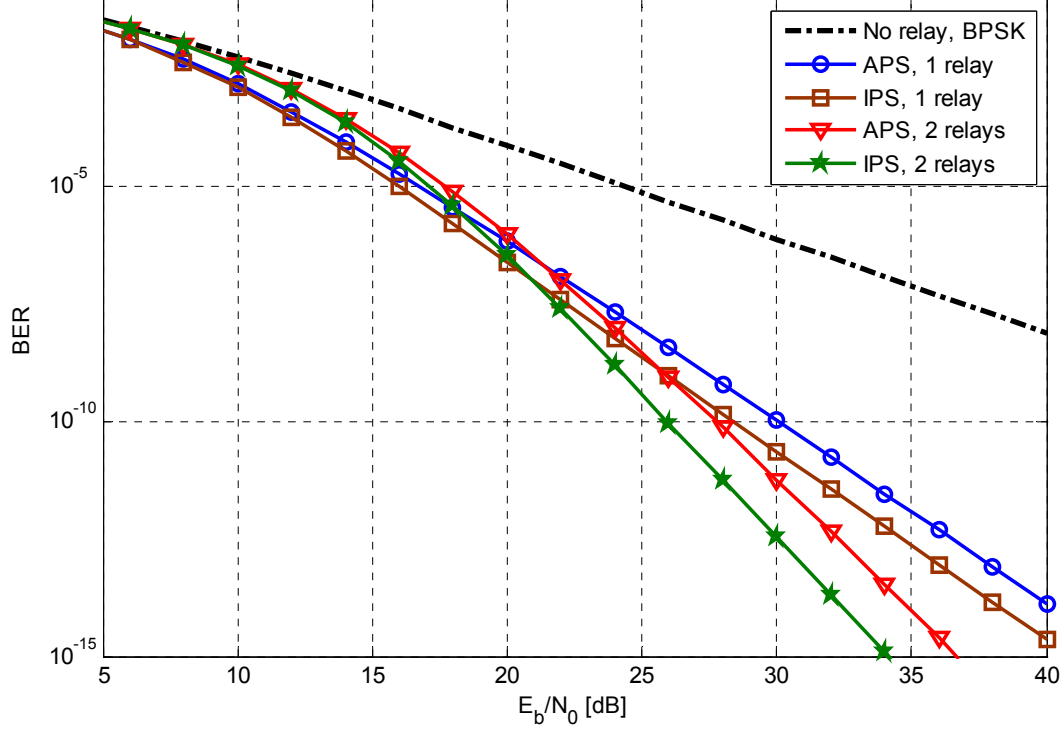
Figure 4.2 MFB bound on BER performance ($L_{SD} = L_{SR_n} = L_{R_nD} = 2$, $G_{SD} = G_{SR_n} = 0\,\mathrm{dB}$, and $G_{R_nD} = 10\,\mathrm{dB}$)

counterpart, and the relative performance gap among them approaches to 2 dB in the high SNR region.

Fig. 4.3 illustrates the effect of different relative path losses in different links on the BER performance of the single-relay assisted scenario. It is assumed that the adopted modulation scheme is QPSK and $\overline{\gamma} = 20$ dB. In Fig. 4.3.a, the MFB-BER of the IPS-based system, under different G_{R_1D} values, is depicted for both OPA and EPA strategies. Fig. 4.3.b shows the associated power allocation parameter, K_0, for corresponding channel realizations. From Fig. 4.3.a, it is observed that the larger G_{SR_1} is, the smaller the gap between the performance of OPA and EPA is. For example, consider the case of $G_{R_1D} = 0\,\mathrm{dB}$. In this case, the gap between OPA and EPA systems is negligible for $G_{SR_1} = 10\,\mathrm{dB}$. However, as G_{SR_1} decreases to 0 dB, the OPA
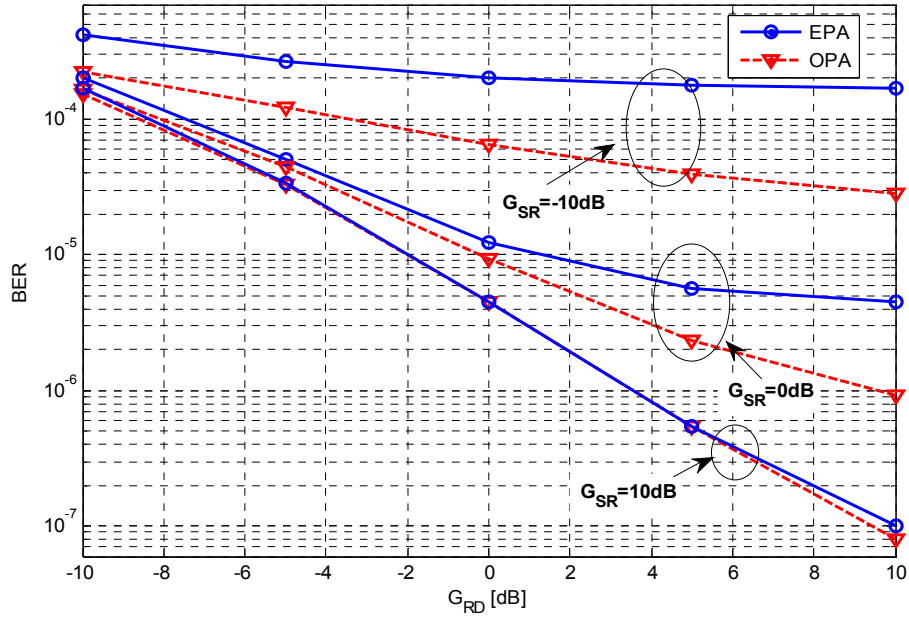
(a)
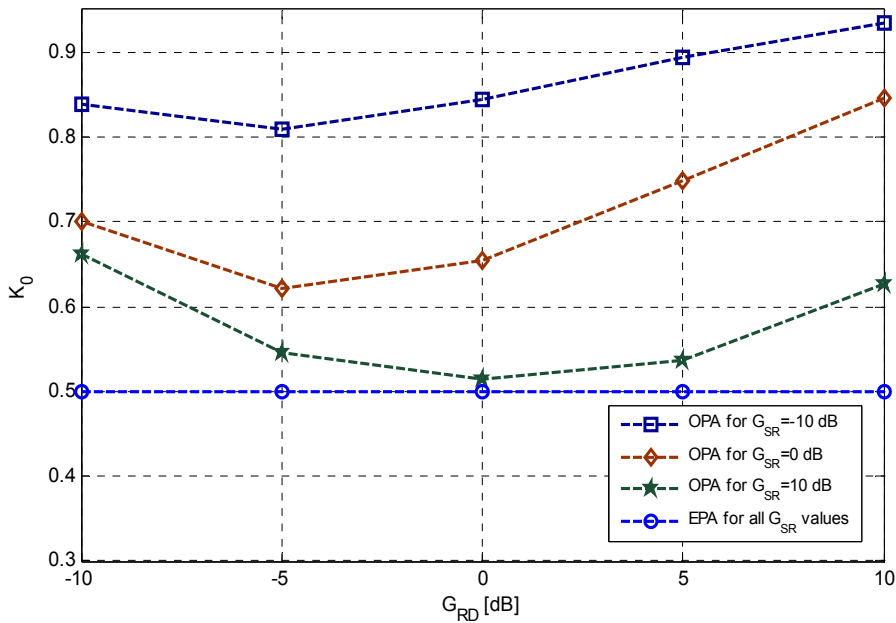
(b)

Figure 4.3 Comparison of the (a) BER and the (b) power allocation parameter, K_0, of the EPA and OPA strategies with respect to different path gains ($M = 1$, $L_{SD} = L_{SR_1} = L_{R_1D} = 2$, $\bar{\gamma} = 20$ dB).

system (with $K_0 = 0.65$) outperforms the EPA counterpart by 0.13 order of magnitude. This gap climbs up to 0.49 order of magnitude when G_{SR_1} becomes -10 dB. It should also be emphasized that the effect of G_{R_1D} on the performance gap between OPA and EPA is not monotonic. Specifically, for any given G_{SR_1}, we observe that when the relay is located far away from the destination (corresponding to low G_{R_1D} region), the performance gap decreases by increasing G_{R_1D} (i.e., by moving the relay towards the destination). However, if the relay keeps moving towards the destination, after a particular distance, the performance gap starts increasing. This non-monotonic behavior is also evident by inspecting the variation of the OPA's K_0 with respect to G_{R_1D} in Fig. 4.3.b.

In Fig. 4.4, we illustrate the performance of some practical equalization schemes and compare them with the derived MFB. Here, we consider a single-relay cooperative system without direct link (i.e., a dual-hop scheme) assuming IPS. Both relay and destination terminals are equipped with equalizers. Two equalization schemes are considered: a) frequency domain (FD) minimum mean square error (MMSE) equalization (FD-MMSE-LE) and b) FD-MMSE decision feedback equalization (FD-MMSE-DFE). In both cases, after equalization, the relay forwards a scaled version of its equalizer's soft output towards the destination. We consider EPA, i.e., $K_0 = K_1 = 0.5$, and assume that the relay is located midway between the source and the destination (i.e., $G_{SR_1} = G_{R_1D} = 0$ dB). The channel lengths are $L_{SR_1} = 2$, $L_{R_1D} = 4$, and the transmission frame size is 100. QPSK is adopted as the modulation type. As earlier noted, the MFB provides a bound on any equalizer. In this respect, we see that the performance of FD-MMSE-LE lies within 4.3 dB of the MFB at a target SER of 10^{-3}. This reduces to 2 dB for FD-MMSE-DFE.
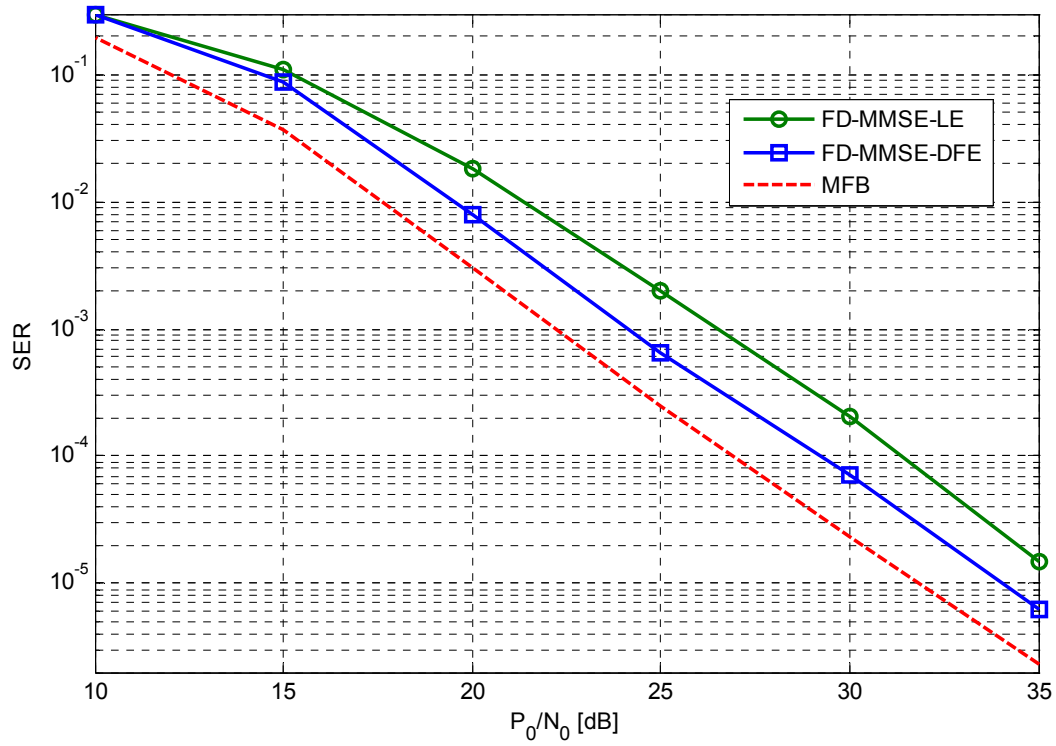
Figure 4.4 Comparison of the performance of practical equalizers with the MFB (dual-hop transmission with $M = 1$, $G_{SR_1} = G_{R_1D} = 0$ dB, $L_{SR_1} = 2$, $L_{R_1D} = 4$, and EPA is in place)

Chapter 5

Frequency Domain Equalization for Single-Carrier
Cooperative HF Systems

5.1 Introduction

For the HF sky wave and NVIS channels with long delay-spread profile (of the order of milliseconds), the complexity of the time domain equalization (TDE) becomes prohibitively high. In this chapter, as an alternative to TDE, we consider the design of frequency domain equalization (FDE) for the SC cooperative systems. In the conventional symbol-spaced method, the received signals at the relay(s) and destination are sampled at a rate equal to the baud rate (or symbol rate) of the system. However, in the fractionally-spaced sampling approach, the received signals are sampled at a rate at least equal to the Nyquist rate. Specifically, we consider the case in which the rate of the fractionally-spaced method is equal to the half of the symbol rate. Under the well designed pulse shaping filters at the source and relay(s), half-baud rate sampling is always more than Nyquist rate and no information loss (in the form of aliasing) occurs as a result of analog-to-digital conversion.

The rest of the chapter is organized as follows: In Section 5.2, we introduce the system model. In Section 5.3, considering both linear and decision feedback structures, we present the derivation of the fractionally-space FDEs (FS-FDEs) and symbol-spaced FDEs (SS-FDEs). Finally, we present simulation results in Section 5.4.

5.2 System Model

In the cooperative system under consideration, the source node S transmits information to the destination node D through the assistance of M relay nodes, $R_1, \cdots, R_M$ (see Fig. 4.1 in Chapter

4). We adopt the HF channel models presented in Section 3.2 of Chapter 3 for the underlying links. Furthermore, it is assumed that the temporal support of channel impulse response in the $A \to B$ link is less than or equal to ℓ_{AB} symbol intervals.

The block diagrams of the source, relay and destination terminals are illustrated in Fig. 5.1. At the source terminal (see Fig. 5.1.a.), a stream of $N \log M$ bits is parsed into N consecutive tuples of $\log M$ bits. Each tuple is mapped (using Gray coding) into a complex channel symbol belonging to a M-point linear-modulation constellation (such as PSK or QAM) with unit average power. The resulting sequence of symbols, denoted by $\mathbf{a} = [a_0, \cdots, a_{N-1}]^T$, is appended by a cyclic prefix (CP) with length N_1, and fed to the transmitter filter at a rate of $1/T_S$ where T_S seconds is the symbol time interval. The impulse response of the transmitter filter is given by the unit-energy root-raised-cosine function, $g(t)$, with the temporal support in the range of $[0, N_{RRC} T_S]$ and the bandwidth of $B_{RRC} = (1+\beta)/(2T_S)$ where $0 \le \beta \le 1$ is the roll-off factor.

After power amplification, the baseband signal transmitted by the source is given by

$$x_S(t) = \sqrt{P_0} \sum_{n=-N_1}^{N-1} \mathbf{a}(<n>_N)g\left(t - nT_S\right) \tag{5.1}$$

where P_0 is the average source power per symbol and can be written as $P_0 = K_0 P_T$ ($0 \le K_0 \le 1$). Here, P_T denotes the average total power budget (i.e., total power of source and relay nodes) for transmitting one symbol. Accordingly, the received signals at the mth relay and the destination are, respectively, given by

$$r_{SR_m}(t) = \sqrt{G_{SR_m} P_0} \sum_{n=-N_1}^{N} \mathbf{a}(<n>_N)g\left(t - nT_S\right) * h_{SR_m}(t) + n_{SR_m}(t) \tag{5.2}$$

$$r_{SD}(t) = \sqrt{P_0} \sum_{n=-N_1}^{N} \mathbf{a}(<n>_N)g\left(t - nT_S\right) * h_{SD}(t) + n_{SD}(t) \tag{5.3}$$

where $n_{SD}(t)$ and $n_{SR_m}(t)$ are the additive white complex Gaussian noises with zero mean and double sided PSD, N_0.
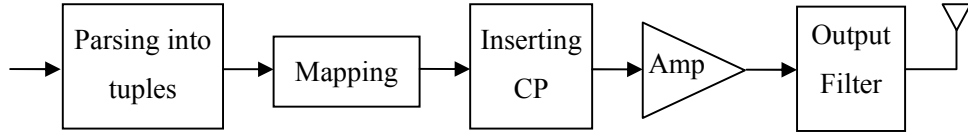
(a)
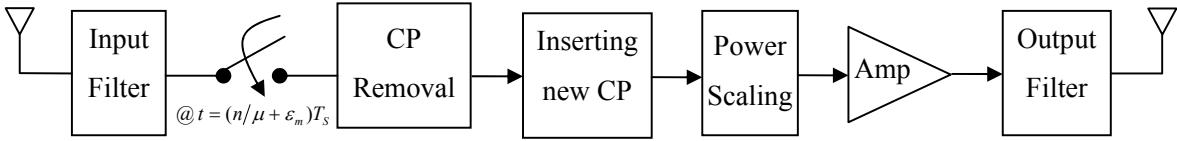
(b)
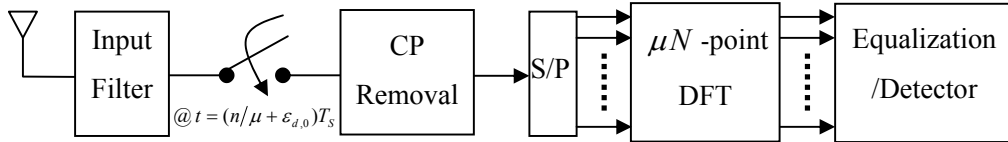
(c)

Figure 5.1 Block diagram of (a) source, (b) relay, and (c) destination

At the relay and destination (see Figs.5.1.b and 5.1.c.), the received signal is passed through the input filters with impulse responses $p_{\mathrm{R}_m}(t)$ and $p_{\mathrm{D}}(t)$, respectively. It is well known that the optimum linear receiver can be realized by matching the input filter to $g(t)$ convolved with the impulse response of the channel and sampling the result at the rate of $1/T_S$ [35]. This means that $p_{\mathrm{R}_m}(t)$ and $p_{\mathrm{D}}(t)$ must be, respectively, matched to $g(t)*h_{\mathrm{SR}_m}(t)$ and $g(t)*h_{\mathrm{SD}}(t)$ in the mth relay and destination. However, in practice, the channel impulse responses are usually time-variant. As a result, the optimum analog matched filters must be adaptively adjusted. A suboptimal solution is to match $p_{\mathrm{R}_m}(t)$ and $p_{\mathrm{D}}(t)$ to the transmitted signal pulse, $g(t)$. On the other hand, in the fractionally-spaced systems, a pre-equalizer shaping filter is not required, and

only an anti-aliasing low-pass filter is used. Therefore, in the following, we assume that $p_{R_m}(t) = p_D(t) = p(t) = g^*(-t)$ for the case of symbol-spaced sampling approach, and ideal low-pass filtering with cut-off frequency of $1/T_S$ is performed for the case of fractionally-spaced method (i.e., $p_{R_m}(t) = p_D(t) = p(t) = \sqrt{T_S/2}\,\text{sinc}(2t/T_S)$).

Assume that $N_1 = \max(\ell_{SD}, \ell_{SR_1}, \cdots, \ell_{SR_M}) + N_{RRC} + N_{sp,1}$ where $N_{sp,1}$ is the number of additional CP symbols inserted to the CPSC signal for the ease of symbol synchronization. The periodicity feature of the DFT allows us to represent the received signals at the destination and the mth relay, respectively, as (see Appendix E)

$$y_{SD}(t) = \sqrt{\frac{P_0}{N}} \sum_{k=-N}^{N} \tilde{H}_{SD}(k)\tilde{a}(k)\exp(j2\pi kt/NT_S) + v_{SD}(t) \tag{5.4}$$

$$y_{SR_m}(t) = \sqrt{\frac{G_{SR_m} P_0}{N}} \sum_{k=-N}^{N} \tilde{H}_{SR_m}(k)\tilde{a}(k)\exp(j2\pi kt/NT_S) + v_{SR_m}(t) \tag{5.5}$$

for $-N_{sp,1}T_S \le t \le NT_S$, where $\tilde{a}(k) = (1/\sqrt{N})\sum_{n=0}^{N-1} \mathbf{a}(n)W_N^{kn}$, $W_N = \exp(-j2\pi/N)$, $\tilde{H}_{SD}(k) = \tilde{h}_{SD}(k)\,\tilde{g}(k)\,\tilde{p}(k)$, $\tilde{H}_{SR_m}(k) = \tilde{h}_{SR_m}(k)\,\tilde{g}(k)\,\tilde{p}(k)$, $\tilde{g}(k) \triangleq \tilde{g}(k/NT_S)/\sqrt{T_S}$, $\tilde{p}(k) \triangleq \tilde{p}(k/NT_S)/\sqrt{T_S}$, $\tilde{h}_{SD}(k) \triangleq \tilde{h}_{SD}(k/NT_S)$, and $\tilde{h}_{SR_m}(k) \triangleq \tilde{h}_{SR_m}(k/NT_S)$. Here, $\tilde{g}(f)$, $\tilde{p}(f)$, $\tilde{h}_{SD}(f)$, and $\tilde{h}_{SR_m}(f)$ are the continuous Fourier transform of, respectively, $g(t)$, $p(t)$, $h_{SD}(t)$, and $h_{SR_m}(t)$. Furthermore, $v_{SD}(t)$ and $v_{SR_m}(t)$ denote the colored Gaussian noise terms with PSD $S_0(f) = N_0\,|\tilde{p}(f)|^2$.

The received signals, $y_{SD}(t)$, and $y_{SR_m}(t)$, are sampled at a rate of μ/T_S where $\mu = 1$ in the symbol-spaced sampling approach, and $\mu = 2$ in the fractionally-spaced sampling scheme. Therefore, from (5.4) and (5.5), we have

$$\mathbf{y}_{SD}(n) = y_{SD}(n\frac{T_S}{\mu} + \varepsilon_{d,0}T_S) = \sqrt{\frac{P_0}{N}} \sum_{k=-N}^{N} \tilde{H}_{SD}(k)\tilde{a}(k)W_N^{-k\varepsilon_{d,0}}W_{\mu N}^{-kn} + \mathbf{v}_{SD}(n) \tag{5.6}$$

$$\mathbf{y}_{SR_m}(n) = y_{SR_m}(n\frac{T_S}{\mu} + \varepsilon_m T_S) = \sqrt{\frac{G_{SR_m} P_0}{N}} \sum_{k=-N}^{N} \tilde{H}_{SR_m}(k)\tilde{a}(k)W_N^{-k\varepsilon_m}W_{\mu N}^{-kn} + \mathbf{v}_{SR_m}(n) \tag{5.7}$$

for $n = 0, \cdots, \mu N - 1$, where $\mathbf{v}_{\mathrm{SD}}(n) = v_{\mathrm{SD}}(nT_S/\mu + \varepsilon_{d,0}T_S)$, $\mathbf{v}_{\mathrm{SR}_m}(n) = v_{\mathrm{SR}_m}(nT_S/\mu + \varepsilon_m T_S)$, $\varepsilon_{d,0}T_S$ is the sampling phase error at the destination during the broadcasting phase, and $\varepsilon_m T_S$ is the sampling phase error at the mth relay $(-N_{sp,1} \le \varepsilon_{d,0}, \varepsilon_m \le 0)$.

Assume that the ith relay is selected to transmit its signal. First, a new CP with a length of $N_2 = \mu(\ell_{\mathrm{R}_i \mathrm{D}} + N_{RRC} + N_{sp,2})$ is inserted into the sampled sequence, $\mathbf{y}_{\mathrm{SR}_i}$. Then, after power scaling and amplification, the resulting signal is applied to the output filter with the rate of μ/T_S. Therefore, the baseband signal transmitted by the ith relay can be expressed as

$$x_{\mathrm{R}_i}(t) = \sqrt{\alpha_{\mathrm{R}_i} P_1} \sum_{n=-N_2}^{\mu N - 1} \mathbf{y}_{\mathrm{SR}_i}(< n >_{\mu N}) g(t - nT_S/\mu) \tag{5.8}$$

where α_{R_i} is the scaling factor to ensure that the average power consumed per symbol by the ith relay is $P_1 = (1 - K_0)P_T$. Assuming that $E\{a(n)a^*(m)\} = \delta(n - m)$, we can calculate α_{R_i} as (see Appendix F)

$$\alpha_{\mathrm{R}_i} = \begin{cases} \dfrac{1}{G_{\mathrm{SR}_i} P_0 \left(1 + \dfrac{1}{N} \displaystyle\sum_{k=1}^{2N-1} (2N - k)\left[g_{\mathrm{RC}}\left(\dfrac{kT_S}{2}\right)\right]^2\right) + 2N_0}, & \text{for FS-FDE} \\[3em] \dfrac{1}{G_{\mathrm{SR}_i} P_0 \left(1 - \dfrac{\beta}{4}\right) + N_0}, & \text{for SS-FDE} \end{cases} \tag{5.9}$$

where $g_{\mathrm{RC}} = g(t) * g^*(-t)$ is the impulse response of a raised cosine filter with the roll-off factor β and symbol rate $1/T_S$. From (5.9), it is observed that in the symbol-spaced sampling systems and for the special case of $\beta = 0$, α_{R_i} is reduced to the well known form of $1/(G_{\mathrm{SR}_i} P_0 + N_0)$ which is known as "average-power scaling" (APS) [52] or "fixed relay gain" [64].

After passing through the $\mathrm{R}_i \to \mathrm{D}$ channel and the input filter of the destination, the received signal at the destination is sampled at the rate of μ/T_S. The resulting signal is given by

$$\mathbf{y}_{\mathrm{R}_i \mathrm{D}}(n) = \sqrt{\frac{\mu G_{\mathrm{R}_i \mathrm{D}} \alpha_{\mathrm{R}_i} P_1}{N}} \sum_{k=-N}^{N} \tilde{H}_{\mathrm{R}_i \mathrm{D}}(k) \tilde{y}_{\mathrm{SR}_i}(k) W_N^{-k\varepsilon_{d,1}} W_{\mu N}^{-kn} + \mathbf{v}_{\mathrm{R}_i \mathrm{D}}(n) \tag{5.10}$$

for $n = 0, \cdots, \mu N - 1$, where $\tilde{H}_{R,D}(k) = \tilde{h}_{R,D}(k)\tilde{g}(k)\tilde{p}(k)$, $\tilde{h}_{R,D}(k) \triangleq \tilde{h}_{R,D}(k/NT_S)$, $\tilde{h}_{R,D}(f)$ is the continuous Fourier transform of $h_{R,D}(t)$, $\tilde{y}_{SR_i}(k) = (1/\sqrt{\mu N})\sum_{n=0}^{\mu N-1} y_{SR_i}(n)W_{\mu N}^{kn}$, $v_{R,D}(n) = v_{R,D}(nT_S/\mu + \varepsilon_{d,1}T_S)$, $v_{R,D}(t)$ is a colored complex Gaussian noise with $S_0(f) = N_0 |\tilde{p}(f)|^2$, and $\varepsilon_{d,1}T_S$ is the sampling phase error at the destination during the relaying phase ($-N_{sp,2} \leq \varepsilon_{d,1} \leq 0$).

5.3 Equalization in the Frequency Domain

Over one broadcasting-relaying cycle, the destination has received two signals, namely, $\mathbf{y}_{SD}$ and $\mathbf{y}_{R,D}$ (of size $\mu N \times 1$) given respectively by (5.6) and (5.10). After taking μN-point DFT of these signals, we have the following cases for the fractionally-spaced frequency-domain equalization (FS-FDE) and symbol-spaced FDE (SS-FDE) systems.

Case 1: FS-FDE

In this case, we have $\mu = 2$, $\tilde{p}(k) = 1/\sqrt{2}$, and $S_0(f) = N_0 T_S \Pi(T_S f/2)/2$ where $\Pi(f)$ is 1 for $-1/2 \leq f \leq 1/2$ and 0, otherwise. Therefore, based on (5.6), (5.7), and (5.10), we can write

$$\tilde{\mathbf{y}}_{FSE,SD} = \mathbf{Q}_{2N} \mathbf{y}_{SD}\big|_{\mu=2} = \mathbf{D}_{FSE}\tilde{\mathbf{a}}_{2N} + \tilde{\mathbf{v}}_{FSE,SD} \tag{5.11}$$

$$\tilde{\mathbf{y}}_{FSE,R,D} = \mathbf{Q}_{2N} \mathbf{y}_{R,D}\big|_{\mu=2} = \mathbf{D}_{FSE,i}\tilde{\mathbf{a}}_{2N} + \mathbf{C}_{FSE,i}\tilde{\mathbf{v}}_{FSE,SR_i} + \tilde{\mathbf{v}}_{FSE,R,D} \tag{5.12}$$

where $\mathbf{Q}_{2N} = [q_{n,k}]$ is the 2N-point DFT matrix with $q_{n,k} = W_{2N}^{kn}/\sqrt{2N}$ ($n,k = 0,1,\cdots,2N-1$), $\tilde{\mathbf{a}}_{2N} = [\tilde{\mathbf{a}}^T | \tilde{\mathbf{a}}^T]^T$, $\tilde{\mathbf{a}} = \mathbf{Q}_N \mathbf{a}$, $\mathbf{D}_{FSE} = \text{diag}\{\mathbf{d}_{FSE}\}$, $\mathbf{D}_{FSE,i} = \text{diag}\{\mathbf{d}_{FSE,i}\}$, $\mathbf{C}_{FSE,i} = \text{diag}\{\mathbf{c}_{FSE,i}\}$, $\mathbf{d}_{FSE}(k) = \sqrt{P_0}\tilde{h}_{SD}([k]_N)\tilde{g}([k]_N)W_N^{-[k]_N\varepsilon_{d,0}}$, $\mathbf{d}_{FSE,i}(k) = \sqrt{2G_{R,D}\alpha_{R_i}P_1 G_{SR_i}P_0}\tilde{h}_{R,D}([k]_N)(\tilde{g}([k]_N))^2$ $\tilde{h}_{SR_i}([k]_N) W_N^{-[k]_N(\varepsilon_{d,1}+\varepsilon_i)}$, $\mathbf{c}_{FSE,i}(k) = \sqrt{2G_{R,D}\alpha_{R_i}P_1} \tilde{h}_{R,D}([k]_N)\tilde{g}([k]_N)W_N^{-[k]_N\varepsilon_{d,1}}$, $k = 0,\cdots,2N-1$, and $[k]_N$ is equal to k if $k \leq N$, and equal to $k - 2N$ if $k > N$. In (5.11) and (5.12), $\tilde{\mathbf{v}}_{FSE,SD}$, $\tilde{\mathbf{v}}_{FSE,SR_i}$, and $\tilde{\mathbf{v}}_{FSE,R,D}$ are, respectively, the 2N-point DFT of $\mathbf{v}_{SD}$, $\mathbf{v}_{SR_i}$, and $\mathbf{v}_{R,D}$.

Case 2: SS-FDE

In this case, we have $\mu = 1$, $\tilde{p}(k) = \tilde{g}^*(k)$, and $S_0(f) = N_0 |\tilde{g}(f)|^2$. Therefore, based on (5.6), (5.7), and (5.10), we can write

$$\tilde{\mathbf{y}}_{SSE,\text{SD}} = \mathbf{Q}_N\,\mathbf{y}_{\text{SD}}\big|_{\mu=1} = \mathbf{D}_{SSE}\tilde{\mathbf{a}} + \tilde{\mathbf{v}}_{SSE,\text{SD}} \tag{5.13}$$

$$\tilde{\mathbf{y}}_{SSE,\text{R}_i\text{D}} = \mathbf{Q}_N\,\mathbf{y}_{\text{R}_i\text{D}}\big|_{\mu=1} = \mathbf{D}_{SSE,i}\mathbf{C}_{SSE,i}\tilde{\mathbf{a}} + \mathbf{C}_{SSE,i}\tilde{\mathbf{v}}_{SSE,\text{SR}_i} + \tilde{\mathbf{v}}_{SSE,\text{R}_i\text{D}} \tag{5.14}$$

where $\mathbf{D}_{SSE} = \text{diag}\{\mathbf{d}_{SSE}\}$, $\mathbf{D}_{SSE,i} = \text{diag}\{\mathbf{d}_{SSE,i}\}$, $\mathbf{C}_{SSE,i} = \text{diag}\{\mathbf{c}_{SSE,i}\}$, $d_{SSE}(k) = \sqrt{P_0}$ $\sum_{m=k,k-N}\tilde{h}_{\text{SD}}(m)\left|\tilde{g}(m)\right|^2 W_N^{-m\varepsilon_{d,0}}$, $d_{SSE,i}(k) = \sqrt{G_{\text{SR}_i}P_0}\sum_{m=k,k-N}\tilde{h}_{\text{SR}_i}(m)\left|\tilde{g}(m)\right|^2 W_N^{-m\varepsilon_i}$, and $c_{SSE,i}(k) = \sqrt{G_{\text{R}_i\text{D}}\alpha_{\text{R}_i}P_1}\sum_{m=k,k-N}\tilde{h}_{\text{R}_i\text{D}}(m)\left|\tilde{g}(m)\right|^2 W_N^{-m\varepsilon_{d,1}}$. In (5.13), and (5.14), $\tilde{\mathbf{v}}_{SSE,\text{SD}}$, $\tilde{\mathbf{v}}_{SSE,\text{SR}_i}$, and $\tilde{\mathbf{v}}_{SSE,\text{R}_i\text{D}}$ are the N-point DFT of $\mathbf{v}_{\text{SD}}$, $\mathbf{v}_{\text{SR}_i}$, and $\mathbf{v}_{\text{R}_i\text{D}}$, respectively.

For both cases, by concatenating the received signals in the frequency-domain into one column vector, we can write

$$\tilde{\mathbf{y}}_i = \mathbf{D}_i\tilde{\mathbf{A}} + \tilde{\mathbf{v}}_i. \tag{5.15}$$

For the case of FS-FDE, we have $\tilde{\mathbf{y}}_i = [\tilde{\mathbf{y}}_{FSE,\text{SD}}^T \mid \tilde{\mathbf{y}}_{FSE,\text{R}_i\text{D}}^T]^T$, $\mathbf{D}_i = [\mathbf{D}_{FSE} \mid \mathbf{D}_{FSE,i}]^T$, $\tilde{\mathbf{A}} = [\tilde{\mathbf{a}}_{2N}^T \mid \tilde{\mathbf{a}}_{2N}^T]^T$, and $\tilde{\mathbf{v}}_i = [\tilde{\mathbf{v}}_{FSE,\text{SD}}^T \mid (\mathbf{C}_{FSE,i}\tilde{\mathbf{v}}_{FSE,\text{SR}_i} + \tilde{\mathbf{v}}_{FSE,\text{R}_i\text{D}})^T]^T$. On the other hand, for the case of SS-FDE, we have $\tilde{\mathbf{y}}_i = [\tilde{\mathbf{y}}_{SSE,\text{SD}}^T \mid \tilde{\mathbf{y}}_{SSE,\text{R}_i\text{D}}^T]^T$, $\mathbf{D}_i = [\mathbf{D}_{SSE} \mid \mathbf{D}_{SSE,i}\mathbf{C}_{SSE,i}]^T$, $\tilde{\mathbf{A}} = \tilde{\mathbf{a}}_{2N}$, and $\tilde{\mathbf{v}}_i = [\tilde{\mathbf{v}}_{SSE,\text{SD}}^T \mid (\mathbf{C}_{SSE,i}\tilde{\mathbf{v}}_{SSE,\text{SR}_i} + \tilde{\mathbf{v}}_{SSE,\text{R}_i\text{D}})^T]^T$.

In the following, we derive the linear and decision feedback FDEs for both cases.

5.3.1 Linear Equalization (LE)

The structure of the LE is depicted in Fig. 5.2. The objective of the linear minimum-mean-square error (MMSE) equalization is to find a weighting matrix, $\mathbf{M}_{LE,i}$, such that $E[\|\,\tilde{\mathbf{x}}_i - \tilde{\mathbf{a}}\,\|^2] = E[\|\,\mathbf{x}_i - \mathbf{a}\,\|^2]$ is minimized where $\tilde{\mathbf{x}}_i = \mathbf{M}_{LE,i}\tilde{\mathbf{y}}_i$ and $\mathbf{x}_i = \mathbf{Q}_N^*\tilde{\mathbf{x}}_i$.
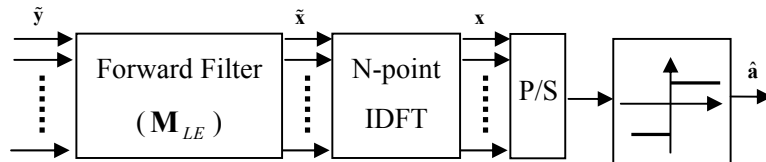

Figure 5.2 Internal structure of the linear equalizer

64

Based on the so-called orthogonality principal, we have

$$E\left[(\tilde{\mathbf{x}} - \tilde{\mathbf{a}})\tilde{\mathbf{y}}^*\right] = \mathbf{0} \tag{5.16}$$

where we have dropped the sub-index i for the convenience. As a result, the weighting matrix is given by

$$\mathbf{M}_{LE} = \mathbf{JD}^*\left(\mathbf{DJ}^*\mathbf{JD}^* + \mathbf{\Gamma}_{\tilde{\mathbf{v}}}\right)^{-1} = \left(\mathbf{I} + \mathbf{JD}^*\mathbf{\Gamma}_{\tilde{\mathbf{v}}}^{-1}\mathbf{DJ}^*\right)^{-1}\mathbf{JD}^*\mathbf{\Gamma}_{\tilde{\mathbf{v}}}^{-1} \tag{5.17}$$

where $\mathbf{J} = \mathbf{1}_{1\times 2\mu} \otimes \mathbf{I}_N$, and $\mathbf{\Gamma}_{\tilde{\mathbf{v}}} = N_0[\mathbf{I}_{2N} \mid \mathbf{C}_{FSE}\mathbf{C}_{FSE}^* + \mathbf{I}_{2N}]^T$ for the FS-FDE and $\mathbf{\Gamma}_{\tilde{\mathbf{v}}} = N_0[\mathbf{I}_N \mid \mathbf{C}_{SSE}\mathbf{C}_{SSE}^* + \mathbf{I}_N]^T$ for the SS-FDE. The second equality in (5.17) is based on the matrix-inversion lemma[1].

After calculating $\tilde{\mathbf{x}} = \mathbf{M}_{LE}\mathbf{y}$, an N-point IDFT is applied, and the resulting vector, $\mathbf{x}$, is fed to a slicer device, operating on a symbol-by-symbol basis, to make a hard estimation about the transmitted vector $\mathbf{a}$. Defining the error autocorrelation matrix as $\mathbf{R}_{\mathbf{e}} = (1/N)E[(\mathbf{x}-\mathbf{a})(\mathbf{x}-\mathbf{a})^*]$, we have

$$\mathbf{R}_{\mathbf{e}} = \frac{1}{N}\mathbf{Q}_N^*E\left[\mathbf{Q}_N(\mathbf{x}-\mathbf{a})(\mathbf{x}-\mathbf{a})^*\mathbf{Q}_N^*\right]\mathbf{Q}_N = \frac{1}{N}\mathbf{Q}_N^*E\left[(\mathbf{M}_{LE}\mathbf{y}-\mathbf{Q}_N\mathbf{a})(\mathbf{M}_{LE}\mathbf{y}-\mathbf{Q}_N\mathbf{a})^*\right]\mathbf{Q}_N. \tag{5.18}$$

By inserting (5.17) into (5.18) we obtain

$$\mathbf{R}_{\mathbf{e}} = \frac{1}{N}\mathbf{Q}^*\left(\mathbf{I}_N + \mathbf{JD}^*\mathbf{\Gamma}_{\tilde{\mathbf{v}}}^{-1}\mathbf{DJ}^*\right)^{-1}\mathbf{Q}. \tag{5.19}$$

Therefore, the associated MSE of the LE method is given by

$$MSE_{LE} = \text{trace}\left(\mathbf{R}_{\mathbf{e}}\right) = \frac{1}{N}\text{trace}\left(\left(\mathbf{I}_N + \mathbf{JD}^*\mathbf{\Gamma}_{\tilde{\mathbf{v}}}^{-1}\mathbf{DJ}^*\right)^{-1}\right). \tag{5.20}$$

---

[1] For matrices A, B, C, and D of compatible dimensions, it holds that $(\mathbf{A} + \mathbf{BCD})^{-1} = \mathbf{A}^{-1} - \mathbf{A}^{-1}\mathbf{B}(\mathbf{C}^{-1} - \mathbf{D}\mathbf{A}^{-1}\mathbf{B})^{-1}\mathbf{D}\mathbf{A}^{-1}$.

5.3.2 Decision-Feedback Equalization (DFE)

The structure of the DFE is depicted in Fig. 5.3. Similar to the LE, the received signal is first applied to a frequency-domain feed-forward filter, and then, returned back to the time domain via an IDFT operation to feed a symbol-by-symbol (hard-decision) slicer. However, in contrast to the LE, each detected symbol lines up in the input port of a feedback filter to contribute in the ISI reduction over the symbols that have not yet been detected. The output of the feedback filter at time instance n, $\mathbf{u}(n)$, can be considered as an estimation made based on $\hat{\mathbf{a}}(0), \cdots, \hat{\mathbf{a}}(n-1)$ about the ISI generated by the first $(n-1)$ transmitted symbols on the nth one. This output is then subtracted from $\mathbf{x}(n)$, and the resulting signal, i.e., $\mathbf{t}(n) = \mathbf{x}(n) - \mathbf{u}(n)$, is passed through the slicer where a hard estimation about the transmitted symbol $\mathbf{a}(n)$ is made. Feedback processing is carried out in the time domain through a time-varying finite impulse response (FIR) filter. Considering an $N \times N$ unit lower triangular matrix $\mathbf{B}_{DFE}$, the output of the filter at time instance n, $\mathbf{u}(n)$, can be modeled as $\mathbf{u}(n) = (\mathbf{B}_{DFE,n} - \mathbf{I}_{N,n})\hat{\mathbf{a}}_n$ where $\mathbf{B}_{DFE,n}$ is the nth row of the matrix $\mathbf{B}_{DFE}$, $\mathbf{I}_{N,n}$ is the nth row of the matrix $\mathbf{I}_N$, and $\hat{\mathbf{a}}_n \triangleq [\hat{\mathbf{a}}(0), \cdots, \hat{\mathbf{a}}(n-1), \mathbf{0}_{1 \times (N-n)}]^T$.
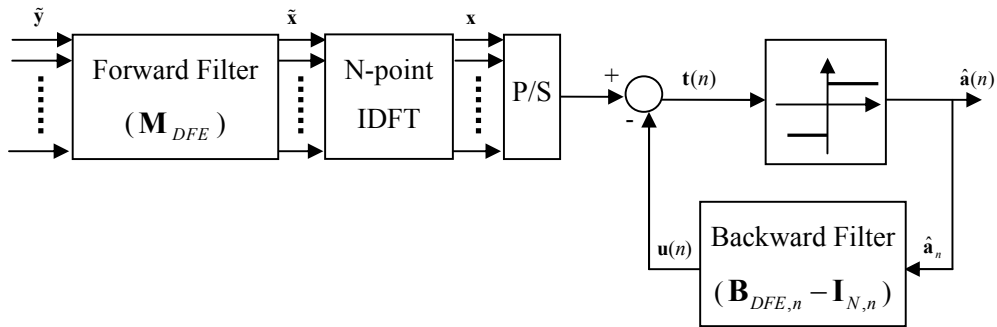

Figure 5.3 Internal structure of the DFE equalizer

A performance measure of the DFE receiver is the error at the input of the decision device, i.e., $\mathbf{e} = \mathbf{t} - \mathbf{a}$. In the MMSE based equalization, the feed-forward matrix $\mathbf{M}_{DFE}$ and the feedback

matrix $\mathbf{B}_{DFE}$ are designed to minimize $E \| \mathbf{e} \|^2$. Using the standard assumption of correct past decisions, we have

$$\begin{aligned}
\| \mathbf{e} \|^2 &= \| \mathbf{t} - \mathbf{a} \|^2 = \| \mathbf{Q}_N \left(\mathbf{t} - \mathbf{a} \right) \|^2 \\
&= \| \tilde{\mathbf{x}} - \mathbf{Q}_N \left(\mathbf{B}_{DFE} - \mathbf{I}_N \right) \mathbf{a} - \mathbf{Q}_N \mathbf{a} \|^2 = \| \tilde{\mathbf{x}} - \mathbf{Q}_N \mathbf{B}_{DFE} \mathbf{a} \|^2
\end{aligned} \tag{5.21}$$

Following the same approach as in [65], we first assume that $\mathbf{B}_{DFE}$ is fixed and we obtain the matrix $\mathbf{M}_{DFE}$ which minimizes $E \| \mathbf{e} \|^2$. Using the orthogonality principle, we can write

$$E \left[\left(\tilde{\mathbf{x}} - \mathbf{Q}_N \mathbf{B}_{DFE} \mathbf{a} \right) \tilde{\mathbf{y}}^* \right] = 0. \tag{5.22}$$

By inserting $\tilde{\mathbf{x}} = \mathbf{M}_{DFE} \mathbf{y}$ into (5.22) and after some straightforward manipulations, $\mathbf{M}_{DFE}$ is given by

$$\begin{aligned}
\mathbf{M}_{DFE} &= \mathbf{Q} \mathbf{B}_{DFE} \mathbf{Q}^* \mathbf{J} \mathbf{D}^* \left(\mathbf{D} \mathbf{J}^* \mathbf{J} \mathbf{D}^* + \mathbf{\Gamma}_{\tilde{\mathbf{v}}} \right)^{-1} \\
&= \mathbf{Q} \mathbf{B}_{DFE} \mathbf{Q}^* \left(\mathbf{I} + \mathbf{J} \mathbf{D}^* \mathbf{\Gamma}_{\tilde{\mathbf{v}}}^{-1} \mathbf{D} \mathbf{J}^* \right)^{-1} \mathbf{J} \mathbf{D}^* \mathbf{\Gamma}_{\tilde{\mathbf{v}}}^{-1}
\end{aligned} \tag{5.23}$$

where the second equality is based on the matrix inversion lemma. By defining $\mathbf{R}_{\mathbf{e}} = (1/N) E (\mathbf{t} - \mathbf{a})(\mathbf{t} - \mathbf{a})^*$, we have

$$\mathbf{R}_{\mathbf{e}} = \frac{1}{N} \mathbf{Q}_N^* E \left[\left(\mathbf{M}_{DFE} \mathbf{y} - \mathbf{Q}_N \mathbf{B}_{DFE} \mathbf{a} \right) \left(\mathbf{M}_{DFE} \mathbf{y} - \mathbf{Q}_N \mathbf{B}_{DFE} \mathbf{a} \right)^* \right] \mathbf{Q}_N. \tag{5.24}$$

By replacing (5.23) into (5.24), we obtain

$$\mathbf{R}_{\mathbf{e}} = \frac{1}{N} \mathbf{B}_{DFE} \mathbf{Q}^* \left(\mathbf{I} + \mathbf{J} \mathbf{D}^* \mathbf{\Gamma}_{\tilde{\mathbf{v}}}^{-1} \mathbf{D} \mathbf{J}^* \right)^{-1} \mathbf{Q} \mathbf{B}_{DFE}^* \tag{5.25}$$

Using the results in [65], trace($\mathbf{R}_{\mathbf{e}}$) is minimized by setting $\mathbf{B}_{DFE} = \mathbf{U}^{-1}$, where $\mathbf{U}$ is a unit lower triangular matrix given by the Cholesky decomposition of $\mathbf{Q}^* \left(\mathbf{I} + \mathbf{J} \mathbf{D}^* \mathbf{\Gamma}_{\tilde{\mathbf{v}}}^{-1} \mathbf{D} \mathbf{J}^* \right)^{-1} \mathbf{Q}$ in the form of $\mathbf{U} \Delta \mathbf{U}^*$ where Δ is a diagonal matrix with positive diagonal elements. Therefore, the MSE associated to the DFE is given by

$$MSE_{DFE} = \text{trace}(\mathbf{R_e}) = \frac{1}{N}\text{trace}(\Delta) .$$

(5.26)

Based on the MSE expressions derived in (5.20) and (5.26), we have the following proposition about the performance of the cooperative FS-FDE and SS-FDE equalization techniques under consideration.

Proposition: The performance of FS-FDE based cooperative equalizers does not depend on the sampling-phase error. On the other hand, in SS-FDE-based cooperative equalization, sampling-phase errors affect the system performance.

Proof: From (5.20) and (5.26), it is observed that the term $\mathbf{JD}^*\mathbf{\Gamma}_{\tilde{v}}^{-1}\mathbf{DJ}^*$ is the only term that may reflect the dependency of the MSE of the LE and DFE techniques on the sampling-phase errors. Based on the underlying structure of $\mathbf{\Gamma}_{\tilde{v}}$ and $\mathbf{D}$, $\mathbf{JD}^*\mathbf{\Gamma}_{\tilde{v}}^{-1}\mathbf{DJ}^*$ is an $N \times N$ diagonal matrix whose kth diagonal entry is given by

$$\frac{\displaystyle\sum_{m=k,k-N}\left(P_0\left|\tilde{h}_{SD}(m)\tilde{g}(m)\right|^2 + 2G_{RD}\alpha_R P_1 G_{SR} P_0\left|\tilde{h}_{RD}(m)\tilde{h}_{SR}(m)\left(\tilde{g}(m)\right)^2\right|^2\right)}{2G_{RD}\alpha_R P_1 N_0 \displaystyle\sum_{m=k,k-N}\left|\tilde{h}_{RD}(m)\tilde{g}(m)\right|^2 + N_0}$$

(5.27)

for the case of FS-FDE and

$$\frac{P_0}{G_{RD}\alpha_R P_1 N_0\left|\displaystyle\sum_{m=k,k-N}\tilde{h}_{RD}(m)\left|\tilde{g}(m)\right|^2 W_N^{-m\varepsilon_{d,1}}\right|^2 + N_0}\left\{\left|\sum_{m=k,k-N}\tilde{h}_{SD}(m)\left|\tilde{g}(m)\right|^2 W_N^{-m\varepsilon_{d,0}}\right|^2\right.$$

$$\left. + G_{SR}G_{RD}\alpha_R P_1\left|\left(\sum_{m=k,k-N}\tilde{h}_{SR}(m)\left|\tilde{g}(m)\right|^2 W_N^{-m\varepsilon}\right)\left(\sum_{m=k,k-N}\tilde{h}_{RD}(m)\left|\tilde{g}(m)\right|^2 W_N^{-m\varepsilon_{d,1}}\right)\right|^2\right\}$$

(5.28)

for the case of SS-FDE. From (5.27), we note that the performance of the FS-FDE is independent of the sampling-phase errors. On the other hand, from (5.28), we observe that MSE depends on the sampling-phase errors in the SS-FDE method, and the superposition of the aliasing roll-off components occurs. This superposition, for certain clock phases, may result in a spectral null,

and subsequently, in the degradation of the SS-FDE performance [35], [36]. In the simulation results provided in the next section, we will demonstrate that this dependency significantly degrades the performance of the SS-FDE equalizers.

5.4 Numerical Results

In this section, we investigate the BER performance of cooperative systems with different equalization techniques based on Monte Carlo simulations. Throughout this section, it is assumed that the selection of relays is based on maximizing the SNR at destination from the MFB point of view, c.f., Chapter 4, (4.22), $\beta = 0.5$, and the adopted modulation scheme is BPSK and QPSK for the non-cooperative (i.e., direct transmission) and cooperative systems, respectively. Following the waveform specification in MIL-STD 188-110A/B/C, it is assumed that the number of symbols in each packet is 32, and $T_S = 1/2400$ seconds. Also, unless otherwise specified, the underlying links among different nodes are typical slowly-time-varying ($f_d \leq 2\,\mathrm{Hz}$) and frequency-selective HF skywave/NVIS channels consisting of two propagation paths with the same attenuations and a delay spread equal to $5T_S\,(\approx 2.1)$ msec.

Fig. 5.4 shows the BER performance of the linear SS-FDE and FS-FDE systems for $E_b/N_0 = 20\,\mathrm{dB}$, and various sampling-phase errors at the relay(s) and destination terminals when the delay spread is $5T_S$ (Fig. 5.4.a) and 2 msec (Fig. 5.4.b). It is assumed that $G_{\mathrm{SR}_m} = G_{\mathrm{R}_m\mathrm{D}} = 0$ dB and EPA ($K_0 = 0.5$) is in place. It is observed that the performance of SS-FDE systems is highly dependent on the variations of the sampling-phase error. In particular, for certain values of errors, the BER performance of the cooperative scheme approaches to that of no-relay system whereas FS-FDE successfully compensates the phasing-error and retains the cooperative diversity. A comparison between Fig. 5.4.a and Fig. 5.4.b shows that the underlying channel profile does affect the behavior and the amount of variation of the BER performance with respect to phasing-errors. Specifically, for the delay spread of $5T_S$, the performances of the FS-FDE and
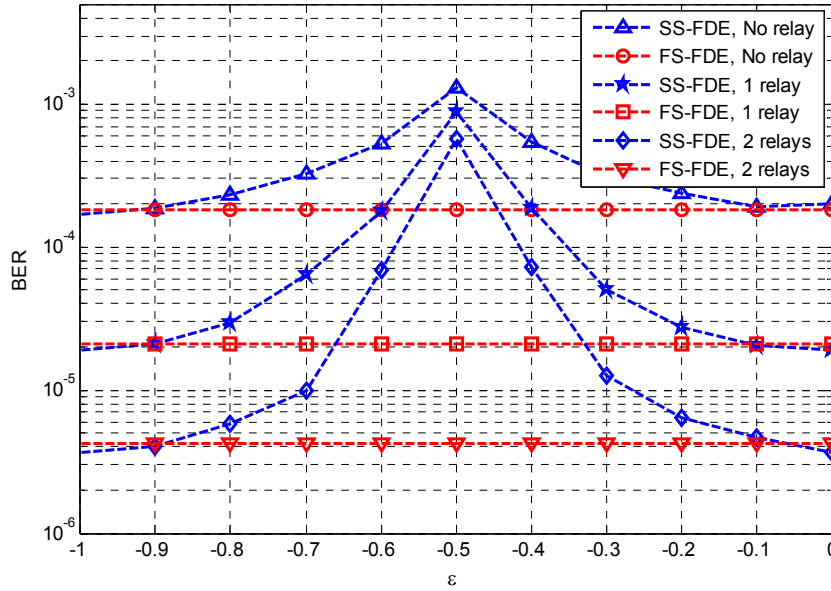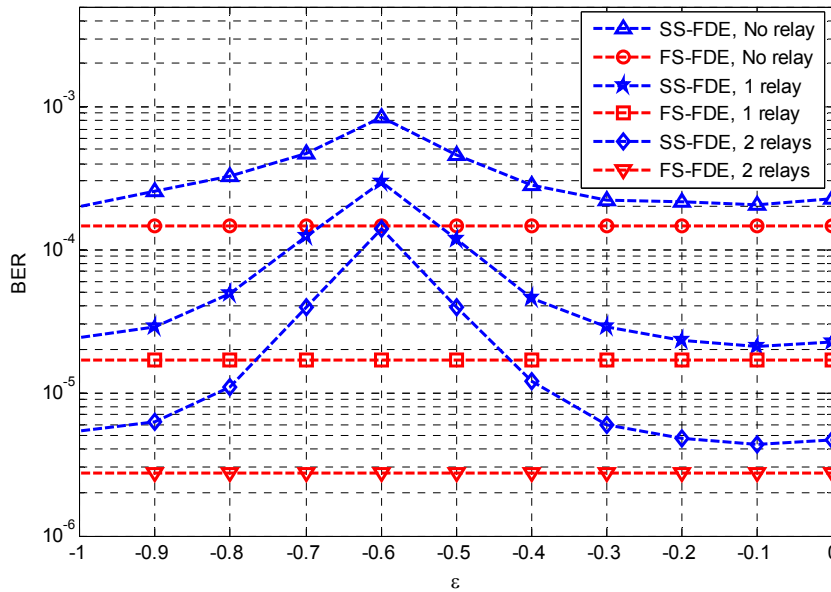
Figure 5.4 BER performances of the SS-FDE and FS-FDE systems with different number of relays. In (a), delay spread is $5T_S$ and in (b), delay spread is 2msec.

SS-FDE are the same when the phasing error is zero (or $-T_s$), and the highest degradation of the SS-FDE occurs at the phasing-error equal to $-0.5T_s$. On the other hand, when the delay spread is 2 msec (Fig. 5.4.b), FS-FDE-based system outperforms the SS-FDE-based counterpart even under the no phasing error scenario, and the highest degradation of the SS-FDE-systems takes place when the phasing-error is equal to $-0.6T_s$.

Fig. 5.5 displays the BER performance of FS-FDE- and SS-FDE- based linear equalization for different number of relays. We consider an HF network scenario with sky wave source-to-relay(s)/destination and NVIS relay-to-destination links (see Fig. 3.2 in Chapter 3) with $G_{SD} = G_{SR_m} = 0\,dB$, and $G_{R_mD} = 10\,dB$. By solving the optimum (from MFB perspective) power allocation problem (see Chapter 4, eq. (4.23)), the value of K_0 is found to be 0.77 and 0.67 for
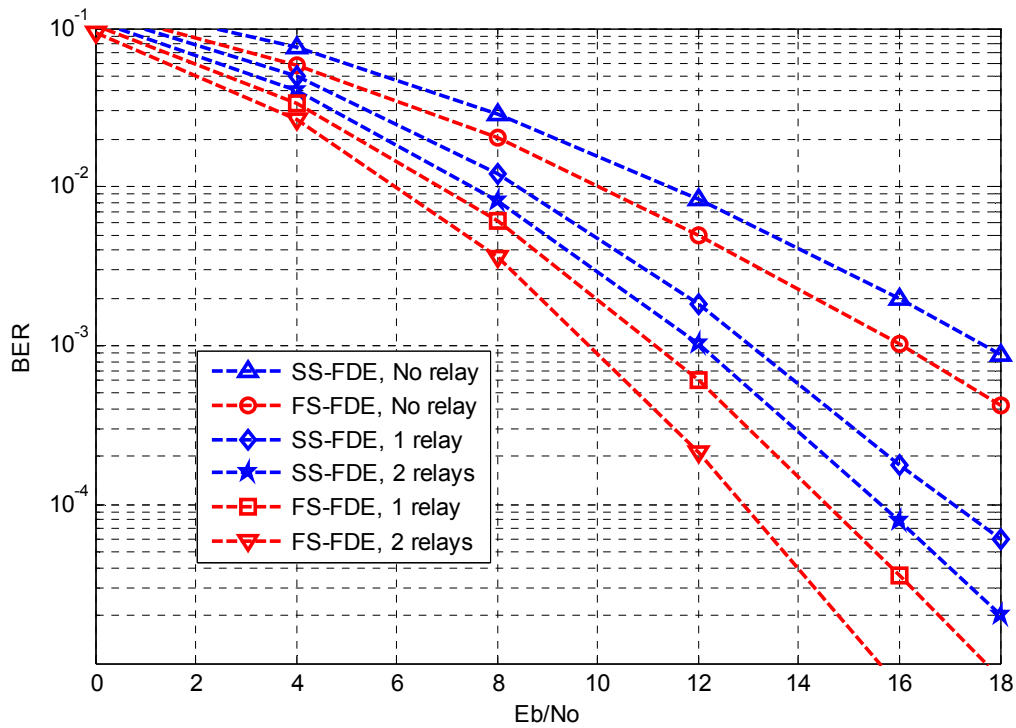

Figure 5.5: BER performances of SS-FDE and FS-FDE systems with different number of relays. $G_{SR_m} = 0\,dB$, $G_{R_mD} = 10\,dB$, $L_{SD} = L_{SR_m} = L_{R_mD} = 2$, random phase error, and MFB based OPA is in place.

the one- and two-relay cooperative systems under consideration, respectively. Moreover, the sampling phase error at the relay(s) and destination terminals is randomly chosen with uniform distribution from the interval $[-T_S, 0]$ for each transmitted block. It is observed from Fig. 5.5 that the FS-FDE method outperforms the SS-FDE approach. Specifically, at a target BER of 10^{-3}, the performance gap between the FS-FDE- and SS-FDE-based methods is 1.6 dB for the non-cooperative scenario. This performance gap climbs up to 1.9 and 2.25 dB for cooperative systems with one and two relays, respectively.

Fig. 5.6 shows the BER performance of DFE- and LE- techniques for both SS-FDE and FS-FDE assuming single-relay cooperative systems under the uniform random sampling phase errors. We assume that $G_{SD} = G_{SR_m} = 0\,\text{dB}$, $G_{R_mD} = 10\,\text{dB}$, $L_{SD} = L_{SR_m} = 5$, $L_{R_mD} = 10$, and the
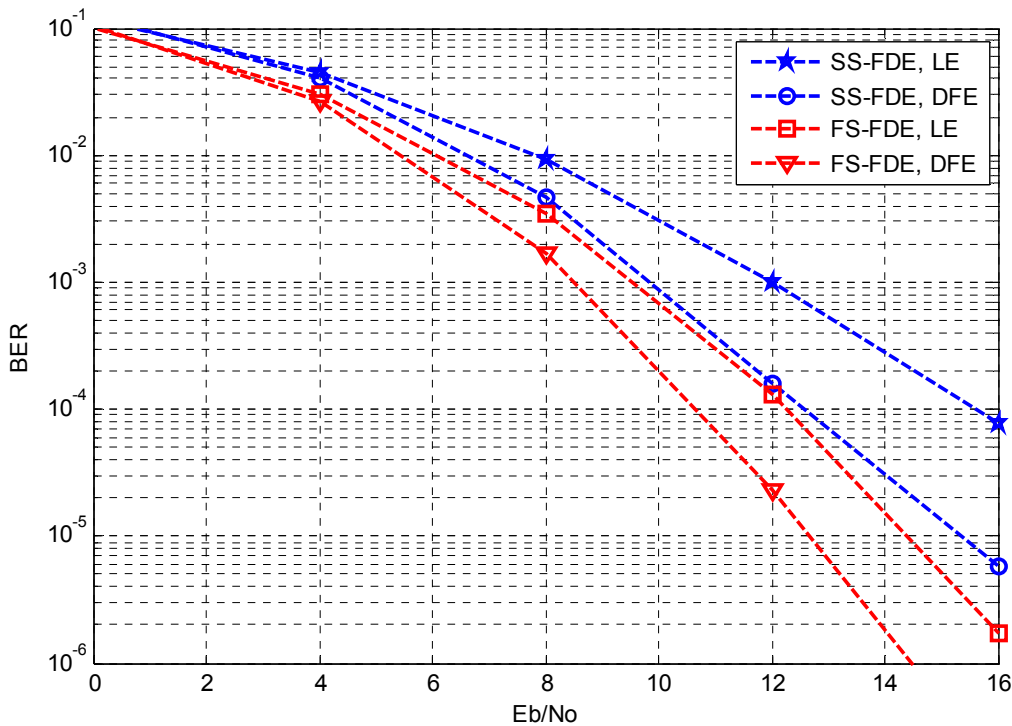

Figure 5.6 BER performances of single-relay assisted SS-FDE and FS-FDE systems with LE and DFE equalization. $G_{SR_m} = 0\,\text{dB}$, $G_{R_mD} = 10\,\text{dB}$, $L_{SD} = L_{SR_m} = 5$, $L_{R_mD} = 10$, random phase error, and MFB based OPA is in place.

72

delay between consecutive paths is T_s. For this case, the optimum value of K_0 is 0.82. It is observed from Fig.5.6 that the DFE methods outperform the corresponding LE approaches. Specifically, at a target BER of 10^{-4} , the performance gap between the DFE- and LE-methods are 1.6 and 3 dB for the SS-FDE- and FS-FDE-based systems, respectively. Moreover, based on Fig. 5.6, FS-FDE systems (with either LE or DFE technique) outperform the SS-FDE systems in exploiting the available multipath diversity of the underlying channels.

In Fig. 5.7, we investigate the effect of time-variation of the HF sky wave/NVIS links on the performance of the SC cooperative systems. We consider uni-Gaussian Doppler PSD with different Doppler spreads, namely $f_d = 2,5$ and 10 Hz. Comparison with Fig. 5.5 indicates that time selectivity induced by ionosphere brings negligible degradation for typical HF channels with 2 Hz Doppler spread. However, as Doppler spread increases, the performance of the system gradually degrades. Different techniques can be used to overcome the induced inter-carrier interference (ICI), e.g. see [66] and references therein.
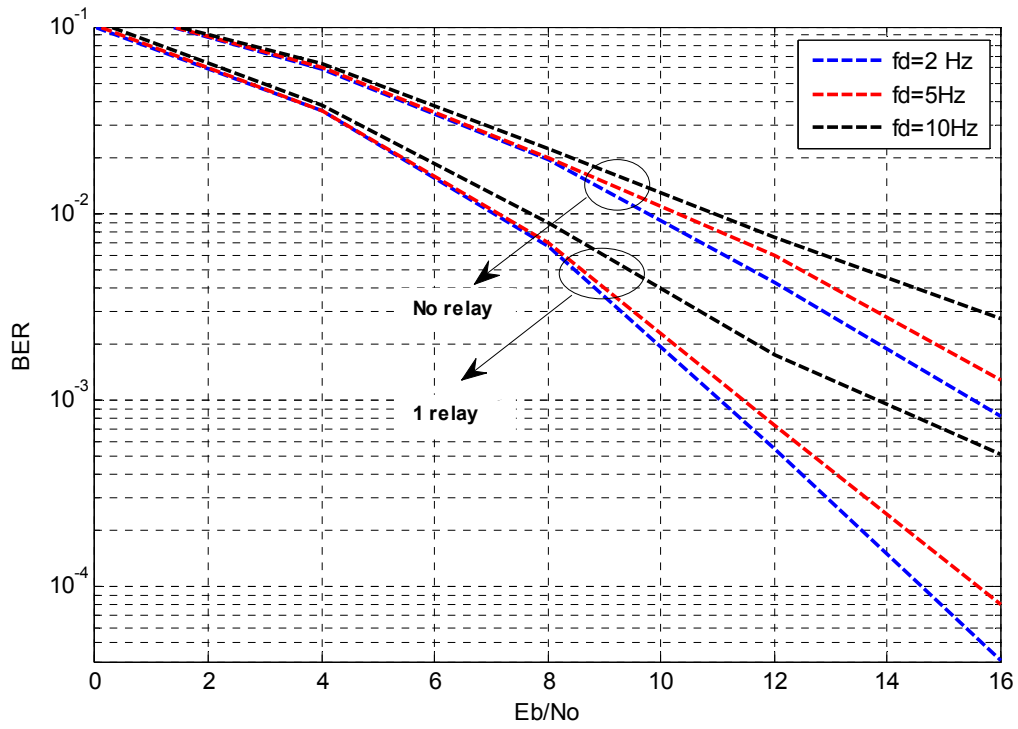
Figure 5.7 BER performance of the cooperative systems under the time varying channel assumption. $G_{\mathrm{SR}_m} = 0\,\mathrm{dB}$, $G_{\mathrm{R}_m\mathrm{D}} = 10\,\mathrm{dB}$, $L_{\mathrm{SD}} = L_{\mathrm{SR}_m} = L_{\mathrm{R}_m\mathrm{D}} = 2$, random phase error, and MFB based OPA is in place.

Chapter 6

Conclusions and Future Work

6.1 Conclusions

In this work, we proposed cooperative communication as an effective technique to boost the performance of wireless HF communication systems. In the current HF standards, both single-carrier and multi-carrier techniques have been adopted in the physical layer. As a result, we have considered cooperation strategies in conjunction with both single-carrier and multi-carrier based physical layers. Specifically, in Chapter 3, we investigated multi-carrier AaF cooperative HF communication using BICM-OFDM signaling, which is backward compatible with the current existing HF modems working based on the DRM standard. It was demonstrated that the proposed system achieves full frequency and spatial (cooperative) diversities. Relay selection mechanisms and power allocation strategies were also presented. Extensive simulations confirmed the analytical derivations, and demonstrated the performance under various practical scenarios.

Chapters 4 and 5 considered single-carrier AaF cooperative communication. In Chapter 4, through MFB analysis, we provided a lower bound on the performance of single-carrier non-regenerative cooperative systems. In our derivation, we first demonstrated a relationship between "*the performance of non-regenerative relaying over frequency-selective Rayleigh channels*" and "*the performance of non-regenerative relaying over frequency-flat Nakagami-m channels*". This relationship let us readily take advantage of the existing rich body of analytical results for Nakagami-m fading channels. Moreover, the derived MFB provided an optimum relay selection strategy and an optimum power allocation scheme for the multi-relay cooperative systems.

In chapter 5, we focused on the equalization techniques required to overcome the ISI impairment in practical multi-relay single-carrier AaF cooperative systems over frequency selective channels. Required signal processing in the relay and the structure of the MMSE based linear/decision-feedback equalization filters in the destination were derived for both symbol-spaced and fractionally-spaced approaches. It was demonstrated that, in contrast to symbol-spaced equalizers, aliasing of roll-off factors does not occur in the fractionally-spaced equalizers, so they are robust against the sampling phase errors at the relay and destination nodes.

6.2 Future Work

HF channel is known for the existence of long delays among contributing paths [42], [47]. In high rate signaling, this feature results in many zero taps between the non-zero ones in the TDL model, leading to a sparse channel. Conventional estimation methods ignore this sparse structure, and therefore, their applicability in HF channels is limited. For instance, in the conventional least square (LS) method, some a priori information such as delay spread is assumed to be known. Then, LS method tries to estimate all the coefficients over the channel length determined by the given delay spread. However, due to the sparse channel structure, many of these channel coefficients are actually zero, and as a result, the associated channel estimation error becomes very high. Unlike conventional methods, sparse channel estimation, see e.g. [67], [68] and the references therein, exploits this feature of the channel, not only to improve the estimation performance, but also to reduce the number of channel taps to be estimated. Therefore, it would be of practical importance to develop efficient sparse channel estimators for cooperative HF communication systems.

Another possible research venue is to consider the cooperative automatic-repeat-request (ARQ) technique for the HF communication. ARQ is an essential operation of data link layer in point-to-point communications [69]. The main idea behind ARQ is to let the transmitter know

about the success or failure of the receiver in data packet detection. For this purpose, the receiver sends back an ACK (if it succeeds) or NACK (if it fails) to the transmitter for each numbered packet in the transmitted frame. With regard to forward-error-correction (FEC) methods, conventional ARQ protocols can be considered as an alternative approach to provide reliable data transmission in a closed-loop communication. However, to further increase the reliability of the system, the combination of ARQ and FEC is adopted in a wide range of applications, which is called hybrid-ARQ (HARQ) [69]. The transmitter can respond to repeat requests in different ways, and meanwhile, the receiver has its own options for detection, based on what received after multiple retransmissions for a specific packet. In HARQ-type-I, the transmitter sends the same copies of the packet, and the (memoryless) receiver decodes only based on the latest copy of the packet. In HARQ-type-II, the error correction capability of the receiver is enhanced by applying soft packet combining. In this type of HARQ, retransmissions are either identical to the first transmission or new redundancies from the channel encoder. The former is called Chase-combining HARQ (CC-HARQ) [70] while the latter is named incremental-redundancy HARQ (IR-HARQ) [71].

In the area of HF communication, NATO standard STANAG 5066 considers transmission of the same packet in different iterations (i.e., HARQ-type-I or CC-HARQ). On the other hand, MIL STD 110-141B defines an IR-HARQ protocol for reliable point-to-point communication over the HF channel. In cooperative systems, a cooperative ARQ protocol has been also introduced as an energy conservative cooperation technique [72]. Contrary to in ordinary protocols, in ARQ-based cooperation, relays participate in communication only when the receiver fails to correctly decode. By this mechanism, higher throughput can also be achieved. These features are quite tempting for energy-devouring and narrow-band HF ionospheric communication. Therefore, analysis and design of cooperative ARQ over frequency selective

77

channels, in general, and over HF channels, in particular, suggest promising area for future research.

Another important issue to consider in the practical implementation of HF cooperative systems is synchronization among cooperating nodes. The cooperating nodes are geographically dispersed, and each relies on its local oscillator. Their signals may arrive at the destination with different timing and carrier frequency offsets. Therefore, cooperative schemes need to be implemented taking into account this asynchronous nature. It can be noted that in an OFDM implementation, timing offsets are absorbed into the channel frequency responses, and therefore, can be handled through proper channel equalization. On the other hand, the mitigation of multiple carrier frequency offsets (CFO) becomes more problematic and requires judiciously designed CFO correction algorithms.

Appendices

Appendix A
Derivation of Upper Bound in (3.15)

Noting that $\sigma_n^2 = \alpha_{R_n} P_n G_{R_nD} L_{R_nD} \|\mathbf{h}_{R_nD}\|^2 + 1 \geq \sigma_{k,n}^2$ for any $0 \leq k \leq K-1$, we can rewrite (3.14) as

$$PEP_{SRD} \leq E_{\mathbf{h}_{RD}} \left\{ \prod_{n=1}^{M} \det^{-1} \left(\mathbf{I}_{L_{SR_n}} + \frac{\beta_n d_{\min}^2}{4 L_{SR_n} \sigma_n^2} \Psi_{R_nD}^* \mathbf{J}_n \Psi_{R_nD} \right) \right\} \tag{A-1}$$

where Ψ_{R_nD} is an $L_{SR_n} L_{R_nD} \times L_{SR_n}$ matrix given by $\Psi_{R_nD} = \mathbf{I}_{L_{SR_n}} \otimes \mathbf{h}_{R_nD}$, and $\mathbf{J}_n$ is an $L_{SR_n} L_{R_nD} \times L_{SR_n} L_{R_nD}$ matrix given by $\mathbf{J}_n = \sum_{k \in \Omega} \tilde{\mathbf{V}}_{n,k} \mathbf{v}_{SR_n,k} (\tilde{\mathbf{V}}_{n,k} \mathbf{v}_{SR_n,k})^*$ with $\tilde{\mathbf{V}}_{n,k} = \mathbf{I}_{L_{SR_n}} \otimes \mathbf{v}_{R_nD,k}$. By using Sylvester's determinant theorem [73], and considering the eigenvalue decomposition of $\Psi_{R_nD} \Psi_{R_nD}^*$ in the form of

$$\Psi_{R_nD} \Psi_{R_nD}^* = \mathbf{U}_n \operatorname{diag} \left\{ \left(\underbrace{0, \cdots, 0}_{L_{SR_n} L_{R_nD} - L_{SR_n}}, \underbrace{\|\mathbf{h}_{R_nD}\|^2, \cdots, \|\mathbf{h}_{R_nD}\|^2}_{L_{SR_n}} \right) \right\} \mathbf{U}_n^* \tag{A-2}$$

, we can write

$$PEP_{SRD} \leq E_{\mathbf{h}_{RD}} \left\{ \prod_{n=1}^{M} \det^{-1} \left(\mathbf{I}_{L_{SR_n}} + \frac{\beta_n d_{\min}^2}{4 L_{SR_n} \sigma_n^2} \|\mathbf{h}_{R_nD}\|^2 \mathbf{Q}_n \right) \right\} \tag{A-3}$$

where $\mathbf{Q}_n$ is an $L_{SR_n} \times L_{SR_n}$ submatrix located in the last L_{SR_n} rows and the last L_{SR_n} columns of the matrix $\mathbf{U}_n^* \mathbf{J}_n \mathbf{U}_n$. It can be shown that with any orthonormal matrix $\mathbf{U}_n$, the rank of the matrix $\mathbf{Q}_n$, r_n, is equal to $\min(L_{SR_n}, d_f)$ (See Appendix B in the following).

Note that $\|\mathbf{h}_{R_nD}\|^2$ is a gamma random variable with mean 1 and variance $1/L_{R_nD}$, respectively. Therefore, (A-3) can be represented in the form of

79

$$PEP_{\text{SRD}} \le \prod_{n=1}^{M} \int_{0}^{\infty} (4 + 4\alpha_{R_n} P_n G_{R_n D} L_{R_n D} x_n)^{r_n} \frac{L_{R_n D}^{L_{R_n D}} x_n^{L_{R_n D}-1} \exp(-L_{R_n D} x_n) \ dx_n}{\left(L_{R_n D}-1\right)!\left(\beta_n' x_n + 4\alpha_{R_n} P_n G_{R_n D} L_{R_n D} x_n + 4\right)^{r_n}} \tag{A-4}$$

where $\beta_n' = \beta_n d_{\min}^2 \lambda_n / L_{SR_n}$, and λ_n is the minimum of the non-zero eigenvalues of all possible $\mathbf{Q}_n$ associated with the matrices in the form of $\mathbf{U}_n^* \mathbf{J}_n \mathbf{U}_n$ for any orthonormal matrix $\mathbf{U}_n$. Since the term $4\alpha_{R_n} P_n G_{R_n D} L_{R_n D} x_n$ is always positive in the integral limit of (A-4), and its asymptotic value does not depend on P_T (i.e., $4\alpha_{R_n} P_n G_{R_n D} L_{R_n D} x_n \to 4K_n G_{R_n D} L_{R_n D} x_n / (K_0 G_{SR_n})$, as $P_T \to \infty$), we can upper bound (A-4) by ignoring $4\alpha_{R_n} P_n G_{R_n D} L_{R_n D} x_n$ in the denominator. After expanding the term $(4 + 4\alpha_{R_n} P_n G_{R_n D} L_{R_n D} x_n)^{r_n}$, we have

$$PEP_{\text{SRD}} \le \prod_{n=1}^{M} \sum_{m=0}^{r_n} \xi_{n,m} \frac{L_{R_n D}^{L_{R_n D}}}{\left(L_{R_n D}-1\right)!} \int_{0}^{\infty} \frac{x_n^{L_{R_n D}-1+m} \exp(-L_{R_n D} x_n) \ dx_n}{\left(\beta_n' x_n + 4\right)^{r_n}} \tag{A-5}$$

where $\xi_{n,m}$ is the coefficient of the term x_n^m in the binomial expansion of $(4 + 4\alpha_{R_n} P_n G_{R_n D} L_{R_n D} x_n)^{r_n}$.

Appendix B

Lemma: The rank of matrix $\mathbf{Q}_n$ in (A-3) is equal to $\min(L_{\mathrm{SR}_n}, d_f)$.

Proof: First note that we can re-write $\mathbf{J}_n$ (appeared in (A-1)) as $\mathbf{J}_n = \sum_{k\in\Omega} \mathbf{v}_{n,k} \mathbf{v}_{n,k}^*$ where $\mathbf{v}_{n,k} \triangleq \mathbf{v}_{\mathrm{SR}_n,k} \otimes \mathbf{v}_{\mathrm{R}_n\mathrm{D},k}$. We can represent $\mathbf{v}_{n,k}$ as $\mathbf{v}_{n,k} = [a_k^{-\ell_1}, a_k^{-\ell_2}, \cdots, a_k^{-\ell_{L_n}}]^*$ for some $\ell_1, \cdots, \ell_{L_n} \geq 0$ where $L_n = L_{\mathrm{SR}_n} L_{\mathrm{R}_n\mathrm{D}}$ and $a_k = \exp(2\pi jk/K)$. Assume that we divide the entries of the vector $\mathbf{v}_{n,k}$ into L_{SR_n} subsequent disjoint groups with equal number of $L_{\mathrm{R}_n\mathrm{D}}$ elements. Specifically, the first $L_{\mathrm{R}_n\mathrm{D}}$ entries of $\mathbf{v}_{n,k}$ form the first group, the second $L_{\mathrm{R}_n\mathrm{D}}$ entries form the second group, and so on. Since the elements in both $\mathbf{v}_{\mathrm{SR}_n,k} = \exp(2j\pi k\boldsymbol{\tau}_{\mathrm{SR}_n}/K)$ and $\mathbf{v}_{\mathrm{R}_n\mathrm{D},k} = \exp(2j\pi k\boldsymbol{\tau}_{\mathrm{R}_n\mathrm{D}}/K)$ have different exponents, it is clear that in each of the aforementioned groups, there exists at least one element, say $a_k^{\ell_i}$, whose exponent is unique among all $\mathbf{v}_{n,k}$ entries' exponents (i.e. $\ell_i \neq \ell_j$ for any $j = 1, \cdots, L_n$, $j \neq i$). This is the property which we will use later on.

Defining $\ell_{i,j} = \ell_i - \ell_j$, the matrix $\mathbf{J}_n$ can be written in the form of

$$\mathbf{J}_n = \begin{pmatrix} \sum_{k\in\Omega} a_k^{\ell_{1,1}} & \sum_{k\in\Omega} a_k^{\ell_{1,2}} & \cdots & \sum_{k\in\Omega} a_k^{\ell_{1,L_n}} \\ \sum_{k\in\Omega} a_k^{\ell_{2,1}} & \sum_{k\in\Omega} a_k^{\ell_{2,2}} & \cdots & \sum_{k\in\Omega} a_k^{\ell_{2,L_n}} \\ \vdots & \vdots & \ddots & \vdots \\ \sum_{k\in\Omega} a_k^{\ell_{L_n,1}} & \sum_{k\in\Omega} a_k^{\ell_{L_n,2}} & \cdots & \sum_{k\in\Omega} a_k^{\ell_{L_n,L_n}} \end{pmatrix}. \tag{B-1}$$

Here after, without loss of generality, we assume that $\Omega = \{1, 2, \cdots, d_f\}$. As a result, $\mathbf{J}_n$ can be decomposed into the multiplication of two matrices as [24]

81

$$\mathbf{J}_n = \underbrace{\begin{pmatrix} 1 & 1 & \cdots & 1 \\ a_1^{\ell_{2,1}} & a_2^{\ell_{2,1}} & \cdots & a_{d_f}^{\ell_{2,1}} \\ \vdots & \vdots & \ddots & \vdots \\ a_1^{\ell_{L_n,1}} & a_2^{\ell_{L_n,1}} & \cdots & a_{d_f}^{\ell_{L_n,1}} \end{pmatrix}}_{\mathbf{B}_n} \underbrace{\begin{pmatrix} 1 & a_1^{\ell_{1,2}} & \cdots & a_1^{\ell_{1,L_n}} \\ 1 & a_2^{\ell_{1,2}} & \cdots & a_2^{\ell_{1,L_n}} \\ \vdots & \vdots & \ddots & \vdots \\ 1 & a_{d_f}^{\ell_{1,2}} & \cdots & a_{d_f}^{\ell_{1,L_n}} \end{pmatrix}}_{\mathbf{C}_n} \tag{B-2}$$

where $\mathbf{B}_n$ and $\mathbf{C}_n$ are matrices of sizes $L_n \times d_f$ and $d_f \times L_n$, respectively. Since $\ell_{i,j} = -\ell_{j,i}$, $\mathbf{B}_n$ and $\mathbf{C}_n$ are Hermitian of each other, i.e., $\mathbf{B}_n = \mathbf{C}_n^*$. Therefore, $\mathbf{U}_n^* \mathbf{J}_n \mathbf{U}_n = \mathbf{U}_n^* \mathbf{B}_n \mathbf{C}_n \mathbf{U}_n = \mathbf{U}_n^* \mathbf{C}_n^* \mathbf{C}_n \mathbf{U}_n$ where $\mathbf{U}_n$ is given by (A-2). The aforementioned property about the exponents of the $\mathbf{v}_{n,k}$'s entries shows up itself in the matrix $\mathbf{C}_n$. In particular, if we divide the matrix $\mathbf{C}_n$ into the concatenation of $d_f \times L_{\mathrm{R}_n\mathrm{D}}$ matrices such that $\mathbf{C}_n = [\mathbf{C}_{n,1} | \cdots | \mathbf{C}_{n,L_{\mathrm{SR}_n}}]$, then in each submatrix there exists at least one column with distinct exponent which is unique in the whole matrix $\mathbf{C}_n$. Since we are interested in the submatrix residing in the last L_{SR_n} rows and the last L_{SR_n} columns of $\mathbf{U}_n^* \mathbf{C}_n^* \mathbf{C}_n \mathbf{U}_n$, only the last L_{SR_n} columns of $\mathbf{U}_n$ are important. But we know that the last L_{SR_n} columns of $\mathbf{U}_n$ includes the zero-padded and shifted versions of the vector $\mathbf{h}_{\mathrm{R}_n\mathrm{D}}/\|\mathbf{h}_{\mathrm{R}_n\mathrm{D}}\|$ which is the unique non-zero eigenvector of the matrix $\mathbf{h}_{\mathrm{R}_n\mathrm{D}}\mathbf{h}_{\mathrm{R}_n\mathrm{D}}^*$ with respect to its single non-zero eigenvalue, i.e. $\|\mathbf{h}_{\mathrm{R}_n\mathrm{D}}\|^2$. Therefore, the submatrix including the last L_{SR_n} columns of $\mathbf{U}_n$ can be represented by $\mathbf{I}_{L_{\mathrm{SR}_n}} \otimes \mathbf{h}_{\mathrm{R}_n\mathrm{D}}/\|\mathbf{h}_{\mathrm{R}_n\mathrm{D}}\|$.

Now consider the submatrix which contains the last L_{SR_n} columns of the matrix $\mathbf{C}_n \mathbf{U}_n$. We denote this $d_f \times L_{\mathrm{SR}_n}$ matrix by $\mathbf{Q}_n'$ which is the result of multiplying the matrix $\mathbf{C}_n$ by the last L_{SR_n} columns of the matrix $\mathbf{U}_n$. Therefore, based on the above property about the last L_{SR_n} columns of the matrix $\mathbf{U}_n$, the ith column in the matrix $\mathbf{Q}_n'$ is the weighted sum of the columns of the submatrix $\mathbf{C}_{n,i}$. By taking into account the Vandermonde structure [73] of the matrix $\mathbf{C}_n$ and the fact that there exists at least one column with distinct exponent in each predefined submatrices of $\mathbf{C}_n$, we can conclude that the rank of the matrix $\mathbf{Q}_n'$ is $\min(d_f, L_{\mathrm{SR}_n})$. Finally, since $\mathbf{Q}_n = (\mathbf{Q}_n')^* \mathbf{Q}_n'$, the rank of the matrix $\mathbf{Q}_n$ is the same as the rank of the matrix $\mathbf{Q}_n'$ [73].

Appendix C

Derivation of the Approximation in (3.25)

Defining the argument of the multiplicative term in (3.23) as

$$g_n(K_0, K_n, s) = \frac{1}{\overline{\gamma}_{SR_n} s + 1} + \frac{\left(\overline{\gamma}_{SR_n} + 1\right)\overline{\gamma}_{SR_n} s e^{\frac{\overline{\gamma}_{SR_n} + 1}{\overline{\gamma}_{R_n D}\left(\overline{\gamma}_{SR_n} s + 1\right)}}}{\overline{\gamma}_{R_n D}\left(\overline{\gamma}_{SR_n} s + 1\right)^2} E_1\left(\frac{\overline{\gamma}_{SR_n} + 1}{\overline{\gamma}_{R_n D}\left(\overline{\gamma}_{SR_n} s + 1\right)}\right) \tag{C-1}$$

, we can rewrite (3.23) as $\Phi_{\gamma_D}^{NVIS}(s) = [1/(\overline{\gamma}_{SD} s + 1)]\prod_{n=1}^{M} g_n(K_0, K_n, s)$. At high SNR region ($\overline{\gamma} \to \infty$), we can write [60]

$$\begin{aligned}
g_n(K_0, K_n, \frac{d_{\min}^2}{4}) &\approx \frac{4}{G_{SR_n} K_0 \overline{\gamma} d_{\min}^2} + \int_0^\infty \frac{4e^{-x}}{G_{R_n D} K_n \overline{\gamma} d_{\min}^2 x + 4} dx \\
&\approx \frac{4}{G_{SR_n} K_0 \overline{\gamma} d_{\min}^2} + \int_{\frac{1}{\overline{\gamma}}}^\infty \frac{4e^{-x}}{G_{R_n D} K_n \overline{\gamma} d_{\min}^2 x + 4} dx \\
&\approx \frac{4}{G_{SR_n} K_0 \overline{\gamma} d_{\min}^2} + \frac{4}{G_{R_n D} K_n \overline{\gamma} d_{\min}^2} E_1\left(\frac{1}{\overline{\gamma}}\right) \\
&\approx \frac{4}{G_{SR_n} K_0 \overline{\gamma} d_{\min}^2} + \frac{4\ln(\overline{\gamma})}{G_{R_n D} K_n \overline{\gamma} d_{\min}^2}
\end{aligned}$$

$$\tag{C-2}$$

where $\overline{\gamma} = P_T / N_0$, and we have used $E_1(x) \to -\ln(1/x)$ as $x \to 0$. As a result, at high SNR region, we have

$$\Phi_{\gamma_D}^{NVIS}\left(\frac{d_{\min}^2}{4}\right) \simeq \frac{4}{K_0 \overline{\gamma} d_{\min}^2} \prod_{n=1}^{M}\left(\frac{4}{G_{SR_n} K_0 \overline{\gamma} d_{\min}^2} + \frac{4\ln(\overline{\gamma})}{G_{R_n D} K_n \overline{\gamma} d_{\min}^2}\right) \tag{C-3}$$

which is a posynomial function with respect to $K_0, K_1, \cdots, K_M$ [54].

83

Appendix D

Proof of Equation (4.19)

Lemma 1: Consider X as a Nakagami-m random variable with $E[X]=1$. Then, the pdf and cdf of $Y = aX$ (a is a positive constant) is given by $f_Y(y) = \theta\, y^{m-1}$, and $F_Y(y) = \varphi y^m$ for small enough y where $\theta = m^m a^{-m} / \Gamma(m)$, and $\varphi = m^{m-1} a^{-m} / \Gamma(m)$.

  Proof: See Table I in [63]. ∎

  From Lemma 1, it is easy to show that, at high SNR region, the pdf of the γ_{SD} is given by

$$f_{\gamma_{\mathrm{SD}}}(x) \simeq \frac{L_{\mathrm{SD}}^{\,L_{\mathrm{SD}}} x^{L_{\mathrm{SD}}-1}}{\Gamma(L_{\mathrm{SD}}) K_0^{\,L_{\mathrm{SD}}} \overline{\gamma}^{\,L_{\mathrm{SD}}}} \tag{D-1}$$

and consequently, for the MGF of γ_{SD}, we can write

$$\Phi_{\gamma_{\mathrm{SD}}}(s) = \int_0^\infty \frac{L_{\mathrm{SD}}^{\,L_{\mathrm{SD}}} x^{L_{\mathrm{SD}}-1}}{\Gamma(L_{\mathrm{SD}}) K_0^{\,L_{\mathrm{SD}}} \overline{\gamma}^{\,L_{\mathrm{SD}}}} e^{-sx}\, dx = \eta_0 \left(\overline{\gamma} s\right)^{-L_{\mathrm{SD}}} \tag{D-2}$$

where $\eta_0 = (L_{\mathrm{SD}}/K_0)^{L_{\mathrm{SD}}}$ and the second equality is based on [60, pp. 340]

$$\int_0^\infty x^n \exp(-\mu x)\, dx = \Gamma(n+1)\, \mu^{-n-1} . \tag{D-3}$$

Lemma 2: At high SNR region, the cdf of $\gamma_{\mathrm{SR}_n\mathrm{D}}$ can be approximated by $F_{\gamma_{\mathrm{SR}_n\mathrm{D}}}(x) = \eta'_{0,n}(x/\overline{\gamma})^{L_{\mathrm{SR}_n}} + \eta'_{1,n}(x/\overline{\gamma})^{L_{\mathrm{R}_n\mathrm{D}}}$ where the values of $\eta'_{0,n}$, and $\eta'_{1,n}$ are given by

$$\eta'_{0,n} = \frac{L_{\mathrm{SR}_n}^{\,L_{\mathrm{SR}_n}-1} \left(G_{\mathrm{SR}_n} K_0\right)^{-L_{\mathrm{SR}_n}}}{\Gamma\left(L_{\mathrm{SR}_n}\right)}$$

$$\eta'_{1,n} = \frac{L_{\mathrm{R}_n\mathrm{D}}^{\,L_{\mathrm{R}_n\mathrm{D}}-1} \left(G_{\mathrm{R}_n\mathrm{D}} K_n\right)^{-L_{\mathrm{R}_n\mathrm{D}}}}{\Gamma\left(L_{\mathrm{R}_n\mathrm{D}}\right)}$$

for the case of IPS. On the other hand, in the case of APS, they are obtained as

<div align="center">84</div>

$$
\eta'_{0,n} = \begin{cases}
L_{SR_n}^{L_{SR_n}-1} \sum_{k=0}^{L_{SR_n}} \binom{L_{SR_n}}{k} G_{R_nD}^{-k} G_{SR_n}^{k-L_{SR_n}} \dfrac{K_0^{k-L_{SR_n}} K_n^{-k} L_{R_nD}^{k} \Gamma(L_{R_nD}-k)}{\Gamma(L_{SR_n})\Gamma(L_{R_nD})}, & L_{R_nD} > L_{SR_n} \\[2em]
\dfrac{L_{SR_n}^{L_{SR_n}-1}}{2\Gamma(L_{SR_n})}\left((G_{SR_n}K_0)^{-L_{SR_n}} + \dfrac{L_{SR_n}^{L_{SR_n}}(G_{R_nD}K_n)^{-L_{SR_n}}}{\Gamma(L_{SR_n})}\log\left(\dfrac{cG_{SR_n}\bar\gamma}{L_{SR_n}}\right)\right), & L_{R_nD} = L_{SR_n} \\[2em]
\dfrac{L_{SR_n}^{L_{SR_n}-1}(G_{SR_n}K_0)^{-L_{SR_n}}}{\Gamma(L_{SR_n})}, & L_{R_nD} < L_{SR_n}
\end{cases}
$$

$$
\eta'_{1,n} = \begin{cases}
0, & L_{R_nD} > L_{SR_n} \\[2em]
\dfrac{L_{SR_n}^{L_{SR_n}-1}}{2\Gamma(L_{SR_n})}\left((G_{SR_n}K_0)^{-L_{SR_n}} + \dfrac{L_{SR_n}^{L_{SR_n}}(G_{R_nD}K_n)^{-L_{SR_n}}}{\Gamma(L_{SR_n})}\log\left(\dfrac{cG_{SR_n}\bar\gamma}{L_{SR_n}}\right)\right), & L_{R_nD} = L_{SR_n} \\[2em]
L_{SR_n}^{L_{R_nD}} L_{R_nD}^{L_{R_nD}-1}\Gamma(L_{SR_n}-L_{R_nD})\dfrac{(G_{SR_n}G_{R_nD}K_n)^{-L_{R_nD}}}{\Gamma(L_{SR_n})\Gamma(L_{R_nD})}, & L_{R_nD} < L_{SR_n}
\end{cases}\ .
$$

Proof: See [74] for IPS. For APS relaying, we can rewrite (4.11) as

$$
\gamma_{SR_nD} = \frac{\bar\gamma G_{SR_n} G_{R_nD}VW}{G_{R_nD}V + G_{SR_n}K_0 + \bar\gamma^{-1}}
\tag{D-4}
$$

where $V = K_n \|\mathbf{h}_{R_nD}\|^2 \sim \mathcal{G}(L_{R_nD}, K_n/L_{R_nD})$ and $W = K_0 \|\mathbf{h}_{SR_n}\|^2 \sim \mathcal{G}(L_{SR_n}, K_0/L_{SR_n})$. From (D-4), we have

$$
\begin{aligned}
F_{\gamma_{SR_nD}}(x) = \Pr(\gamma_{SRD} \le x) &= \Pr\left(\frac{VW}{G_{R_nD}V + G_{SR_n}K_0 + \bar\gamma^{-1}} \le \frac{x}{\bar\gamma G_{SR_n} G_{R_nD}}\right) \\
&= \Pr\left(\frac{VW}{G_{R_nD}V + G_{SR_n}K_0 + \varepsilon} \le q(\varepsilon)\right)
\end{aligned}
\tag{D-5}
$$

where, in the last equality, $\varepsilon = \bar\gamma^{-1}$, and $q(\varepsilon) = x/\bar\gamma G_{SR_n} G_{R_nD}$. Accordingly, by replacing L_{SR_n} and L_{R_nD} by m_1 and m_2, respectively, we have the following cases:

Case I ($m_2 > m_1$): In this case, we can write

$$F_{\gamma_{\mathrm{SR}_n\mathrm{D}}}(x) = \Pr\left(W \le \frac{q(\varepsilon)}{V}(G_{\mathrm{R}_n\mathrm{D}}V + K_0 G_{\mathrm{SR}_n} + \varepsilon)\right) = \int_0^\infty F_W\left(\frac{q(\varepsilon)}{v}(G_{\mathrm{R}_n\mathrm{D}}v + K_0 G_{\mathrm{SR}_n} + \varepsilon)\right) f_V(v)\,dv$$

$$\text{(D-6)}$$

Hence, based on the lemma 1, for sufficiently large $\bar{\gamma}$, we have

$$F_{\gamma_{\mathrm{SR}_n\mathrm{D}}}(x) \simeq \frac{m_1^{m_1-1} m_2^{m_2} q(\varepsilon)^{m_1}}{\Gamma(m_1)\Gamma(m_2)} K_0^{-m_1} K_n^{-m_2} \int_0^\infty \left(G_{\mathrm{R}_n\mathrm{D}} + \frac{G_{\mathrm{SR}_n} K_0}{v}\right)^{m_1} v^{m_2-1} \exp\left(-\frac{m_2 v}{K_n}\right) dv \qquad \text{(D-7)}$$

Using binomial expansion theorem and (D-3), we have

$$F_{\gamma_{\mathrm{SR}_n\mathrm{D}}}(x) \simeq \frac{m_1^{m_1-1} \sum_{r=0}^{m_1} \binom{m_1}{r} G_{\mathrm{R}_n\mathrm{D}}^{-r} G_{\mathrm{SR}_n}^{r-m_1} \Gamma(m_2 - r) m_2^{r} K_0^{r-m_1} K_n^{-r}}{\Gamma(m_1)\Gamma(m_2)} \left(\frac{x}{\bar{\gamma}}\right)^{m_1} \qquad \text{(D-8)}$$

Case II ($m_2 < m_1$): In this case, we can write

$$F_{\gamma_{\mathrm{SR}_n\mathrm{D}}}(x) = \int_0^{G_{\mathrm{R}_n\mathrm{D}}q(\varepsilon)} \underbrace{\Pr\left(V > \underbrace{\frac{q(\varepsilon)(K_0 G_{\mathrm{SR}_n} + \varepsilon)}{w - G_{\mathrm{R}_n\mathrm{D}}q(\varepsilon)}}_{\le 0}\right)}_{1} f_W(w)\,dw + \int_{G_{\mathrm{R}_n\mathrm{D}}q(\varepsilon)}^\infty F_V\left(\frac{q(\varepsilon)(K_0 G_{\mathrm{SR}_n} + \varepsilon)}{w - G_{\mathrm{R}_n\mathrm{D}}q(\varepsilon)}\right) f_W(w)\,dw$$

$$\text{(D-9)}$$

for sufficiently large $\bar{\gamma}$, based on Lemma 1, $F_{\gamma_{\mathrm{SR}_n\mathrm{D}}}(x)$ tends to

$$F_{\gamma_{\mathrm{SR}_n\mathrm{D}}}(x) \simeq \frac{m_1^{m_1-1}(G_{\mathrm{SR}_n} K_0)^{-m_1}}{\Gamma(m_1)}\left(\frac{x}{\bar{\gamma}}\right)^{m_1} + \frac{m_1^{m_2} m_2^{m_2-1} \Gamma(m_1 - m_2)\left(G_{\mathrm{SR}_n} G_{\mathrm{R}_n\mathrm{D}} K_n\right)^{-m_2}}{\Gamma(m_1)\Gamma(m_2)}\left(\frac{x}{\bar{\gamma}}\right)^{m_2} \qquad \text{(D-10)}$$

Case III ($m_2 = m_1$): In this case, we can still use (D-9), but the way of manipulating the second integral is different. Specifically, we can rewrite it as

$$\int_{G_{\mathrm{R}_n\mathrm{D}}q(\varepsilon)}^\infty F_V\left(\frac{q(\varepsilon)(K_0 G_{\mathrm{SR}_n} + \varepsilon)}{w - G_{\mathrm{R}_n\mathrm{D}}q(\varepsilon)}\right) f_W(w)\,dw \simeq \frac{m_1^{2m_1-1}\left(G_{\mathrm{R}_n\mathrm{D}} K_n\right)^{-m_1}}{\left(\Gamma(m_1)\right)^2} E_1\left(\frac{m_1 t_0}{K_0}\right)\left(\frac{x}{\bar{\gamma}}\right)^{m_1} \qquad \text{(D-11)}$$

where $t_0 = G_{\mathrm{R}_n\mathrm{D}}q(\varepsilon)/c$, c is an arbitrary constant less than 1. Based on [60, pp. 884], we have $E_1(z) \to \log(1/z)$, as $z \to 0$. As a result, for sufficiently large $\bar{\gamma}$, we have

86

$$F_{\gamma_{\mathrm{SR}_n\mathrm{D}}}(x) \simeq \frac{m_1^{m_1-1}(G_{\mathrm{SR}_n}K_0)^{-m_1}}{\Gamma(m_1)}\left(\frac{x}{\overline{\gamma}}\right)^{m_1} + \frac{m_1^{2m_1-1}\left(G_{\mathrm{R}_n\mathrm{D}}K_n\right)^{-m_1}}{\left(\Gamma(m_1)\right)^2}\log\left(\frac{cG_{\mathrm{SR}_n}\overline{\gamma}}{m_1}\right)\left(\frac{x}{\overline{\gamma}}\right)^{m_1} \tag{D-12}$$

∎

From Lemma 2, the pdf of the $\gamma_{\mathrm{SR}_n\mathrm{D}}$ is given by

$$f_{\gamma_{\mathrm{SR}_n\mathrm{D}}}(x) = \frac{dF_{\gamma_{\mathrm{SR}_n\mathrm{D}}}(x)}{dx} \simeq \frac{L_{\mathrm{SR}_n}\eta'_{0,n}x^{L_{\mathrm{SR}_n}-1}}{\overline{\gamma}^{L_{\mathrm{SR}_n}}} + \frac{L_{\mathrm{R}_n\mathrm{D}}\eta'_{1,n}x^{L_{\mathrm{R}_n\mathrm{D}}-1}}{\overline{\gamma}^{L_{\mathrm{R}_n\mathrm{D}}}} \tag{D-13}$$

Therefore, the MGF of $\gamma_{\mathrm{SR}_n\mathrm{D}}$ can be written as

$$\Phi_{\gamma_{\mathrm{SR}_n\mathrm{D}}}(s) = \int_0^\infty f_{\gamma_{\mathrm{SR}_n\mathrm{D}}}(x)e^{-sx}dx = \eta_{0,n}\left(\overline{\gamma}s\right)^{-L_{\mathrm{SR}_n}} + \eta_{1,n}\left(\overline{\gamma}s\right)^{-L_{\mathrm{R}_n\mathrm{D}}} \tag{D-14}$$

where $\eta_{0,n} = L_{\mathrm{SR}_n}\Gamma(L_{\mathrm{SR}_n})\eta'_{0,n}$ and $\eta_{1,n} = L_{\mathrm{R}_n\mathrm{D}}\Gamma(L_{\mathrm{R}_n\mathrm{D}})\eta'_{1,n}$. Finally, by noting that $\Phi_{\gamma_{\mathrm{D}}}(s) = \Phi_{\gamma_{\mathrm{SD}}}(s)\prod_{n=1}^{M}\Phi_{\gamma_{\mathrm{SR}_n\mathrm{D}}}(s)$ and based on (D-2) and (D-14), the proof is completed.

Appendix E

Fourier Series Representation of CPSC Signals

The Fourier series representation of the CPSC signals, in the desired time interval, originally has been introduced in [37]. Here we explain this method for a more general scenario where besides the CP symbols that prevent the inter-block-interference, additional CP symbols have been also inserted to overcome the sampling phase errors at the receivers.

In general, a CPSC signal such as $x(t)$ can be expressed as

$$x(t) = \sum_{n=-N_{CP}}^{N-1} \mathbf{b}(<n>_N)u(t-nT_S) \tag{E-1}$$

where $\mathbf{b}$ is the N-tuple data-symbol vector, and N_{CP} is the length of CP. Also, $u(t)$ is a signal whose bandwidth and time-support are less than $1/T_S$ and $N_P T_S$, respectively. Therefore, $N_{CP} - N_P \geq 0$ is the number of CP symbols that allow tolerance in the estimation of the beginning of the symbol sequence.

On the other hand, consider $y(t) = \sum_{n=0}^{N-1} \mathbf{b}(n)u(t-nT_S)$ as the CP-free version of $x(t)$. The continuous Fourier transform of $y(t)$ is given by

$$\tilde{y}(f) = \tilde{u}(f)\sum_{n=0}^{N-1} \mathbf{b}(n)\exp\left(-j2\pi nT_S f\right) \tag{E-2}$$

where $\tilde{u}(f)$ is the continuous Fourier transform of $u(t)$. Here, we note that $\tilde{y}(k/NT_S), k = 0,\pm 1,\pm 2,\cdots,\pm N$ are the Fourier series coefficients of the periodic signal $\hat{y}(t) = \sum_m y(t-m/NT_S)$. Specifically, we have

$$\hat{y}(t) = \frac{1}{NT_S}\sum_{k=-N}^{N} \tilde{y}(k/NT_S)\exp\left(j2\pi kt/NT_S\right). \tag{E-3}$$

Moreover, one can easily verify that $\hat{y}(t) = x(t)$, for $-(N_{CP} - N_P)T_S \le t \le NT_S$, and therefore, we can write

$$x(t) = \frac{1}{NT_S} \sum_{k=-N}^{N} \tilde{u}(k)\tilde{b}(k) \exp\left(j2\pi kt / NT_S\right), \quad -(N_{CP} - N_P)T_S \le t \le NT_S \qquad \text{(E-4)}$$

where $\tilde{u}(k) \triangleq \tilde{u}(k/NT_S)$ and $\tilde{b}(k) = \sum_{n=0}^{N-1} \mathbf{b}(n) \exp(-j2\pi nk/N)$.

Appendix F

Denoting the CP-free part of the signal transmitted by the ith relay by $\hat{x}_{R_i}(t)$, the average energy consumed for the transmission of one symbol is given by $P_{Ave} = (1/N)E\{\int |\hat{x}_{R_i}(t)|^2 \, dt\}$. From (5.8), we have

$$
\begin{aligned}
P_{Ave} &= \frac{\alpha_{R_i} P_1}{N} E\left\{ \sum_{n=0}^{\mu N-1} \sum_{m=0}^{\mu N-1} \mathbf{y}_{SR_i}(n)\mathbf{y}_{SR_i}^*(m) \int g\left(t - n\frac{T_S}{\mu}\right) g^*\left(t - m\frac{T_S}{\mu}\right) dt \right\} \\
&= \frac{\alpha_{R_i} P_1}{N} E\left\{ \sum_{n=0}^{\mu N-1} \sum_{m=0}^{\mu N-1} \mathbf{y}_{SR_i}(n)\mathbf{y}_{SR_i}^*(m) g_{RC}\left(\frac{(n-m)T_S}{\mu} \right) \right\}
\end{aligned}
$$

(F-1)

where $g_{RC}(t) = g(t) * g^*(-t)$ is the impulse response of a raised cosine filter with the roll-off factor β, and symbol rate $1/T_S$, which is given by [75]

$$
g_{RC}(t) = \frac{\cos\left(\dfrac{\beta \pi t}{T_S}\right)}{1 - \left(\dfrac{2\beta t}{T_S}\right)^2} sinc\left(\frac{t}{T_S}\right)
$$

(F-2)

with the following Fourier transform

$$
\tilde{g}_{RC}(f) = \begin{cases} T_S & |f| \le \dfrac{1-\beta}{2T_S} \\[2ex] \dfrac{T_S}{2}\left[1 + \cos\left(\dfrac{\pi T_S}{\beta}\left[|f| - \dfrac{1-\beta}{2T_S}\right]\right)\right] & \dfrac{1-\beta}{2T_S} < |f| < \dfrac{1+\beta}{2T_S} \\[2ex] 0 & \dfrac{1+\beta}{2T_S} \le |f| \end{cases}
$$

(F-3)

By plugging $\mathbf{y}_{SR_i}(n)$ and $\mathbf{y}_{SR_i}(m)$ from (5.7) into (F-1), and using $E[a(n)a^*(m)] = \delta(n-m)$, and $E[\mathbf{h}_{SR_i}(l)\mathbf{h}_{SR_i}^*(u)] = (1/L_{SR_i})\delta(l-u)$, we can write

$$
P_{Ave} = \frac{\alpha_{R_i} P_1}{N} \sum_{n=0}^{\mu N-1} \sum_{m=0}^{\mu N-1} \left[\frac{G_{SR_i} P_0}{N} \sum_{k=-N}^{N} |\tilde{g}(k)|^2 |\tilde{p}(k)|^2 W_{\mu N}^{-k(n-m)} + N_0 \delta(n-m) \right] g_{RC}\left(\frac{(n-m)T_S}{\mu} \right).
$$

(F-4)

Now, we have the following cases.

Case I: SS-FDE

In this case, we have $\mu = 1$, $\tilde{p}(k) = \tilde{g}^*(k)$, and therefore,

$$P_{Ave} = \frac{\alpha_{R_i} P_1}{N} \sum_{n=0}^{N-1} \left[N_0 + \frac{G_{SR_i} P_0}{N} \sum_{k=-N}^{N} \left| \tilde{g}(k) \right|^4 \right] \qquad \text{(F-5)}$$

where we have used $g_{RC}((n-m)T_S) = \delta(n-m)$. On the other hand, we have

$$\sum_{k=-N}^{N} \left| \tilde{g}(k) \right|^4 = \frac{N}{T_S} \sum_{k=-N}^{N} \frac{1}{NT_S} \left| \tilde{g}(\frac{k}{NT_S}) \right|^4 \approx \frac{N}{T_S} \int \left| \tilde{g}_{RC}(f) \right|^2 df = N \left(1 - \frac{\beta}{4} \right) \qquad \text{(F-6)}$$

, and therefore, from (F-5), we can write

$$P_{Ave} = \alpha_{R_i} P_1 \left[G_{SR_i} P_0 \left(1 - \frac{\beta}{4} \right) + N_0 \right]. \qquad \text{(F-7)}$$

As a result, by adjusting

$$\alpha_{R_i} = \frac{1}{G_{SR_i} P_0 \left(1 - \dfrac{\beta}{4} \right) + N_0} \qquad \text{(F-8)}$$

the desired equality of $P_{Ave} = P_1$ is held.

Case II: FS-FDE

In this case, we have $\mu = 2$, $\tilde{p}(k) = 1/\sqrt{2}$, and therefore, we have

$$\sum_{k=-N}^{N} \left| \tilde{g}(k) \right|^2 \left| \tilde{p}(k) \right|^2 W_{2N}^{-k(n-m)} = \frac{N}{2} \sum_{k=-N}^{N} \frac{1}{NT_S} \left| \tilde{g}\left(\frac{k}{NT_S} \right) \right|^2 W_{2N}^{-k(n-m)} \approx \frac{N}{2} \int \left| \tilde{g}(f) \right|^2 \exp\left(j2\pi f \frac{(m-n)T_S}{2} \right) df$$

$$= \frac{N}{2} g_{RC} \left(\frac{(m-n)T_S}{2} \right). \qquad \text{(F-9)}$$

As a result, from (F-4), we can write

$$P_{Ave} = \frac{\alpha_{R_i} P_1}{N} \sum_{n=0}^{2N-1} \sum_{m=0}^{2N-1} \left[\frac{G_{SR_i} P_0}{2} \left(g_{RC} \left(\frac{(m-n)T_S}{2} \right) \right)^2 + N_0 \delta(n-m) \right]$$

$$= \alpha_{R_i} P_1 \left[2N_0 + \frac{G_{SR_i} P_0}{2N} \sum_{n=0}^{2N-1} \sum_{m=0}^{2N-1} \left[g_{RC} \left(\frac{(m-n)T_S}{2} \right) \right]^2 \right]$$

$$= \alpha_{\mathrm{R}_i} P_1 \left[2N_0 + G_{\mathrm{SR}_i} P_0 \left(1 + \frac{1}{N} \sum_{k=1}^{2N-1} (2N-k) \left[g_{\mathrm{RC}} \left(\frac{kT_S}{2} \right) \right]^2 \right) \right].$$

(F-10)

Consequently, by forcing the constraint of $P_{Ave} = P_1$, α_{R_i} is given by

$$\alpha_{\mathrm{R}_i} = \frac{1}{G_{\mathrm{SR}_i} P_0 \left(1 + \frac{1}{N} \sum_{k=1}^{2N-1} (2N-k) \left[g_{\mathrm{RC}} \left(\frac{kT_S}{2} \right) \right]^2 \right) + 2N_0} \ .$$

(F-11)

Bibliography

[1] N. M. Maslin, *HF Communications: A Systems Approach*. Springer, 1987.

[2] J. M. Goodman, *HF Communications: Science and Technology*. Van Nostrand Rheinhold, New York, 1992.

[3] IEC, "International Standard 62 272-1, Digital Radio Mondiale (DRM)-Part 1: System Specification," *International Electrotechnical Commission*, 2003.

[4] J. Pennington, "Techniques for medium-speed data transmission over HF channels," *IEE Proc. Commun. Speech and Vision*, 1989.

[5] E. E. Johnson, "Third-generation technologies for HF radio networking," in *IEEE Proc. of Mil. Commun. Conf.*, 1998.

[6] E. E. Johnson, "Interoperability and performance issues in HF e-mail," in *IEEE Proc. of Mil. Commun. Conf.*, 2001.

[7] A. Navarro, R. Rodrigues, J. Angeja, J. Tavares, L. Carvalho, and F. Perdigao, "Video conference over HF packet radio channels," in *IEEE Proc. of Mil. Commun. Conf.*, 2003.

[8] V. Tarokh, N. Seshadri, and A. R. Calderbank, "Space-time codes for high data rate wireless communication: performance criterion and code construction," *IEEE Trans. Inf. Theory*, vol. 44, no. 2, pp. 744 –765, Mar. 1998.

[9] B. Vucetic and J. Yuan, *Space-Time Coding*. Wiley, 2003.

[10] A. Paulraj, R. Nabar, and D. Gore, *Introduction to Space-Time Wireless Communications*. Cambridge University Press, 2003.

[11] E. C. Van Der Meulen, "Three-Terminal Communication Channels," *Advances in Applied Probability*, vol. 3, no. 1, p. 120, 1971.

[12] T. M. Cover and A. E. Gamal, "Capacity theorems for the relay channel," *IEEE Trans. Inf. Theory*, vol. 25, pp. 572–584, 1979.

[13] A. Sendonaris, E. Erkip, and B. Aazhang, "User cooperation diversity. Part I. System description," *IEEE Trans. Commun.*, vol. 51, no. 11, pp. 1927–1938, Nov. 2003.

[14] A. Sendonaris, E. Erkip, and B. Aazhang, "User cooperation diversity. Part II. Implementation aspects and performance analysis," *IEEE Trans. Commun.*, vol. 51, no. 11, pp. 1939–1948, Nov. 2003.

[15] J. N. Laneman, D. N. C. Tse, and G. W. Wornell, "Cooperative diversity in wireless networks: Efficient protocols and outage behavior," *IEEE Trans. Inf. Theory*, vol. 50, no. 12, pp. 3062 – 3080, Dec. 2004.

[16] J. N. Laneman, G. W. Wornell, and D. N. C. Tse, "An efficient protocol for realizing cooperative diversity in wireless networks," in *IEEE Proc. of Inter. Symp. on Inf. Theory*, 2001.

[17] J. N. Laneman and G. W. Wornell, "Distributed space-time-coded protocols for exploiting cooperative diversity in wireless networks," *IEEE Trans. Inf. Theory*, vol. 49, no. 10, pp. 2415–2425, Oct. 2003.

[18] A. Bletsas, A. Khisti, D. P. Reed, and A. Lippman, "A simple Cooperative diversity method based on network path selection," *IEEE J. Sel. Areas Commun.*, vol. 24, no. 3, pp. 659–672, Mar. 2005.

[19] H. Chen, A. B. Gershman, and S. Shahbazpanahi, "Filter-and-Forward Distributed Beamforming in Relay Networks With Frequency Selective Fading," *IEEE Trans. Signal Process.*, vol. 58, no. 3, pp. 1251 –1262, Mar. 2010.

[20] H. J. Strangeways, "Estimation of signal correlation at spaced antennas for multi-moded ionospherically reflected signals and its effect on the capacity of SIMO and MIMO HF links," in *IET Inter. Conf. on Ionospheric Radio Systems and Techniques*, 2006.

[21] M. Sharp, A. Scaglione, and S. Galli, "Distributed Randomized Space-Time Coding for HF Transmission," in *IEEE Proc. of Mil. Commun. Conf.*, 2006.

[22] T. Banwell, J. Dixon, J. Koshy, D. Waring, A. Scaglione, and M. Sharp, "Distributed carrier synchronization for HF cooperative communication employing randomized space time block coding," in *IEEE Proc. of Mil. Commun. Conf.*, 2009.

[23] G. Caire, G. Taricco, and E. Biglieri, "Bit-interleaved coded modulation," *IEEE Trans. Inf. Theory*, vol. 44, no. 3, pp. 927 –946, May 1998.

[24] E. Akay and E. Ayanoglu, "Achieving Full Frequency and Space Diversity in Wireless Systems via BICM, OFDM, STBC, and Viterbi Decoding," *IEEE Trans. Commun.*, vol. 54, no. 12, pp. 2164 –2172, Dec. 2006.

[25] M. R. Heidarpour and M. Uysal, "Cooperative BICM-OFDM systems for frequency-selective relay channels," in *Asilomar Conf. on Signals, Systems and Computers*, 2011.

[26] T. Islam, R. Schober, R. K. Mallik, and V. K. Bhargava, "Analysis and Design of Cooperative BICM-OFDM Systems," *IEEE Trans. Commun.*, vol. 59, no. 6, pp. 1742 – 1751, Jun. 2011.

[27] H. Gacanin and F. Adachi, "Broadband analog network coding," *IEEE Trans. Wireless Commun.*, vol. 9, no. 5, pp. 1577 –1583, May 2010.

[28] Y. Liang, A. Ikhlef, W. Gerstacker, and R. Schober, "Cooperative Filter-and-Forward Beamforming for Frequency-Selective Channels with Equalization," *IEEE Trans. Wireless Commun.*, vol. 10, no. 1, pp. 228 –239, Jan. 2011.

[29] P. Wu and R. Schober, "Cooperative Frequency-Domain Beamforming for Broadband SC-FDE Systems," in *IEEE Proc. of Global Telecommun.*, 2011.

[30] H. Mheidat, M. Uysal, and N. Al-Dhahir, "Equalization Techniques for Distributed Space-Time Block Codes With Amplify-and-Forward Relaying," *IEEE Trans. Signal Process.*, vol. 55, no. 5, pp. 1839 –1852, May 2007.

[31] J. E. Mazo, "Exact matched filter bound for two-beam Rayleigh fading," *IEEE Trans. Commun.*, vol. 39, no. 7, pp. 1027 –1030, Jul. 1991.

[32] S. A. Fechtel and H. Meyr, "A new method of evaluating the matched-filter bound for uncoded and trellis-coded transmission over frequency-selective fading diversity channels," in *IEEE Proc. of Global Telecommun.*, 1992.

[33] F. Ling, "Matched filter-bound for time-discrete multipath Rayleigh fading channels," *IEEE Trans. Commun.*, vol. 43, no. 234, pp. 710 –713, Apr. 1995.

[34] J. R. Barry, D. G. Messerschmitt, and E. A. Lee, *Digital Communication: Third Edition*. Norwell, MA, USA: Kluwer Academic Publishers, 2003.

[35] R. D. Gitlin and S. B. Weinstein, "Fractionally-spaced equalization: An improved digital transversal equalizer," *Bell Syst. Tech. J.*, vol. 60, pp. 275–296, Feb. 1981.

[36] G. Ungerboeck, "Fractional Tap-Spacing Equalizer and Consequences for Clock Recovery in Data Modems," *IEEE Trans. Commun.*, vol. 24, no. 8, pp. 856 – 864, Aug. 1976.

[37] F. Pancaldi and G. M. Vitetta, "Block channel equalization in the frequency domain," *IEEE Trans. Commun.*, vol. 53, no. 3, pp. 463 – 471, Mar. 2005.

[38] M. V. Clark, "Adaptive frequency-domain equalization and diversity combining for broadband wireless communications," *IEEE J. Sel. Areas Commun.*, vol. 16, no. 8, pp. 1385 –1395, Oct. 1998.

[39] R. Kalbasi, D. D. Falconer, A. H. Banihashemi, and R. Dinis, "A Comparison of Frequency-Domain Block MIMO Transmission Systems," *IEEE Trans. Veh. Technol.*, vol. 58, no. 1, pp. 165 –175, Jan. 2009.

[40] E. Biglieri, J. Proakis, and S. Shamai, "Fading channels: information-theoretic and communications aspects," *IEEE Trans. Inf. Theory*, vol. 44, no. 6, pp. 2619 –2692, Oct. 1998.

[41] IPS Radio and Space Services, "Introduction to HF Radio Propagation." available at www.ips.gov.au.

[42] B. Goldberg, "300 kHz-30 MHz MF/HF," *IEEE Transactions on Communication Technology*, vol. 14, no. 6, pp. 767 –784, Dec. 1966.

[43] "http://www.itu.int/oth/R0A0400000F/en." .

[44] "http://elbert.its.bldrdoc.gov/hf.html." .

[45] ITU, "Method for the prediction of the performance of HF circuits," *ITU-R Recommendations P. 533*, 2009.

[46] C. Watterson, J. Juroshek, and W. Bensema, "Experimental Confirmation of an HF Channel Model," *IEEE Transactions on Communication Technology*, vol. 18, no. 6, pp. 792 –803, Dec. 1970.

[47] ITU, "Testing of HF Modems with Bandwidths of up to 12kHz Using Ionospheric Channel Simulator," *ITU-R Recommendations F. 1487*, 2000.

[48] M. C. Gill, *Coded-Waveform Design for High Speed Data Transfer over High Frequency Radio Channels*. PhD thesis, University of South Australia, 1998.

[49] J. E. M. Nilsson and T. C. Giles, "Wideband multi-carrier transmission for military HF communication," in *IEEE Proc. of Mil. Commun. Conf.*, 1997.

[50] C. A. Pantjiaros, J. A. Wylie, J. Brown, G. F. Gott, and P. J. Laycock, "Extended UK models for high frequency spectral occupancy," *IEE Proc. of Commun.*, Jun. 1998.

[51] H. Ochiai, P. Mitran, and V. Tarokh, "Variable-Rate Two-Phase Collaborative Communication Protocols for Wireless Networks," *IEEE Trans. Inf. Theory*, vol. 52, no. 9, pp. 4299 –4313, Sep. 2006.

[52] H. Mheidat and M. Uysal, "Impact of receive diversity on the performance of amplify-and-forward relaying under APS and IPS power constraints," *IEEE Commun. Lett.*, vol. 10, no. 6, pp. 468 –470, Jun. 2006.

[53] M. Abramowitz and I. A. Stegun, Eds., *Handbook of Mathematical Functions: with Formulas, Graphs, and Mathematical Tables*, 1st ed. Dover Publications, 1965.

[54] S. Boyd and L. Vandenberghe, *Convex Optimization*. Cambridge Univ. Press, 2004.

[55] Y. Ding and M. Uysal, "Amplify-and-forward cooperative OFDM with multiple-relays: performance analysis and relay selection methods," *IEEE Trans. Wireless Commun.*, vol. 8, no. 10, pp. 4963 –4968, Oct. 2009.

[56] M. Uysal, "Diversity analysis of space-time coding in cascaded Rayleigh fading channels," *IEEE Commun. Lett.*, vol. 10, no. 3, pp. 165 – 167, Mar. 2006.

[57] M. Russell and G. L. Stuber, "Interchannel interference analysis of OFDM in a mobile environment," in *IEEE Conf. Veh. Technol.*, 1995.

[58] W. G. Jeon, K. H. Chang, and Y. S. Cho, "An equalization technique for orthogonal frequency-division multiplexing systems in time-variant multipath channels," *IEEE Trans. Commun.*, vol. 47, no. 1, pp. 27 –32, Jan. 1999.

[59] M. K. Simon and M.-S. Alouini, *Digital Communication over Fading Channels*, 2nd ed. Wiley-IEEE Press, 2004.

[60] I. S. Gradshteĭn, I. M. Ryzhik, A. Jeffrey, and D. Zwillinger, *Table of Integrals, Series, And Products*. Academic Press, 2007.

[61] D. Senaratne and C. Tellambura, "Unified Exact Performance Analysis of Two-Hop Amplify-and-Forward Relaying in Nakagami Fading," *IEEE Trans. Veh. Technol.*, vol. 59, no. 3, pp. 1529 –1534, Mar. 2010.

[62] Whittaker, *A Course in Modern Analysis*, 4th ed. Cambridge Univ. Press, 1990.

[63] Z. Wang and G. B. Giannakis, "A simple and general parameterization quantifying performance in fading channels," *IEEE Trans. Commun.*, vol. 51, no. 8, pp. 1389 – 1398, Aug. 2003.

[64] M. O. Hasna and M.-S. Alouini, "A performance study of dual-hop transmissions with fixed gain relays," *IEEE Trans. Wireless Commun.*, vol. 3, no. 6, pp. 1963 – 1968, Nov. 2004.

[65] A. Stamoulis, G. B. Giannakis, and A. Scaglione, "Block FIR decision-feedback equalizers for filterbank precoded transmissions with blind channel estimation capabilities," *IEEE Trans. Commun.*, vol. 49, no. 1, pp. 69 –83, Jan. 2001.

[66] B. K. Ng and D. Falconer, "A novel frequency domain equalization method for single-carrier wireless transmissions over doubly-selective fading channels," in *IEEE Proc. of Global Telecommun.*, 2004.

[67] S. F. Cotter and B. D. Rao, "Sparse channel estimation via matching pursuit with application to equalization," *IEEE Trans. Commun.*, vol. 50, no. 3, pp. 374 –377, Mar. 2002.

[68] C. Carbonelli, S. Vedantam, and U. Mitra, "Sparse Channel Estimation with Zero Tap Detection," *IEEE Trans. Wireless Commun.*, vol. 6, no. 5, pp. 1743 –1763, May 2007.

[69] S. Lin and D. J. Costello, *Error Control Coding: Fundamentals and Applications*. Prentice Hall, 2004.

[70] D. Chase, "Code Combining–A Maximum-Likelihood Decoding Approach for Combining an Arbitrary Number of Noisy Packets," *IEEE Trans. Commun.*, vol. 33, no. 5, pp. 385 – 393, May 1985.

[71] J. Hagenauer, "Rate-compatible punctured convolutional codes (RCPC codes) and their applications," *IEEE Trans. Commun.*, vol. 36, no. 4, pp. 389 –400, Apr. 1988.

[72] B. Zhao and M. C. Valenti, "Practical relay networks: a generalization of hybrid-ARQ," *IEEE J. Sel. Areas Commun.*, vol. 23, no. 1, pp. 7 –18, Jan. 2005.

[73] D. A. Harville, *Matrix Algebra From a Statistician's Perspective*. Springer, 1997.

[74] Y. Yang, J. Ge, and Y. Gao, "Power Allocation for Two-Way Opportunistic Amplify-and-Forward Relaying over Nakagami-m Channels," *IEEE Trans. Wireless Commun.*, vol. 10, no. 7, pp. 2063 –2068, Jul. 2011.

[75] J. Proakis and M. Salehi, *Digital Communications*. McGraw-Hill Education, 2007.